Investigations on polyaniline based systems for technologically important applications and some novel polymers as prospective candidates for fabricating polymer light emitting diodes

Thesis submitted to

Cochin University of Science & Technology

in partial fulfilment of the requirements for the award of

Doctor of Philosophy

by

Sreekanth J Varma

Department of Physics,
Cochin University of Science & Technology,
Kochi- 682022, India

September, 2012

Investigations on polyaniline based systems for technologically important applications and some novel polymers as prospective candidates for fabricating polymer light emitting diodes

Ph.D thesis in the field of material science

Author:

Sreekanth J Varma

Division for Research in Advanced Materials
Department of Physics
Cochin University of Science and Technology
Cochin-682022, Kerala, India
Email: sreekanthvarma@gmail.com

Supervisor:

Dr.S.Jayalekshmi

Professor,
Division for Research in Advanced Materials
Department of Physics
Cochin University of Science and Technology
Cochin-682022, Kerala, India
Email: jayalekshmi@cusat.ac.in

Cover Image: Novel light emitting polymers, TBPV1 (top) and P2 (bottom) and, an OLED with green emission (middle)

September 2012

Department of Physics
Cochin University of Science and Tecnology
Cochin - **682022**

Dr. S. Jayalekshmi
Professor

23rd August 2012

Certificate

Certified that the work presented in the thesis entitled "**Investigations on polyaniline based systems for technologically important applications and some novel polymers as prospective candidates for fabricating polymer light emitting diodes**" is an authentic record of the bonafide research work done by Mr. Sreekanth J Varma, under my guidance and supervision in the Department of Physics, Cochin University of Science and Technology, Kochi-682022, and no part of it has been included in any other thesis submitted previously for the award of any degree.

Dr. S Jayalekshmi
Supervising Guide

Declaration

I do hereby declare that the work presented in the thesis entitled "**Investigations on polyaniline based systems for technologically important applications and some novel polymers as prospective candidates for fabricating polymer light emitting diodes**" is based on the original research work done by me under the guidance and supervision of Dr. S Jayalekshmi, Professor, Department of Physics, Cochin University of Science and Technology, Kochi-682 022 and no part of it has been included in any other thesis submitted previously for the award of any degree.

Kochi-682 022 **Sreekanth J Varma**

23rd August 2012

"Holy light !

Illuminate the way that we may

gather the good we planted"

Isha Upanishad

Words of Gratitude…

All through the past so many years I have been fortunate to be associated with a lot of people who have shaped my thinking and sharpened my logical understanding. From the classrooms to the research lab, it has been a long journey and each step has been taken with the encouragement of my teachers. They have kindled in me the desire to learn and the courage to pursue my dreams. A mere ‘thank you’ cannot express my gratitude to them for having stood by me all these years.

Research has been an enriching experience and the able guidance of Dr. S.Jayalekshmi, Professor, Department of Physics, Cochin University of Science and Technology has been my strength. Her relentless encouragement, benevolent support and scholarly suggestions have helped me at every stage of my work. She has appreciated my suggestions and boosted my confidence to take up challenging tasks. In all my walks through the dark worlds of doubts and uncertainties, she lighted the way, showed the way. I thank her profusely with realization that no words can properly express my indebtedness to her.

At this juncture, I would like to place on record my deepest sense of gratitude to Dr. S. Prathapan, Associate Professor, Department of Applied Chemistry, CUSAT. He has played a pivotal role in making my dream of fabricating polymer LEDs come true. I am indebted to you, sir, for all the selfless support and proficient guidance.

I am extremely thankful to Prof. B. Pradeep, Head of the Department of Physics, CUSAT, Kochi, and former Department Heads, Prof. M.R. Anantharaman, Prof. Godfrey Louis and Prof. Ramesh Babu T for providing all the necessary facilities and the environment to carry out fruitful research. I have been privileged throughout the period of my research work to be associated with Prof. M. K. Jayaraj, Department of Physics, CUSAT. He has extended his helping hand whenever needed, and guided me through the course of research work. I take this opportunity to thank all the faculty members of the Department of Physics, CUSAT for their encouragement and cooperation.

I convey my sincere thanks to the administrative, library and laboratory staff of the Department of Physics for their help and assistance.

I take this opportunity to thank Dr. Rani Joseph, Professor, Department of Polymer Science and Rubber Technology for giving me the opportunity to work in the exciting field of conducting polymers. I am privileged to have started my career in research under her able tutelage. I acknowledge with gratitude the cooperation extended to me by the faculty members, research scholars and the non-teaching staff of the Department of PS&RT.

I consider myself fortunate to have been associated with Dr. C.P.R. Nair, Scientist – SG & Head, VSSC, Thiruvananthapuram during my research work. He has been a well-wisher and a strong motivator. Thank you sir, for your generous support.

Special thanks to Dr. Narayanan Unni and Prof. Deepak Gupta for having made my days at the IIT, Kanpur constructive and memorable

with the successful fabrication of PLEDs. I wish to thank Dr. Asha Awasti, Dr. Ashish Gupta Dr. J.Narain and Awnish for their assistance and timely help.

I owe a lot to Vidya G., Research scholar, PS& RT, CUSAT for helping me in achieving the target of realizing the polymer LEDs in practice.

I have a great friend and collaborator in Dr. Soney Varghese. He has generously helped me to use the experimental facilities of NIT, Calicut and I am extremely grateful for the fruitful discussions I had with him. Subhash and Uvais need special mention for their prompt and timely assistance.

Friends are my strength. Dr. Suma K.K, Dr. Jude Mendez, Dr. Sinto Jacob, Dr. Anoop Anand and Mr. Anoop P.D have been a great source of inspiration.

I remember late Dr. K.Raveendranath, my colleague in DREAM laboratory, CUSAT, with great reverence. He inspired me to write my first research paper. My special thanks to Dr. M Amrithesh, Dr. Arun K J, Ms. Sreevalsa, Ms. Jeeju, Ms. Dhannia, Ms. Sajimol, Mr. Rajive Tomy, Mr. Anil Kumar, Mr. Francis Xavier, Mr. Anand P B, the DREAM team. Though I would like to acknowledge all the research scholars of the Dept. of Physics for their help personally, I prefer to restrict it to a ‘thank you’ due to the length of the list. Let me take this opportunity to thank the faculty and non-teaching staff of the International School of Photonics, CUSAT for their support. My colleagues in the Dept. of Applied Chemistry deserve a special mention for their help and support.

It is my pleasure to thank Prof. Ravindranathan Kartha, NIPER, Chandigarh and Prof. D. Sakthi Kumar, Toyo Univeristy, Japan who helped to overcome many obstacles in my research career.

The financial assistance provided by the University Grants Commission in the form of UGC-RFSMS fellowship is gratefully acknowledged.

I dedicate this thesis to my Achan and Amma who have supported me all these years and given me the strength to fulfil my dreams. Without the unconditional love and emotional backing given by my family, I would never have been able to complete the research work. I fondly remember the good times I spent with my late grandfather who drove home the importance of education in one's life.

I bow in reverence before the Supreme Power for the blessings showered upon me.

Sreekanth J Varma

Preface

Until about 30 years ago all carbon based polymers were rigidly regarded as insulators. The idea that plastics could be made to conduct electricity would have been considered to be absurd. Indeed, plastics have been extensively used by the electronics industry because of this very property. They were utilized as inactive packaging and insulating materials. This perspective was overturned by the pioneering work by ***Alan J. Heeger, Alan MacDiarmid and Hideki Shirakawa*** with the introduction of doped polymers with tunable electrical conductivity extending from semi conducting to the superconducting range. They were awarded Nobel prize in Chemistry in the year 2000 *"For the discovery and development of conductive polymers."* This has triggered extensive research in the field of conducting polymers, otherwise called synthetic metals during the past few years owing to the ever increasing interest in their technological and industrial applications.

Polyaniline (PANI) is one of the most stable conducting polymers ever studied. It is environmentally stable both in conducting (doped) and non-conducting (de-doped) forms. It occupies a unique position among the conducting polymers and is well known for the excellent electrical and optical properties. PANI has immense applications in the fields of polymer LEDs, photovoltaics, batteries, electrostatic charge dissipative coatings, electromagnetic shielding, and sensors. PANI has been identified as one of the most technologically and industrially important conducting polymers owing to its unique processability together with the availability of relatively inexpensive precursors and better yields of polymerization. The electrical conduction mechanism in PANI has been widely investigated.

Conducting polymers can respond to various external stimuli and hence represent a new class of ‘intelligent materials’. The inherent stability of PANI and its tunable electrical and optical properties make it an ingenious element suited for various optoelectronic device applications. The

method adopted for polymerization and the reaction conditions strongly influence the morphology and, optical and electrical properties of PANI.

Conducting polymer nanocomposites belongs to a class of advanced composite materials that can be used for very interesting applications. Blends of carbon nanotubes and other nanoparticles with conducting polymers resulting in the formation of composites have now received a great deal of attention. These composites exhibit the properties of their constituents with synergetic effects and are promising candidates for use in organic light emitting diodes, photovoltaic cells**,** batteries and supercapacitors. The pressure sensing properties in nanostructured and micro-structured polyaniline and its composites has not been investigated in detail. The response to applied pressure in polyaniline and its composites can be effectively used for sensor applications.

Quantum confinement effects are well-known and investigated extensively in metals and inorganic semiconductors in their nano dimensions. Nano sized materials exhibit entirely different properties compared to their bulk analogues. For example, gold appears in different colours and show modified electrical properties when the size is reduced below the confinement regime. Reports on confinement effects in polymers are very scarce. Polyaniline is a low cost conducting polymer, which can be easily synthesized in bulk quantities. The altered emission properties as a result of the confinement effects in PANI thin films offer prospects of being utilized as emissive layers in polymer light emitting diodes.

Only a few papers have been published, related to the synthesis of highly crystalline PANI films with ordered structure and high electrical conductivity. The reported conductivity values range from 200-400 S/cm in chemical oxidative polymerized PANI samples and from 1000-1200 S/cm in those samples prepared using self-stabilized dispersion polymerization. There is a strong relation between dc electrical conductivity and crystallinity of polyaniline and the conductivity gets enhanced with increase in crystallinity.

The highly ordered and crystalline thin films of PANI can be used as the anode material for polymer light emitting diodes.

Light emitting polymers (LEP) have drawn considerable attention because of their numerous potential applications in the field of optoelectronic devices. Till date, a large number of organic molecules and polymers have been designed and devices fabricated based on these materials. Optoelectronic devices like polymer light emitting diodes (PLED) have attracted wide-spread research attention owing to their superior properties like flexibility, lower operational power, colour tunability and possibility of obtaining large area coatings. PLEDs can be utilized for the fabrication of flat panel displays and as replacements for incandescent lamps. The internal efficiency of the LEDs mainly depends on the electroluminescent efficiency of the emissive polymer such as quantum efficiency, luminance-voltage profile of LED and the balanced injection of electrons and holes. Poly (*p*-phenylenevinylene) (PPV) and regio-regular polythiophenes are interesting electro-active polymers which exhibit good electrical conductivity, electroluminescent activity and high film-forming properties. A combination of Red, Green and Blue emitting polymers is necessary for the generation of white light which can replace the high energy consuming incandescent lamps. Most of these polymers show very low solubility, stability and poor mechanical properties. Many of these light emitting polymers are based on conjugated extended chains of alternating phenyl and vinyl units. The intra-chain or inter-chain interactions within these polymer chains can change the emitted colour. Therefore an effective way of synthesizing polymers with reduced π-stacking, high solubility, high thermal stability and high light-emitting efficiency is still a challenge for chemists. New copolymers have to be effectively designed so as to solve these issues. Hence, in the present work, the suitability of a few novel copolymers with very high thermal stability, excellent solubility, intense light emission (blue, cyan and green) and high glass transition temperatures have been investigated to be used as emissive layers for polymer light emitting diodes.

The whole research work presented in the thesis is portrayed in eight chapters as detailed below:

The **first chapter** gives a general introduction to conducting polymers, polyaniline (PANI) and its composites, their history, synthesis procedures and applications.

The **second chapter** deals with the theoretical aspects and details of all the experimental techniques used in the present studies. A brief discussion on the various synthesis methods, resulting polymeric structures, properties, device fabrication methods, etc. has also been included in this section.

The investigations carried out on the pressure sensing properties of polyaniline and its composites with multi-walled carbon nanotubes (MWNT) and polyvinyl chloride (PVC) are portrayed in **Chapter 3**. The change in electrical conductivity with applied pressure in pressed pellets of these samples has been investigated. It is observed that for all the samples, a considerable change in dc electrical conductivity values occurs even for very low applied pressure. Out of all the samples investigated, CSA doped PANI is found to be the best with appreciable percentage variation of electrical conductivity with applied pressure and negligible hysteresis effects. The work highlights the prospects of utilizing doped polyaniline and its composites for pressure sensing applications.

Chapter 4 is devoted to the studies on quantum confinement effects in ultra-thin films (50 nm, 100nm and 150 nm) of polyaniline pursued through spectroscopic investigations. Considerable blue-shift in the UV-Vis absorption and photoluminescence spectra has been observed in these ultra-thin films when compared to the bulk analogue, which is a clear indication of quantum confinement effects. The intense blue emission observed in these ultra-thin PANI films can be of practical application in realizing cost-effective and efficient polymer light emitting diodes.

Chapter 5 gives a detailed account of the various synthesis routes of PANI thin films with exceptionally good crystallinity and their characterization. X-ray diffraction has been used to analyze the extent of crystallinity in these highly ordered films. Cubic, monoclinic and triclinic crystal structures have been found to match with the observed XRD data of these synthesized film samples. These highly conducting and ordered films can be of potential application as anode materials for polymer LEDs.

Chapter 6 deals with the structural and optical characterization of two, novel, light emitting copolymers based on thienylene-biphenylenevinylene with excellent solubility, thermal stability and glass transition temperatures. Attempts have been made to fabricate prototype polymer LEDs using these copolymers as emissive layers. The current-voltage (I-V) characteristics of these prototype devices exhibit the diode characteristics necessary for PLEDs. An orange-red emission has been observed in the electroluminescence spectrum of these prototype devices.

C**hapter 7** gives an account of the characterization of another set of novel**,** light emitting, segmented block polymers based on poly (phenylenevinylene) derivatives. Prototype PLED devices have been fabricated using two polymers which emit light in the blue and green regions. I-V characteristics of these devices also show the diode characteristics necessary for PLEDs. The electroluminescence spectra of these prototype devices have been recorded. Both the devices emit light in the green region. The polymers have been found to be suitable candidates for PLED applications as evident from their I-V characteristics and electroluminescence spectra.

The general conclusions and the scope for future work are included in **chapter 8.**

CONTENTS

Chapter **8**

Summary and Future Prospects ---------- -185 - 192

List of Publications

In peer-reviewed journals related to the present work:

1. **S.J.Varma**, Jerin George, Jeeju.P.P, S.Jayalekshmi, "Quantum confinement effects in highly conducting, ultrathin Polyaniline films pursued through spectroscopic investigations", ***Journal of Luminescence***, 132 (2012) 801-805

2. **S.J.Varma**, Francis Xavier P.A, Soney Varghese and S.Jayalekshmi, "Synthesis and studies on exceptionally crystalline polyaniline thin films", ***Polymer International***, (2012) *(DOI 10.1002/pi.4131).*

3. **S.J.Varma,** S.Jayalekshmi, "On the prospects of Polyaniline and Polyaniline/MWNT Composites for possible pressure sensing applications", ***Journal of Applied Polymer Science***, Vol. 117 (2010) 138–142

4. Vidya.G, **SreekanthJ.Varma**, S.Prathapan, S.Jayalekshmi, Rani Joseph, Novel, Novel, Highly Soluble, Intense Green Light Emitting Thienylene-Biphenylenevinylene Polymers: Synthesis, Characterization, Molecular Assembly and Photophysical Studies, ***Advanced Materials*** (Communicated)

5. Vidya.G, **SreekanthJ.Varma,** S.Prathapan, S.Jayalekshmi, Rani Joseph, Substituent Effects on Light-Emitting Segmented Block PPV Copolymers: Synthesis, Structural and photophysical Studies, ***Macromolecules*** (Communicated)

6. Vidya.G, **SreekanthJ.Varma,** S.Prathapan, S.Jayalekshmi, Rani Joseph, Synthesis and Characterization of New Intense Blue-Light Emitting Ring Substituted Semicrystalline Segmented PPV Block Copolymer, ***Polymer*** (Communicated)

Other publications in peer-reviewed journals:

7. M. Sajimol Augustine, **S.J. Varma**, P.A. Francis Xavier and S. Jayalekshmi, "Enhanced photoluminescence in oleic acid modified polyaniline", *Transactions of the Indian Institute of Metals*, 64 (2011) 209-212

8. Pullarkat P Jeeju, Augustine M Sajimol, Vallath G Sreevalsa, **Sreekanth J Varma** and S Jayalekshmi, "Size-dependent optical properties of transparent, spin-coated polystyrene/ ZnO nanocomposite films" *Polymer International*, 60 (2011) 1263–1268

9. M.Amrithesh, K.P.Chandni, S.Jayalekshmi, FebinKurian, **S.J.Varma**, On the interesting optical transitions observed in polyaniline films in the conducting and insulating states, *Optoelectronics and Advanced Materials – Rapid Communications*, Vol. 3, No. 2, February 2009, p. 149 – 154

10. Novel Polypyrrole films with excellent crystallinity and good thermal stability, P.P.Jeeju, **S. J.Varma**, P.A.Francis Xavier, A.M.Sajimol, S.Jayalekshmi, *Materials Chemistry and Physics* – (2012) doi:10.1016/ j.matchemphys.2012.03.072

International/National Conferences:

11. **Sreekanth J. Varma**, S.Jayalekshmi, "Carbon Nanotube - Polymer Nanocomposites for Possible Pressure Sensor Applications" *Proc. of **SPIE*** Vol. 7037, 703716, (2008)

12. **S.J.Varma**, Francis Xavier and S. Jayalekshmi, "An investigation on the high temperature response of highly conducting polyaniline films" *Proc. International conference on Advances in Polymer Technology*, Feb. 26-27, 2010, India, Page No. 119

13. **S.J.Varma**, et al., "A quest for quantum confinement in highly conducting polyaniline thin films through spectroscopic investigations", *Proc. International conference ICMST*, October 2010, Thiruvananthapuram

14. **S.J.Varma**, S. Jayalekshmi, Proc. International Conference on "*Material Science Research and Nanotechnology (ICMSRN 2008)*", 27-29th February 2008, Kodaikanal, Tamilnadu, India, 46, P 153

15. **Sreekanth.J.Varma**, Rani Joseph, Honey John, Mani. T.K; PP 17, Proc. National Conference "*New Horizons in Theoretical & Experimental Physics (NHTEP 2007)*", October 8-10 (2007), Cochin, India

16. Francis Xavier, Amrithesh.M, **S.J.Varma**, Jeeju P. P and S. Jayalekshmi, "Studies on Polyaniline – functionalised carbon nanotube composite films with exceptional high dc electrical conductivity, *Proc. International symposium for research scholars on metallurgy, material science and engineering (ISRS 2010)*, December 20-22, 2010, ELPM-5, Page No. 199

17. Francis Xavier, **S.J.Varma,** and S. Jayalekshmi, "An investigation on the high temperature response of H_3PO_4 doped PANI and PANI-MWNT composites", *Proc. International conference on Advances in Polymer Technology*, Feb. 26-27, 2010, India, Page No. 115

18. Francis Xavier P. A, Bobins Augustine, **S. J. Varma**, Jeeju P. P, Amrithesh.M and S. Jayalekshmi, Functionalization of Multiwalled Carbon Nanotubes as a route to synthesize highly conducting Polymer-Nanocomposites", *Proc. ICMST*, October 2010,Thiruvananthapuram, HPS05, pp 8.34.

19. SajimolAugustine.M**, S.J.Varma**, Francis Xavier and S. Jayalekshmi, Enhanced photoluminescence behaviour of PANI/ZnOnanocomposite prepared from oleic acid capped ZnO nanoparticles", *Proc. ICMST*, October 2010, Thiruvananthapuram.

20. Jeeju P. P, **S J. Varma**, Francis Xavier P.A, S.Jayalekshmi, “Polypyrrole films with excellent crystallinity and good thermal stability”, *Proc. ICMST*, October 2010, Thiruvananthapuram.

21. SajimolAugustine.M, **S.J.Varma**, Francis Xavier and S. Jayalekshmi, “Enhanced photoluminescence in oleic acid modified Polyaniline”, Proc. Proc. ‘ISRS 2010’, IITM, Chennai.

22. Jeeju.P.P, **Sreekanth.J.Varma**, Amrithesh.M, S.Jayalekshmi, “Polypyrrolenanorods with appreciable crystallanity and good optical absorption characteristics”, *Second International Conference on frontiers in Nanoscience& Nanotechnology: Cochin Nano- 2009*, page 144

23. R.Mohan, Srikanth Naik, M. Rao, **S.J.Varma**, A. M Shanmugharaj, Soney Varghese, Preparation and Characterization of Ferroelectric Polymer-Ceramic Nanocomposites for Non-volatile Memory Applications, *Proc. International conference on Advances in Polymer Technology*, Feb. 26-27, 2010, India, Page No. 330

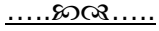

Chapter 1

CONDUCTING POLYMERS, PROPERTIES AND APPLICATIONS: A BRIEF OUTLINE

Contents

This chapter begins with a short introduction to the history of conducting polymers and then evolves into the fundamentals of charge transport in these polymers. One of the most important conducting polymers, polyaniline, its properties and applications are detailed here. A very distinctive class of conjugated conductive polymers, the light emitting polymers, are being portrayed and its application as emissive layers in polymer light emitting diodes is explained. The objectives of the present investigations and the motivation behind the work also form an integral part of the present chapter.

1.1 Conducting Polymers: A Brief Introduction

The history of humanity has been crowned by many landmarks, highlighting the breath taking innovations contributed by pioneers who believed in the potential of science. The humble origins of polymers can be traced back to the contributions of Henri Braconnotin 1777 and Christian

Schonbeinin 1846, which led to the discovery of the macromolecule, nitrocellulose. Since then, similar macromolecules have formed an indispensable part of our lives from simple plastic carry bags to the very sophisticated light emitting diode based displays. An intrinsically conducting polymer (ICP) is a conjugated system combining the optical, electrical, electronic and magnetic properties of a metal and the mechanical properties and process ability of a polymer. ICPs are more commonly called synthetic metals. These organic materials are comprised mainly of carbon, hydrogen and simple heteroatoms like nitrogen and sulphur. Lots of the unique properties associated with the conducting polymers, also called conjugated polymers, originate due to π-conjugation.

Conductive polymers (CP) are electrically conducting at room temperature, a phenomenon unknown in everyday plastics and organic polymers like polyethylene and polyesters. Attempts to synthesize conductive organic materials started in 1891 with F.Goppelsroeder synthesizing polyaniline [1].Though the non-conducting forms of CPs were well known, not much interest was paid to their other interesting properties. Interest in organic semiconductors started in the late 1950s and the highest electrical conductivity value reported was about 10^{-3} S cm^{-1}. Polyacetylene with semi conducting nature was first synthesized by Natta et.al in 1958 as a black powder. Depending on how the polymer was processed and manipulated, its conductivity was found to vary from 7×10^{-11} to 7×10^{-3} Sm^{-1}. Little theoretically postulated the possibility of superconductivity in polymers and put forward the model of a polyene chain with cyanine dye-like substituents [2]. The world-wide interest in CPs pinnacled when scientists of IBM showed that polysulfurnitride was

superconducting in crystalline form [3]. Around this time in 1974 Hideki Shirakwa's group produced a silvery thin film by mistake. The polymer, though metallic in appearance, was not conducting. In 1977 Shirakawa, MacDiarmid and Heeger found that oxidation with chlorine, bromine and iodine vapours resulted in the enhancement of the conductivity of polyacetylene films by 10 orders of magnitude. The procedure of treating polymers with halogens was called doping by analogy with the doping of semiconductors. Doping involves the partial addition (reduction) or removal (oxidation) of electrons to or from the π-system of the polymer backbone [4, 5, 6]. Films prepared by this method were found to have conductivity values of 0.4 Scm^{-1} for bromine doped and 38 Scm^{-1} for iodine doped samples. Later, electrical conductivity around 3000 S $cm^{-1}$was reported by Heeger for iodine doped films [7, 8, 9]. It was found that a transition in conductivity occurs when polymers and polymer derivatives are doped with a weak oxidizing or reducing agent. Alan J Heeger, Alan G MacDiarmid and Hideki Shirakawa were jointly awarded the Nobel Prize in Chemistry in 2000 for their pioneering work related to the discovery and development of conducting polymers.

A conducting polymer in its undoped or neutral state is called a pristine polymer. Doping is a process that gives the conducting polymer its identity. During this process an organic polymer with insulating or semiconducting properties (conductivity in the range 10^{-10} to 10^{-5} S cm^{-1}) becomes a polymer having metal like conductivity (1-10^{4} Scm^{-1}). Dopants can be small anions/ cations like ClO_4^-or Na^+ or large polymeric species like polyvinyl sulfonic acid and poly styrene sulfonic acid [10].

It is found that during controlled addition of small non-stoichiometric quantities of known chemical species, there is enormous change in the physical and structural properties of the polymer. There is no difficulty to regain the original polymer as doping is a reversible process. Both chemical and electrochemical methods can be employed for doping [6]. The level of doping influences the conductivity of the polymer and one can obtain films with conductivity anywhere between that of the non-doped and the fully doped forms of the polymer. A 100% doping level is not possible due to various structural constraints of the polymer. An insulator like the conventional polymer, when blended with a conducting polymer in various proportions can produce the conducting form [11]. A few important conjugated conducting polymers are shown in figures 1.1(a) to 1.1(f).

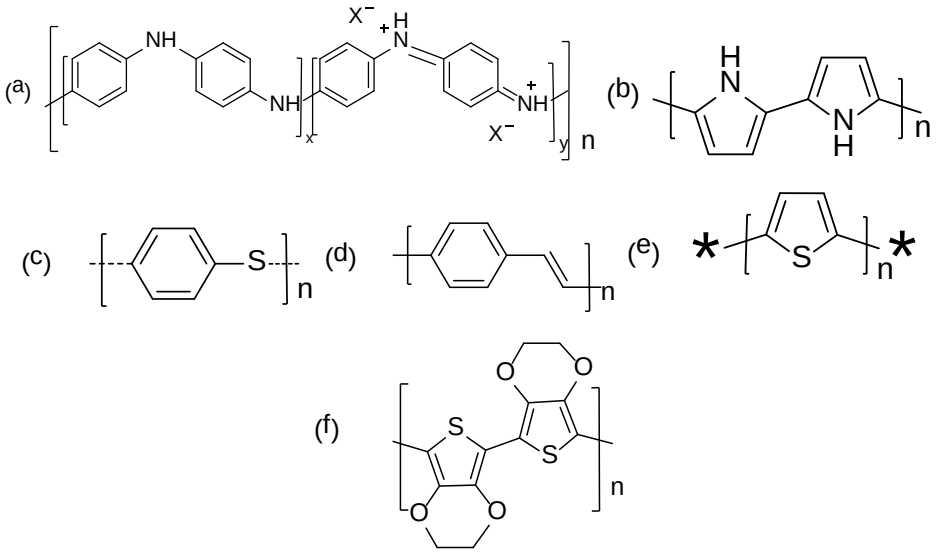

Figure 1.1: (a) Polyaniline (Emeraldine Salt), (b) Polypyrrole, (c) Poly (phenylene sulphide), (d) Poly (phenylenevinylene), (e) polythiophene and (f) Poly(3,4-ethylenedioxythiophene) (PEDOT)

1.2 Principles of electrical conduction in CPs

Electrical conductivity of a material is a measure of the flow of electric current through it for a given applied voltage. It is measured in reciprocal ohms or Siemens per centimeter [12]. The number density of charge carriers **(n)** and their mobility **(μ)** in the material decide the conductivity.

$$\sigma = n\mu e \quad \text{----------} \quad (1)$$

where 'e' is the charge of the electron. For semiconductors and electrolyte solutions, an additional term due to holes has to be added to the above equation. For metals, conductivity increases as temperature decreases while for semiconductors and insulators it decreases with decreasing temperature. Electrical conductivity is an anisotropic property i.e.it depends on direction [7].

The electronic configuration of conjugated polymers is different from ordinary polymers. Broad valence and conduction bands are developed by the extended overlap of π orbitals in conducting polymers. The valence and the conduction bands can be classified as π and π* orbital bands. There is one unpaired π electron per carbon atom in a CP. The carbon orbitals are sp^2p_z hybridized in π orbitals and there is overlapping of orbitals of successive carbon atoms. This leads to delocalization of electrons along the backbone of the polymer which is the path for charge mobilization. Chain symmetry, which is determined by the number and kind of atoms in the repeating unit, decides the electronic structure and hence the conducting properties of the CPs. In conducting polymers, π and π* orbitals are generally termed highest occupied

molecular orbital (HOMO) and lowest unoccupied molecular orbital (LUMO) respectively. The electrically conducting polymers have been aptly called as the "fourth generation of polymeric materials" by Professor BengtRånby in his lecture at the Nobel Symposium (NS-81) in 1991 [13].

In the doped polymer systems, the introduction of charges leads to a relaxation or structural distortion of the polymer about the charge. Due to this distortion energy E_d, localized electronic states are formed in the forbidden gap [14].The ionization energy in this case is less than that required to remove an electron from the HOMO level by a small amount (E_{pol}). If this energy is greater than the distortion energy, a polaron is formed. Polaron is defined as a radical cation (an unpaired electron) that is locally associated with a structural distortion in the CP. In other words, polaron is a charge in the extended lattice that is stabilized by local distortion of the lattice [14].

Usually when an electron is removed, a distortion in the structure occurs locally which tends to stabilize the charge associated with the removal of electron. When this happens in an extended lattice as in the case of a CP chain, it is through a strong electron-phonon coupling and the polaron is said to have a binding energy given by E_{pol}-E_d. No conductivity results from polaron formation as the conduction band is empty and the valence band is full. The forbidden gap now accommodates a new and half occupied electronic level that is localized. The removal of a second electron happens via the formation of another polaron at a different location in the CP chain and there are now two polarons. It is also possible that the second electron can be removed from the polaron itself resulting in the formation of a bipolaron. To decide which process is favourable one has to see the lattice

distortion produced in both the cases. It is inferred from theoretical and experimental studies that the distortion energy E_d required to generate polaronic and bipolaronic distortions are the same. The bipolaron in these systems is more stable than two polarons. There is a Coulombic repulsion between the two positive charges that form the polaron but is stable due to electron-phonon coupling. Electron removal is also possible by doping with a counter ion. It is also possible to have the production of negatively charged polarons and bipolarons by n-type doping of the CPs. Neutral polarons and bipolarons are hypothetical structures that are thought to be the structural distortions before the removal of electrons. In the case of p-type doping, the bipolaron levels are empty andare fully occupied in n-type doping and hence spinless. Though there is liberal use of band theory and other concepts from semiconductor physics, for CPs, a different theoretical model is needed. ESR experiments carried out with highly doped CPs with high intrinsic conductivity are found to give no evidence for the presence of unpaired electrons. In these experiments, rather spinless charge carriers have been identified [15, 16].

The normal aromatic structure of a CP is interrupted significantly in the region where polarons/ bipolarons are present. In many cases, the benzenoid type structure is replaced by a quinoid structure in that region. The polarons and bipolarons are mobile and can propagate along the chain of the CP. They act as charge carriers at suitable levels of concentration. From the CP structures and the idea of mobility, the two charges in the bipolaron are delocalized over several monomer units (6-8) and not over the entire lattice [17].

1.3 A brief introduction to Polyaniline

One of the most important and explored ICPs is polyaniline. Polyaniline (PANI) can be synthesized by very simple chemical and electrochemical routes from aniline or, its ring- or N-substituted derivatives [18]. Polyanilines can exist in different forms and oxidation states as shown in figures 1.2(a) to 1.2(d) [19, 20]

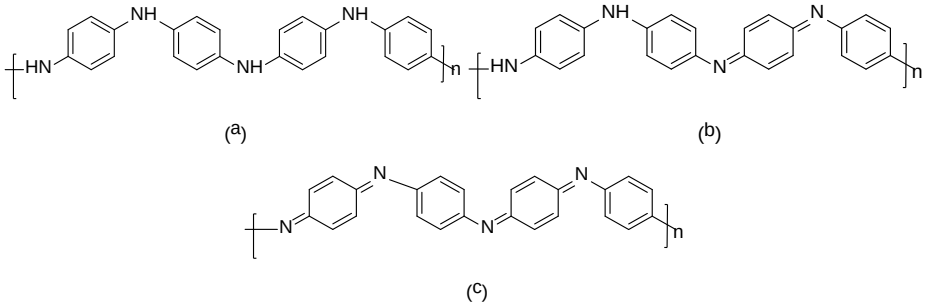

Figure 1.2: Different oxidation states of PANI (a)Leucoemeraldine base (LEB – fully reduced) (b) Emeraldine base (EB - partially oxidised) and (c) Perigraniline base (PNB – fully oxidised)

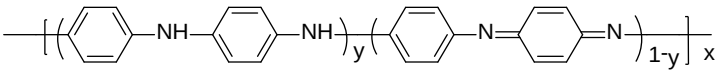

Figure 1.2: (d): Base form of polyaniline – General structure with reduced and oxidised repeat units

Some forms of PANI can be 'doped', chemically or electrochemically to produce highly conducting PANI powders and films with a substantial increase in electrical conductivity of the order of 10^{10} to 10^{12} [18, 21]. Protonation of the EB form gives the conductive form of PANI called the Emeraldine salt (ES) as given in figure 1.3. Only the imine nitrogen atoms in the polymer backbone can be protonated in whole or in part to get the corresponding salts. A delocalised poly-semiquinone radical cation forms

as a result of the complete protonation of imine nitrogen atoms in the Emeraldine base form of PANI. The degree of protonation depends on the EB oxidation state and the pH value of the aqueous acid medium in which the polymerization is carried out. De-protonation of the ES form leads to the formation of EB form of PANI [18, 19, 20].

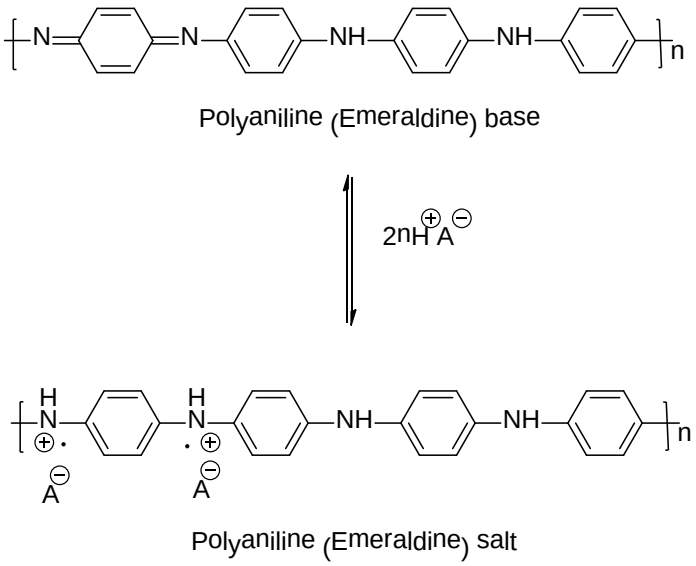

Figure 1.3: Scheme of proton doping in PANI

Doping is the central and unique concept that distinguishes intrinsically conducting polymers from other polymers. Doping an insulating or a semi-conducting polymer results in a significant increase in its electrical conductivity which can go up to the metallic regime. It is a reversible process by which the original properties can be reverted without any or little change in the polymer backbone. By properly varying the doping rate, polymers ranging from insulating to highly conducting can be synthesized. Conducting polymers were initially doped by redox methods until the discovery of protonic acid doping. A

redox reaction involves the partial addition (reduction) or partial removal (oxidation) of electrons from the π system of the polymer backbone. In this method, the number of electrons associated with the polymer backbone changes. But in protonic acid doping, the number of electrons associated with the polymer backbone remains unchanged. Leucoemeraldine base (non-conjugated backbone) form of polyaniline can be transformed to conjugated structure by p-doping and the EB form of PANI becomes conjugated by protonic acid doping [14, 18, 22]. EB form of PANI was the first among the conducting polymers which was made conducting via protonic acid doping (non-redox method). This has increased the conductivity of EB form of PANI by about 10 orders of magnitude [1, 21].

In a typical oxidative polymerization of aniline, the first formed product is the perigraniline form of polyaniline. The polymerization is slower initially, but once the oligomers are formed, it becomes very fast. Perigraniline is a sufficiently strong oxidizing agent which oxidatively polymerizes the excess aniline in the reaction medium to Emeraldine state. This is because perigraniline form has an oxidation potential greater than that required to polymerize aniline. Perigranilinegets reduced by itself to form the Emeraldine form of polyaniline. Hence, the Emeraldine form of PANI is formed as a result of (a) self-reduction of the perigraniline form and (b) oxidative polymerization of aniline by the perigraniline form [22, 23].

A large number of synthesis routes and types of dopants have been identified for producing polyaniline, its derivatives and composites. The charge transport properties of these polymers and their composites have been studied extensively [14]. Based on the promising properties of

polyaniline and its composites, their potential have been identified for a variety of applications including the design of conductive coatings [24], sensors [21, 25, 26], electrostatic charge dissipation systems [27], electromagnetic shielding devices [28, 29], supercapacitors [30], organic photovoltaic devices [31], organic and polymer light emitting diodes [32] and rechargeable batteries [33].

The volume of scientific work related to polyaniline is ever increasing irrespective of the enormous number of papers published till date, owing to its very special tunable features. More than 61,800 articles have been published and 20,000 patents filed worldwide, related to polyaniline, till date. The basic science underlying the structure and polymerization mechanism in polyanilines has been well-explored. Pure PANI forms with the same oxidation states have been reproduced and a large number of application fields for this polymer have been identified [10]. The richness in the physics and chemistry of polyanilines which allows the suitable modifications of the optical, electrochemical, magnetic and structural properties is extremely fascinating and attracts the curiosity of global researchers. There is still ample scope for further research on the fundamental aspects of polyaniline and on identifying novel applications.

1.4 Light Emitting Polymers (LEP)

Conjugated polymers represent a distinctive class of semiconductors that combine the optical and the electronic properties of inorganic semiconductors with the processing advantages and mechanical properties of polymers. Of these, light emitting polymers play an important role in

designing many optoelectronic devices like the polymer light emitting diodes [34, 35], polymer photovoltaic cells [36], sensors [37] and lasers [38]. For a conjugated polymer to be light emitting, it should exhibit fluorescence as well as conduct electricity. An electroluminescent polymer is the one which emits light when an electric field is applied to it. A giant leap in the field of electroluminescent polymers began with the discovery of Sir Richard Friend and his co-workers [35] in which they demonstrated green-yellow coloured electroluminescence in a single-layer device with poly (p-phenylenevinylene) (PPV) as the emissive layer, ITO as the anode and aluminium as the cathode. This discovery in 1990 has given rise to a remarkable growth of interest in polymer LEDs. Since then, there has been extensive research in this field and numerous light emitting polymers have been synthesized and devices fabricated. Poor solubility, photo-stability and thermal stability, and low luminescence intensity of these polymers were some of the challenges faced by the researchers. To resolve these issues, many novel polymers, copolymers and their blends were designed and devices fabricated with light emission over the whole visible spectrum with excellent emission intensity and efficiency [39]. The light emission from these polymers and copolymers was suitably tuned by modifying the band gap through selective attachments of functional groups in the backbone. Chemical structures of a few commercially available light emitting polymers and copolymers are shown in figures 1.4(a) to 1.4(g).

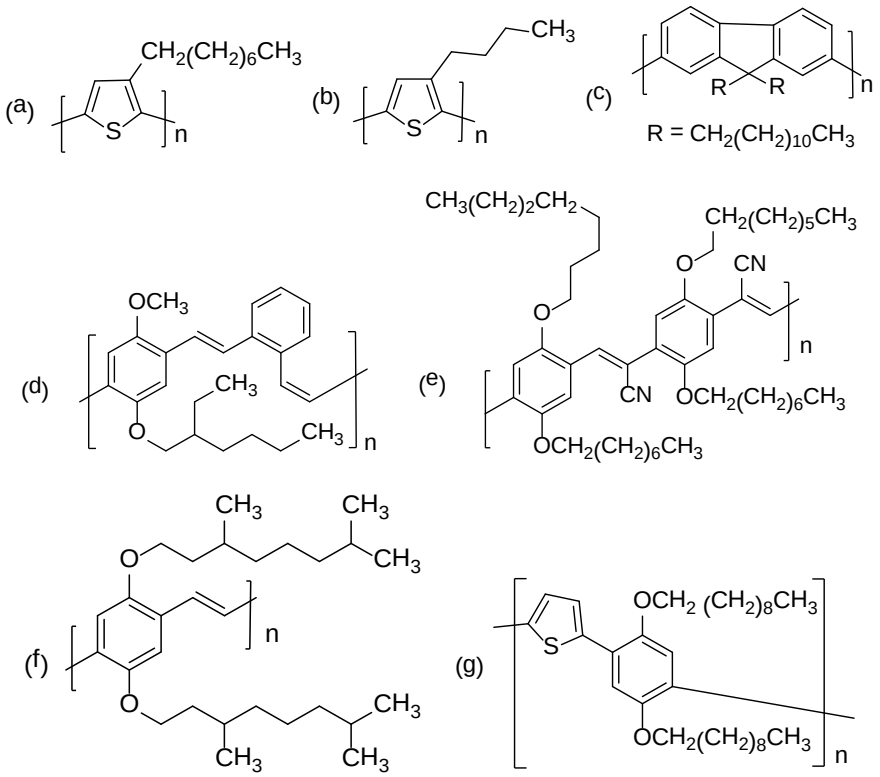

Figure 1.4: (a) Regioregular Poly(3-octylthiophene-2,5-diyl), (b) regioregular Poly(3-butylthiophene-2,5-diyl),(c) Poly(9,9-di-n-dodecylfluorenyl-2,7-diyl), (d) Poly[(o-phenylenevinylene)-alt-(2-methoxy-5-(2-ethylhexyloxy)-p-phenylenevinylene)], (e) Poly(2,5-di(octyloxy)cyanoterephthalylidene), (f) Poly[2,5-bis(3′,7′-dimethyloctyloxy)-1,4-phenylenevinylene] and (g) Poly[(2,5-didecyloxy-1,4-phenylene)-alt-(2,5-thienylene)]

1.5 Polymer Light Emitting Diodes

Electroluminescence (EL) in organic materials was first demonstrated by Bernanose and co-workers at Universite de Nancy, France in 1953. The pioneering discovery of conducting polymers by Heeger, MacDiarmid, and Shirakawa in 1977 opened the vista of a new field of polymer semiconductors for which they were awarded the Nobel Prize in Chemistry for the year 2000. Electroluminescence from polymer films was first observed by Roger Partridge in the year 1983 at the National

Physical Laboratory in the United Kingdom. The device consisted of a film of poly (N-vinylcarbazole) up to 2.2 micrometres thick located between two charge injecting electrodes. Ching W. Tang and Steven Van Slykefirst introduced the efficient organic light-emitting devices (OLED) in 1987 [40]. This device had a novel multi-layer structure with separate hole transporting and electron transporting layers so that recombination and light emission occurred in the middle of the organic emissive layer. The introduction of the multi-layer structures resulted in considerable reduction of device operating voltages and improvements in efficiency which accelerated the current OLED research and device production. Organic small molecules based light emitting devices (OLEDs) have been commercialized by lots of companies like Kodak, Sony, Philips, Nokia, Samsung and OSRAM Opto-semiconductors [39]. Research into polymer electroluminescence gained its strength when J. H. Burrougheset et al, at the Cavendish Laboratory in Cambridge demonstrated a highly efficient green light-emitting polymer based device using 100 nm thick films of poly (p-phenylenevinylene) in the year 1990. This initiated a world-wide search for new light emitting polymers and device architectures with improved efficiency and life-time. Since 1990, PLED technology is probably one of the most important applications in organic electronics, which has accelerated the researchers to search for new light emitting polymers and copolymers, in spite of the unprecedented advancements in polymer photovoltaics and polymer based microelectronics [39, 41, 42].

Polymer light emitting device technology is an easy-to-use approach with numerous advantages. Light weight and thin displays with

very high brightness and contrast can be realized for portable applications. These high-resolution displays can be viewed from very wide angles. All colours can be achieved with the same polymer backbone by suitably engineering the chemical structure and a wide range of red, blue and green emitting polymers are commercially available. The devices having any shape and non-planar displays operating at very low voltages can be fabricated. The response time of polymer displays is very short which is of the order of 10 to 10^2 ns compared to that of liquid crystal displays which is around 10ms. Polymer based displays do not require any back-lighting like the liquid crystal displays. Polymers can be solution processed, spin-coated or ink-jet printed on transparent, plastic substrates to fabricate flexible displays. Although, PLEDs possess these advantages over other technologies, the life-time, environmental stability and efficiency of PLEDs have to be improved further for wide-spread commercial applications [39, 41].

The simplest polymer light emitting diode consists of an emissive layer (a film of light emitting polymer) of about 100nm sandwiched between two electrodes, the anode and the cathode (figure 1.5). The anode is an optically transparent material of high work function, usually, indium tin oxide (ITO) and the cathode is a highly reflecting metal of low work function like calcium, magnesium or aluminium. When a forward bias greater than the difference between anode and cathode work functions is applied to the device, electrons from the cathode and holes from the anode are injected into the LUMO (π^*) and the HOMO (π) energy levels of the emissive layer respectively. The injected positive and negative charge carriers (positive and negative polarons) form bound

polaron-excitons and the radiative decay of these excitons results in electroluminescence [42].

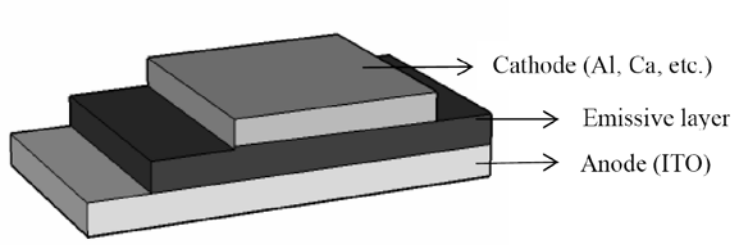

Figure 1.5: Structure of a single layer PLED

There are a number of factors that determine the efficiency of PLEDs. The mismatch of electrode work functions with the HOMO-LUMO levels of the light emitting polymer is one of the prime factors affecting the emission intensity and efficiency. Effective charge injection can occur only when the anode and the cathode work functions are comparable to the HOMO and the LUMO energy levels of the emissive polymer respectively. The injected charge carriers can form either singlet or triplet excitons according to spin statistics. In electroluminescence, only the singlet excitons can decay radiatively. In most of the light emitting polymers, the hole mobility is greater than the electron mobility which results in the formation of excitons near the cathode and hence a non-radiative decay can occur due to image force interactions. To overcome this problem, a hole injection and transport layer (HITL), usually, Poly (3,4-ethylenedioxythiophene) poly (styrenesulfonate) (PEDOT:PSS) or PANI, is used in between the anode and the emissive layer. The likelihood of recombination within the light emitting polymer can be increased by suitably choosing the HITL, where the holes are blocked and localized within the active layer of the device (LEP).The HITL decreases the

barrier height and enhances the hole injection. It also reduces the leakage current and planarizes the rough and spiked ITO surface to avoid any chances of shorting [39, 41, 42].

The schematic diagram of a polymer LED with ITO/PANI/emissive layer/cathode architecture is illustrated in figure 1.6 and the energy band diagrams of single layer and two-layer PLEDs in the forward bias [42] are shown in figures 1.7(a) and 1.7 (b) respectively.

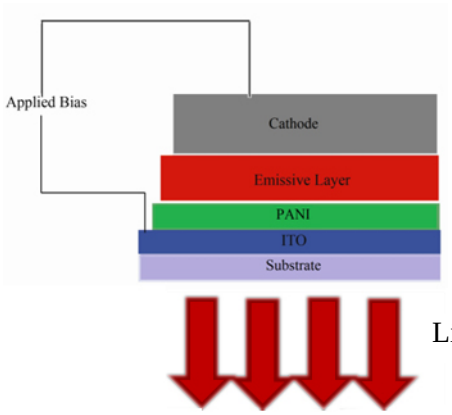

Figure 1.6: Illustration of a two-layer PLED structure under forward bias

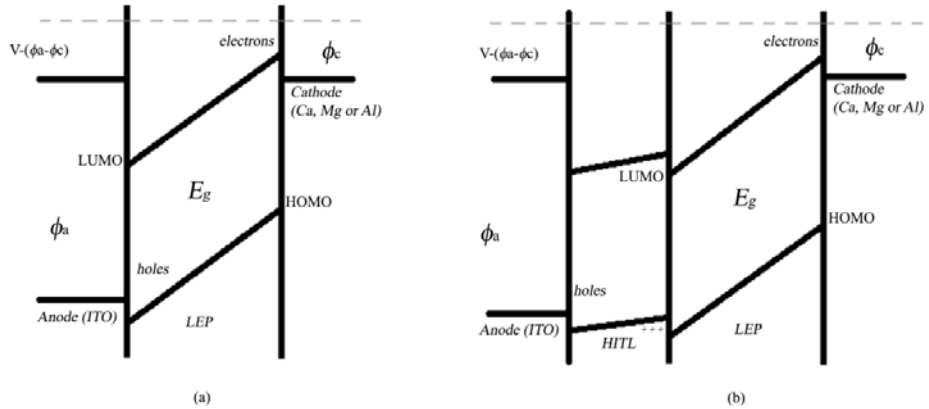

Figure1.7: Energy band diagram of a (a) single layer device and (b) double layer device under forward bias of 'V' volts where 'E_g'- the energy band gap of LEP, ϕ_a- anode work function and ϕ_c- cathode work function

1.6 Objectives of the present work

The interesting tunable characteristics of polyaniline have made it one of the most popular and extensively studied conducting polymers. Polyaniline (PANI) can be synthesized through many simple chemical and electrochemical routes, and in different forms and morphologies. Composites of polyaniline can be synthesized from a variety of conducting and non-conducting fillers. Although a lot of research work has been conducted in PANI, there are certain areas where the properties of this polymer has not been fully utilized or studied extensively. The sensitive dependence of electrical conductivity on applied pressure is one such property that can be used for realizing low cost and good quality pressure sensors.

The optical and electrical properties of PANI have been effectively controlled by doping and side chain attachments. There are established routes to synthesize PANI in insulating, semiconducting and highly conducting forms. Quantum confinement effect is well known in inorganic semiconductors where the bulk properties can be tuned to any desired levels by suitably reducing the dimensions to the nanometre regime. The possibility of quantum confinement of charge carriers has not been pursued in detail in any form of PANI.

The electrical conductivity of polyaniline that can be enhanced through doping process has reached the saturation limits. Further enhancement in conductivity can be achieved only by improving the crystallinity or order within and among the PANI chains. The reported extent of crystallinity in conducting PANI is found to be very low.

Light emitting polymers belong to a class of conjugated polymers, subjected to extensive investigations during the past few decades. There have been numerous studies conducted worldwide in search of new, efficient and stable, conjugated light emitting polymers, since 1990, for applications in polymer light emitting diodes, polymer photovoltaic devices, sensors and actuators. The problems associated with low photo-stability, molecular aggregation effects and short life-time of these polymers have prevented the widespread commercialization of the polymer based devices, although these devices have many other advantages. Newer polymers and copolymers with improved stability and life-time are being synthesized and device architectures modified, by scientists all over the world to overcome these issues.

Taking into consideration, all these aspects, the objectives of the present work can be summarized as follows:

1) To synthesize polyaniline (PANI) and its composites using different routes and various dopants to suit specific applications
2) To investigate the prospects of using PANI and PANI composites as candidates for pressure sensing applications
3) To carry out detailed investigations on quantum confinement effects in ultrathin films of polyaniline
4) To synthesize and characterize polyaniline films with much enhanced crystallinity and order within polymer chains
5) To fabricate polymer light emitting diodes based on a few novel semiconducting polymers (hybrid and segmented block copolymers) having excellent emission characteristics and thermal stability

References

[1] Goppelsroeder, F. *Die International ElektrochemischeAusstellung* **18,** 978;**19,**1047 (1891)

[2] Little, W.A., *Phys.Rev.*,**135**, A1416 (1964)

[3] Greene, R.Street, G.B., and Süter, L.J., *Phys. Rev. Lett.*, **34**, 577 (1975)

[4] A.G. MacDiarmid and A.J.Heeger, *Synth. Met.*,1,**101** (1979/80)

[5] T.A.Skotheim,(ed.), *Handbook of conducting polymers*, 1&2 , Marcel Dekker, NewYork (1986)

[6] M.G.Kanatzidis, *Chemical &Engineering News*, **3**December,36 (1990)

[7] Conductive polymers, The Nobel Prize in Chemistry, (2000)Kungl. Vetenskapsakademien, The Royal Swedish Academy of Sciences

[8] Chiang, C.K., Fincher, C.R.Jr., Park, Y.W., Heeger, A.J.Shirakawa, H., Louis, E.J., Gau, S.C., and MacDiarmid, A.G.,*Phys.Rev.Lett.*,**39**,1098 (1977)

[9] Ito,T., Shirakawa,H., andIkeda,S., *J.Polym.Sci.,Polym.Chem.Ed.*,**12,**1 (1974)

[10] Prasanna Chandrasekhar, *Conducting Polymers, Fundamentals and Applications: A practical approach*, Kluwer Academic Publishers, London (1999) pp1-22, 383-386

[11] [11] K.E.Ziemelis, A.T.Hussain, D.D.C.Bradley, R.H. Friend, J.Rilhe and G.Wegner, *Phys.Rev.Lett.*,**66**,2231 (1991)

[12] [12] Menke,K. and Roth,S. *Chemie in unsererZeit*, **20,** 33 (1986); Pekker S., and Janossy,a.(1986).*Handbook of conducting polymers* (Skotheim, T.A., ed.), Marcel Dekker, New York , pp45

[13] Alan J.Heeger, Semi conducting and Metallic Polymers: The Fourth Generation of Polymeric Materials, *The Journal of Physical Chemistry B*, **105**, Sept 13, (2001)

[14] Prasanna Chandrasekhar, *Conducting Polymers: Fundamentals and Applications*, Kluwer Academic Publishers, London (1999) pp 16-21, 25-30, 101-124

[15] Diaz, A.F.,Kanazawa, K.K., Gardini, G.P., *J.Chem Soc. Chem. Commun.*,635-636(1979)

[16] Scott, J.C., Pfluger, P., Krounbi, M.T.,Street, G.B.,*PhysRev.B*, **28**, 2140 (1983)

[17] Herbert Naarmann, *Handbook of polymer synthesis* (II edition), chapter 12-conducting polymers

[18] Alan G.MacDiarmid and Arthur J. Epstein, *Faraday Discuss. Chem. Soc*., **88**, 317-332 (1989)

[19] Meixiang Wan, Conducting Polymers with Micro or Nanometer Structure, Tsinghua University Press, Springer, New York (2008), pp16-38

[20] Donald L Wise et al, *Electrical and Optical Polymer Systems*, Marcel Dekker, Inc., New York, (1998), pp366-370

[21] S. J. Varma, S. Jayalekshmi, *J. Appl. Polym. Sci.*, **117**, 138–142 (2010)

[22] Hari Singh Nalwa, *Handbook of Organic Conducting Molecules and Polymers: Vol. 2*, John Wiley & Sons, New York (1997), pp 505-566

[23] Tereje A. Skotheim and John R.Reynolds, *Conjugated Polymers: theory, Synthesis, Properties and Characterization*, CRC Press, Taylor & Francis Group, New York (2006), pp 7.1 – 7.40

[24] E.PeterMaziarz et al, *J. Am. Soc. Mass. Spectrom.*, **11,** 659–663 (2000)

[25] S.K. Dhawan et al, *Sens. Actuators, B,* **40**, 99-103 (1997)

[26] DipakDutta et al, *J. Colloid Interface Sci.*, **283**, 153-159 (2005)

[27] ParveenSaini et al, *Polym. Adv. Technol.,* **23,** 343–349 (2012)

[28] S.K Dhawan, N Singh and S Venkatachalam, *Synth. Met.*, **125,** *389-393* (2001)

[29] S Koul, R Chandra and S.K Dhawan, *Polymer*, **41**, 9305-9310 (2000)

[30] Kwang Sun Ryu et al, *J. Power Sources*, **103**, 305-309 (2002)

[31] Shibu Zhu et al, *J. Solid State Chem.*, **190**, 174-179 (2012)

[32] HabibaBejbouj et al, *Mater. Sci. Eng., B,* **166,** 185-189 (2010)

[33] Masayuki Morita et al, *J. Power Sources*, **54**, 214-217 (1995)

[34] Mark T.Bernius et al, *Adv. Mater.*, **12**, 1737-1750 (2000)

[35] J.Burroughes et al, *Nature*, **347,** 539- 541(1990)

[36] F.C.Crebs, Polymeric Solar Cells: Materials, Design, Manufacture, DEStech Publications, (2010), pp 20-41

[37] Y.Chuo et al, *IEEE Sensors*,155 - 159 (2010)

[38] MohamadSalehAlSalhi et al, *Int. J. Mol. Sci.*,**12**, 2036-2054 (2011)

[39] Zhigang Li and Hong Meng, *Organic Light Emitting Materials and Devices*, Taylor & Francis Group, USA (2007), pp 45-294

[40] Tang and VanSlyke, *Appl. Phys. Lett.*, **51**, 913–915 (1987)

[41] Joseph Shinar, *Organic Light Emitting Devices: A Survey*, AIP Press, Springer, New York (2004), pp 1-34

[42] Gregory P. Crawford, *Flexible Flat panel Displays*, John Wiley & Sons Ltd., UK (2005), pp 219-477

…..ൟ…..

Chapter 2

RELEVANT EXPERIMENTAL TECHNIQUES

Contents

This chapter begins with a brief account of the methods adopted to synthesize polyaniline samples with interesting structural, electrical and optical properties, and evolves into the discussion on the effects of various parameters of synthesis on the significant structural, electrical and optical characteristics. It is followed by a brief explanation of the theoretical aspects of various experimental tools used in the present work including Fourier Transform Infrared Spectroscopy (FTIR), UV-Vis-NIR spectroscopy, Photoluminescence (PL) Spectroscopy, Raman spectroscopy, X -ray diffraction (XRD), Thermo-gravimetric Analysis (TGA), Scanning Electron Microscopy (SEM and Atomic Force Microscopy (AFM). A detailed account of the processes involved in the assembling of single and multi-layer polymer light emitting diodes is also addressed in this chapter.

2.1 Synthesis of polyaniline (PANI) via chemical methods

Conducting polymers, especially polyaniline, can be synthesized through numerous chemical and electrochemical routes [1, 2, 3, 4, 5]. In the present work, the synthesis of polyaniline has been carried out via two chemical routes, the chemical oxidative polymerization and

dispersion polymerization. The variations in the reaction parameters like the reaction temperature, type and concentration of the dopants, rate of addition of the oxidant, etc. are found to yield polyaniline samples with different optical, electrical and structural characteristics.

2.1.1 Chemical Oxidative Polymerization

This typical "in-a-beaker" type of synthesis of polyaniline involves the use of a chemical oxidant and an acid medium. Oxidant generates a radical cation from the aniline monomer which initiates the polymerization [1]. In a typical synthesis, aniline monomer is mixed with an acid and the oxidant is added to this solution while stirring. The mixture is stirred for several hours, washed with de-ionised water and filtered to obtain polyaniline. The green coloured polyaniline thus obtained is dried at 50^{o}C in dynamic vacuum and ground to fine powder [2, 3, 4, 6]. This is one of the simplest chemical methods to synthesize conducting polyaniline. A typical chemical oxidative polymerization is illustrated in figure 2.1.

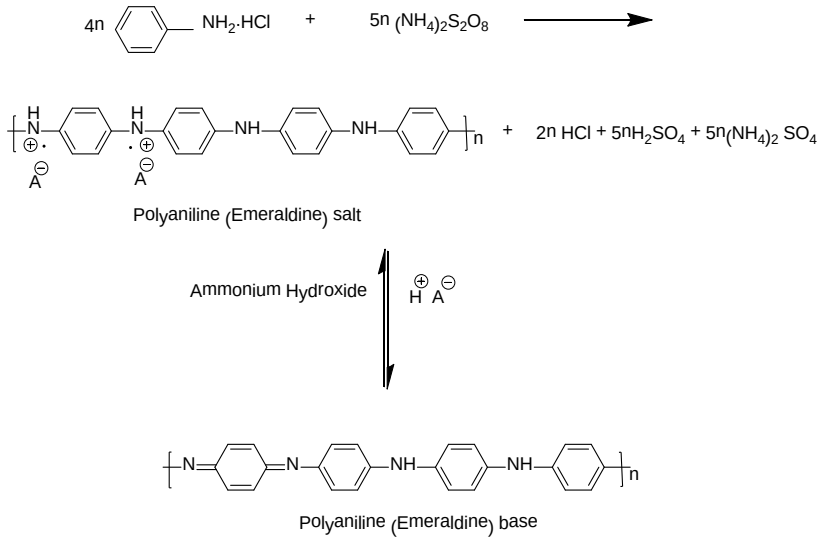

Figure 2.1: Illustration of chemical oxidative polymerization

2.1.2 Dispersion polymerisation

Dispersion polymerization is the best chemical method to synthesize non-oriented, air-stable and highly conducting, polyaniline films. The process involves the production of an insoluble polymer in the form of a stable colloidal dispersion from a monomer dissolved in an organic liquid or water, the stability being provided by an interfacial stabilizer [7, 8]. In a typical synthesis, an aqueous acidic solution of aniline and chloroform in the ratio 2:1 (vol./vol.) is stirred to form a turbid colloidal solution. The monomer, anilium hydrochloride, which is relatively insoluble in the aqueous phase when the temperature is lower than ~ -10^0C, because of the presence of the organic, hydrophobic parts, acts as the interfacial stabilizer. The polymerization of the monomer molecules on the surface of the organic solvent is initiated by the drop-wise addition of an aqueous solution of the oxidant, ammonium persulphate to the dispersion, which generates the radicals in the aqueous phase. As the PANI chains grow and the molecular weight becomes sufficiently high, they move towards the interface as a result of the polymer's insolubility in the organic and aqueous phases. The resulting PANI molecules grow together and aggregate to form a three-dimensional honeycomb network. In this method, external stabilizers and metal-salt anti-freeze agents for low temperature polymerization are not required and, less-branched PANI molecules with almost similar molecular weights can be synthesized. Polyaniline with very high molecular weight can also be synthesized using this method [9, 10]. The films of dispersion polymerized PANI are reported to be metallic in nature with electrical conductivity as high as 1300 S/cm [8].

2.1.3 The effects of dopants, oxidant and reaction temperature

Dopants play a significant role in determining the morphology of PANI in various synthesis methods. Polyaniline structures with different morphologies can be obtained by suitably controlling the dopant concentration, the nature of do pants, stirring type and conditions, and other parameters like pH of the reaction medium and reaction temperature. For example, a tubular morphology can be obtained when β-Naphthalene sulphonic acid (β-NSA) is used as the dopant [11]. The diameter of the tubules can be controlled from a few micrometres to nanometres by suitably varying theβ-NSA concentration. The rate of addition of the oxidant also plays an important role in the morphology of polyaniline. Slower addition leads to the formation of micro-structured and long chained polyanilines whereas immediate addition results in nanostructured forms. The electrical conductivity and crystallinity of polyaniline can be significantly improved when the reaction temperature is reduced [11]. The solubility of PANI depends on the type of dopants, the synthesis method and the precursors used. The freshly synthesized PANI sample is always in the acid-doped, Emeraldine salt (ES) form. The acid-doped PANI can be de-doped using ammonia solution to get the de-protonated, Emeraldine base (EB) form. The EB form can be re-doped using suitable dopants such as d-10-camphorsulphonic acid (CSA) to enhance the solubility in conventional organic solvents. In some other synthesis methods, dopants like DEHSSA [12], β-NSA [13] and DBSA [14, 15] are used to enhance the solubility of PANI without undergoing de-protonation and re-doping processes. The Scanning Electron Microscope (SEM) images of a few polyaniline samples synthesized using various routes and dopants are shown in figures 2.2(a) to 2.2(h) and figure 2.3.

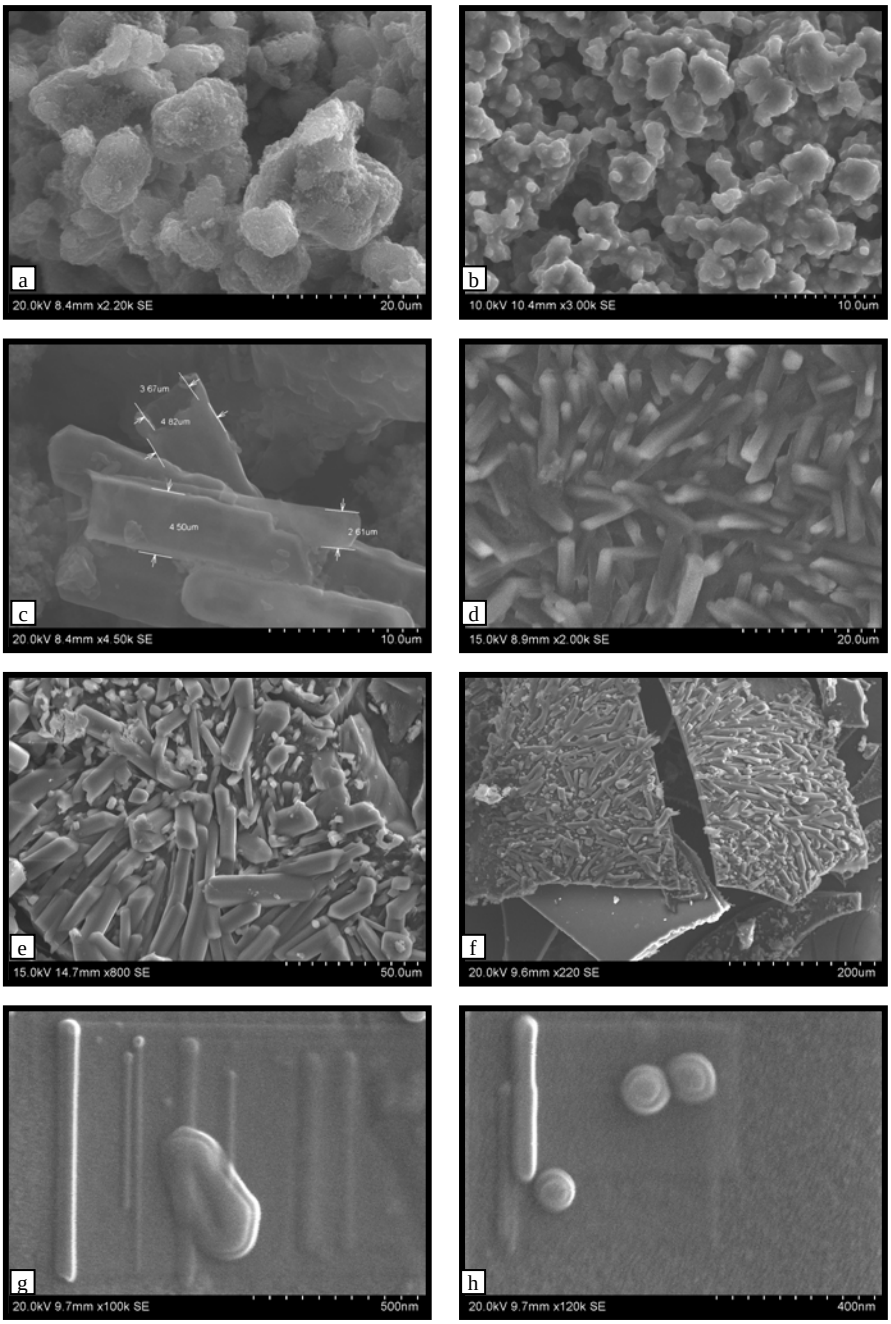

Figure 2.2: Chemical oxidative polymerization: (a) HCl doped (insoluble), (b) CSA re-doped (soluble), (c) NSA doped (partly soluble),(d) HCl doped (by ultrasonication), (e) CSA re-doped (ultrasonicated),

(f) scratched film surface of (e) and (g, h) DBSA doped film surface (ultrasonicated)

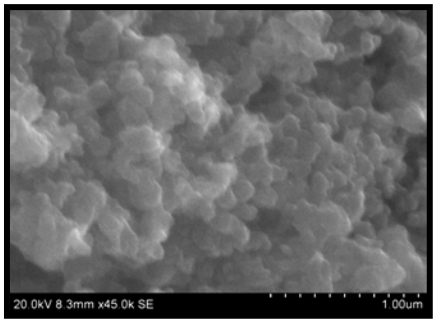

Figure 2.3: Dispersion polymerized PANI (orthophosphoric acid doped)

The chemical structures of polyaniline doped with CSA and the sulphonated (SPAN) forms are shown in figures 2.4 (a) and (b). PANI in the protonated form is insoluble in organic and aqueous solutions. Efforts have been directed towards making PANI soluble in its protonated form, which is a key issue in utilizing PANI as a commercial product in technologically important applications[16]. The solubility of PANI can be improved upon sulphonation by the incorporation of N-alkyl-sulphonic acid pendant groups [16, 17, 18], by micro-emulsion polymerization [19], dopant-induced [20], self-doping polymerization [21] and controlled relative molecular mass [22] methods.

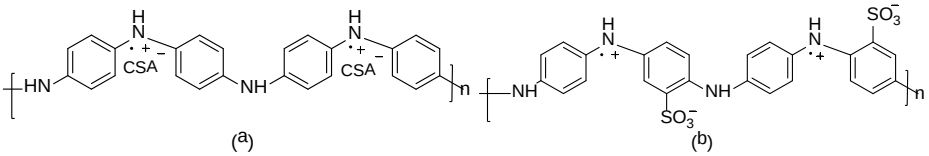

Figure 2.4: Structures of (a) CSA doped PANI (b) SPAN

2.2 Characterization Techniques

In this section, a detailed account of the characterization techniques employed in elucidating the various sample properties is being portrayed.

2.2.1 Fourier Transform Infrared Spectroscopy (FTIR)

Fourier Transform Infrared Spectroscopy is a chemically-specific technique to identify chemical compounds and substituent groups. In this method, infrared radiation is passed through the sample where some of it gets absorbed and some transmitted. The resulting spectrum is a molecular fingerprint of the sample representing the absorption and transmission. This spectrum is unique for that particular sample and no two materials have the same IR spectrum. FTIR can provide the identity of unknown materials, quality of the sample and determine the amount of components in the mixture. The absorption peaks arise due to various frequencies associated with different modes of vibration of the atoms that make up the material. The size of the peaks tells about the amount of material present in the sample. It is a non-destructive method. These factors make FTIR an indispensable characterization tool to investigate the structure and composition of various types of materials.

The main optical part of an FTIR spectrometer is a Michelson interferometer. A parallel beam of radiation from the infrared source, usually a heated element or a glow bar, is directed to the interferometer which has a beam splitter and two mirrors. The beam splitter is a plate of a transparent material such as KBr, coated usually, with germanium in such-a-way that 50% of the incident radiation is reflected and the remaining transmitted. Thus, half of the radiation goes to the first mirror which is fixed and the other half to the movable mirror. The reflected

radiation parts return from both these mirrors along the same path and recombine to a single beam at the beam splitter. This can result in constructive or destructive interference depending on the relative path-lengths from the beam splitter to the mirrors. The so-obtained interferogram contains data points which bear the information of all the infrared frequencies emanated from the source. All frequencies can be measured simultaneously by detecting the interferogram which in turn makes extremely fast measurements. The beam is then directed to the sample where it is transmitted through or reflected off the surface of the sample, depending on the type of analysis performed. Specific frequencies characteristic of the sample are absorbed. The beam finally passes through the specially-designed detector to measure the interferogram. The digitised signal is sent to the computer for Fourier transform and is finally presented to the user as the FTIR spectrum of the sample. Initially, the background spectrum is charted without any sample inside. The Fourier transform interferogram is then compared with the background spectrum for plotting the transmittance spectrum [23].Schematic diagram of the FTIR spectrophotometer is shown in figure 2.5.

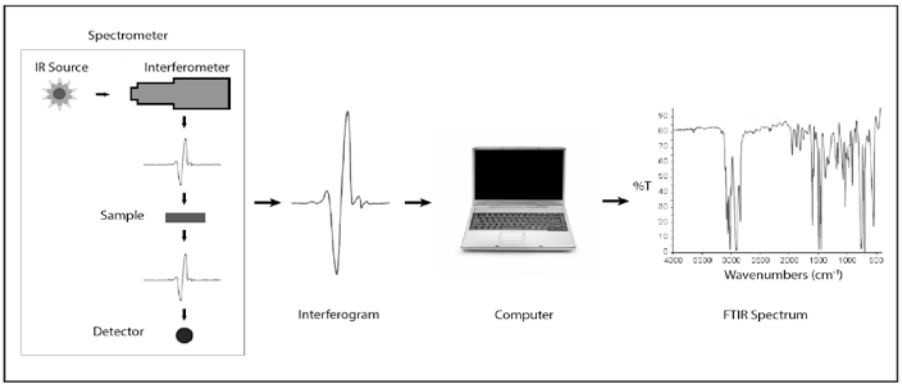

Figure 2.5: Schematic diagram of FTIR spectrophotometer

The FTIR spectra of the samples investigated in the present work are recorded using Bruker Tensor 27 (Germany) and Thermo Nicolet, Avatar 370(USA) spectrometers.

2.2.2 UV-Vis-NIR Spectroscopy

Ultraviolet–visible spectroscopy or ultraviolet-visible spectrophotometry (UV-Vis) denotes the absorption or reflectance spectroscopy in the ultraviolet-visible spectral region which also comprises the near infra-red region (NIR). The nature of chemical groups present in the sample determines the absorption of light in this region. Each filled-molecular orbital in the ground state of a polymer molecule contains two electrons of equal and opposite spin. When a radiation of energy in the UV-VIS region falls on the sample, one of the electrons in the highest-occupied molecular orbital (HOMO) is excited to the lowest-unfilled molecular orbital (LUMO). There can be various possible transitions which are σ-σ^*, n-σ^*, π-π^* and n-π^* depending on the sample under consideration. By analyzing the UV-VIS absorption spectra of materials, it is possible to estimate the absorption coefficient α, direct and indirect band-gap energies and the density of states. The effect of doping on the electronic structure of the materials can also be understood from the UV-Vis absorption spectrum [24, 25]. Schematic diagram of the UV-Vis spectrometer is shown in figure 2.6.

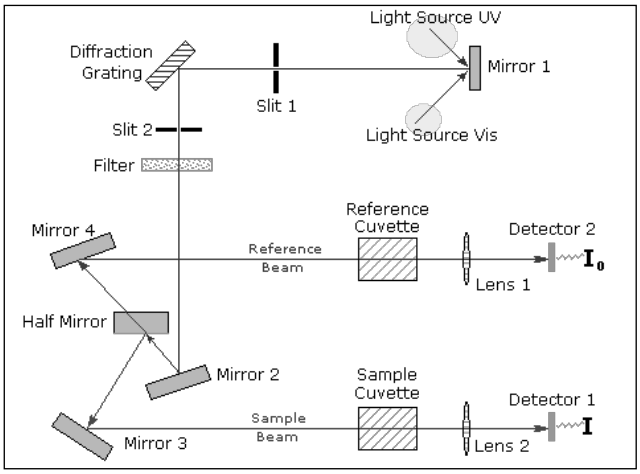

Figure 2.6: Schematic diagram of the UV-Vis spectrometer

In the present study, Jasco V 570 UV-VIS-NIR spectrometer has been used for analyzing the polymer samples. It consists of a deuterium lamp (190-350nm) and a halogen lamp (330-2500nm), and uses a single monochromator. It also has two detectors, one of which is the photomultiplier tube and the other, the lead sulphide (PbS) photoconduction cell. The spectrometer has a resolution of 0.1nm in the UV-VIS region and 0.5nm in the NIR region.

2.2.3 Photoluminescence Spectroscopy (PL)

In the process of photoluminescence (PL), a fraction of the absorbed light energy is emitted by the material in the visible or near-visible region. The excitation source can be IR, visible, UV or X-rays. Photoluminescence can be categorized into fluorescence and phosphorescence. The main factor that differentiates the two is the life-time of emission. Fluorescence is marked by emission during excitation or within 10^{-8} seconds after excitation, where 10^{-8} seconds is the order of life-time of the atomic state corresponding to the allowed dipole transition in the visible region. In

phosphorescence, the emission is not spontaneous, can take microseconds or even hours after the removal of the excitation source [26, 27]. Excitons are responsible for PL emission in polymers. An exciton is a stable, bound electron-hole pair state. In a polymer, an exciton is formed when an electron in the LUMO level combines with a hole in the HOMO level. The singlet excitons, de-localized over the polymer chain, are responsible for PL in conjugated polymers. Emission of light occurs when a singlet exciton decays radiatively to the ground state [28]. In the absence of any emission, the excitation energy is converted into rotational or vibrational motion within the polymer through non-radiative decay processes. The difference between the absorption and emission maxima of the spectrum is called the Stoke's shift which occurs when the emission from the lowest vibrational excited state relaxes to various vibrational levels of ground state.

In the present work, the PL measurements have been carried out using Jobin Yvon Fluorolog 3 spectrofluorimeter (Model: FL3-22) which has a 450W xenon lamp as source, PMT detector (Model: R928P) and a T-box type sample compartment module.

2.2.4 Raman Spectroscopy

Raman spectroscopy is based on Raman effect which is related to the scattering of light when a monochromatic radiation passes through a transparent substance. Sir C.V.Raman found that the scattered energy consists of certain other discrete frequencies in addition to the incident frequency (Rayleigh scattering). Raman effect can be explained in terms of quantum theory of radiation. A radiation of frequency 'ν' is treated as a stream of particles or photons of energy 'hν' where h is the Planck's

constant. A perfectly elastic collision of photons with molecules of a substance does not change the energy of the incident beam and the detector receives radiation of frequency 'ν'. If the collision is inelastic, energy is exchanged between the photons and molecules in accordance with the quantum laws. This change in energy corresponds to the change in the vibrational or rotational energy of the molecule. If the photon gains energy, the scattered radiation has a frequency higher (anti-Stoke's) than the incident radiation and if the molecule gains energy, the radiation is scattered with a lower frequency (Stoke's).The resultant lines of modified frequencies are called Raman lines. Stoke's radiation is generally more intense than anti-Stoke's. The energy level diagram depicting Raman scattering is shown in figure 2.7.

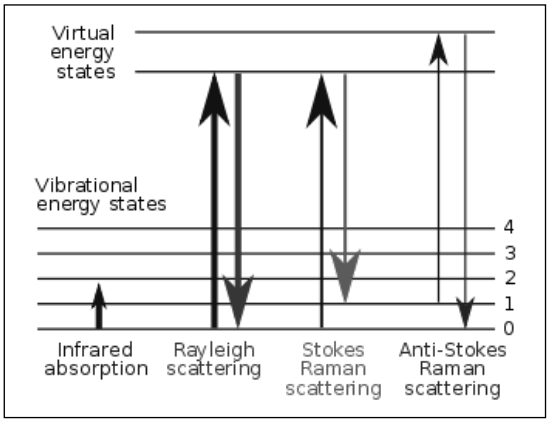

Figure 2.7: Energy level diagram depicting Raman scattering

Most of the Raman lines are strongly polarized. The essential condition for a molecule to exhibit Raman effect is a change in polarizability. Homo-nuclear diatomic molecules like oxygen and hydrogen do not give rise to any infrared or microwave spectra but exhibit rotational Raman lines. Hence, Raman technique gives structural

data unobtainable from other techniques and is thus complementary to infrared and microwave studies. The presence of a centre of symmetry in the molecule, as in hydrogen, oxygen and carbon dioxide, is reflected in the Raman spectrum. For oxygen and carbon dioxide, every alternate rotational level is absent and for hydrogen, the spectral lines are of alternating intensity. It is seen that in molecules with centre of symmetry, Raman active vibrations are IR inactive and vice-versa and in the absence of any centre of symmetry, vibrations may be both Raman and IR active. Raman effect is also called incoherent scattering and is generally considered as the optical analogue of Compton effect.

A Raman spectrometer is an optical device that measures the intensity of the scattered light from the sample relative to its Stoke's shift from the wavelength of the exciting laser radiation. Microscopic areas can be analyzed using a micro-Raman spectrometer configured with lasers of different wavelengths which can be used according to the type of samples used. The micro-Raman spectrometer combines the features of a Raman spectrometer and a microscope which can carry out Raman spectroscopy as well as digital imaging of a sample. The sample is illuminated with a laser of narrow wavelength through the spectrometer objective and the objective of the microscope is used to collect the scattered light from the sample. The laser is focused to form an image at the entrance aperture of the spectrometer. A diffraction grating in the spectrometer separates the scattered radiation from the sample into Stoke's shifted frequencies and these frequencies are focused on to a CCD array detector. Each individual pixel on the array measures the intensity of the frequencies and directs this data on to a computer where it is converted into a Raman spectrum. The

spectrum displays the intensity of the inelestically scattered light in terms of the exciting laser in wavenumbers. Raman spectrum gives a unique spectrum of the material under consideration. Raman data can be used to identify the molecule and its functional groups [23]. The schematic diagram of a micro-Raman spectrometer is shown in figure 2.8.

Jobin Yvon Horibra LABRAM-HR micro-Raman spectrophotometer (Japan) with 488nm argon-ion laser as source has been used for sample analysis in the present studies.

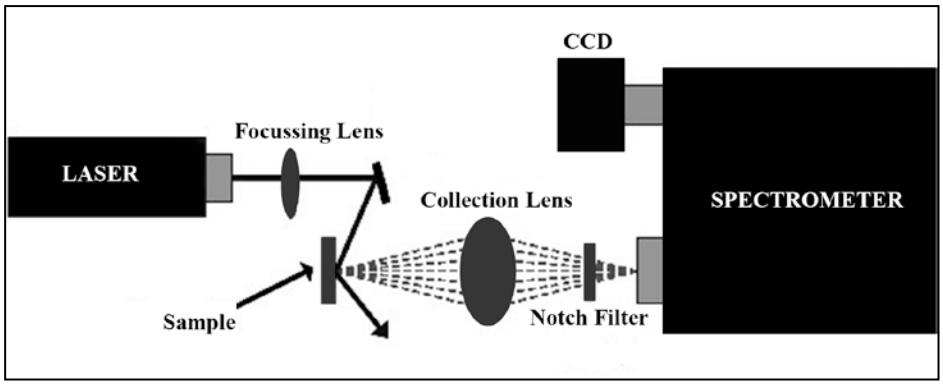

Figure 2.8: Schematic diagram of a micro-Raman spectrometer

2.2.5 X-ray Diffraction (XRD)

X-ray diffraction is one of the major tools in structure determination of various crystalline materials. Materials are broadly classified as crystalline and amorphous depending on whether or not they possess a long range order. Materials behave in different ways when they are exposed to X-rays depending on the presence or absence of long-range order. Crystalline materials show very sharp and well-defined X-ray patterns whereas amorphous or non-crystalline materials show broad and diffuse patterns. X-rays exhibit wave nature like the visible light. When visible light falls on a diffraction grating, which consists of a series of lines separated by a distance comparable to the wavelength of the incident beam, it gets diffracted and shows a series of bands with alternate bright and dark regions. Similarly a crystal lattice, where the molecules are arranged in a regular fashion separated by very small distances comparable to the wavelength of X-rays, acts as a diffraction grating. When X-rays are incident on the crystal lattice, the incident radiation is diffracted to give the pattern which is the fingerprint of the material. Schematic diagram of an X-ray diffraction set-up is shown in figure 2.9.

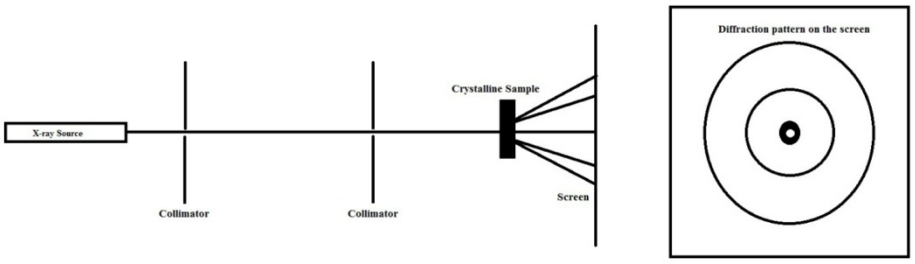

Figure 2.9: Schematic diagram of X-ray diffraction set-up

X-ray diffraction is a very useful non-destructive technique to study the internal structure of polymers, especially the doped, conductive polymers. Most of the polymers diffract X-rays to give diffraction patterns, the majority of which are amorphous in nature, with the exception of a few polymers which give rise to quite crystalline XRD patterns. Polymers are not completely crystalline or ordered and they do not have a perfectly ordered lattice. Since the polymers contain both crystalline and amorphous regions, the X-ray diffraction patterns may contain a mixture of sharp and diffused patterns. The crystallinity of a polymer is expressed in terms of the crystalline or ordered fraction it possesses. The sharp peaks correspond to the ordered regions and the diffused, broader portions correspond to the irregular ones. To some extent, crystallinity has a significant influence on the degradation of the polymer. Degradation happens in amorphous regions easily when compared to the crystalline regions. The ordered regions have a higher density compared to the amorphous regions in polymers. The bulk properties like Young's modulus, hardness, tensile strength, etc. of polymers also depend on the crystalline portions present inside. Thus, X-ray diffraction is a very important tool in analyzing these important properties of polymers [29].

Rigaku X-ray diffractometer (Japan) with Cu-Kα radiation of wavelength, λ = 1.542 Å was used for obtaining the XRD patterns of the powder and film samples in the present study. A tube current of 20mA and an accelerating potential of 30kV was applied to the X-ray tube.

2.2.6 Thermo-gravimetric Analysis (TGA)

Thermo-gravimetric analysis is a technique to analyze the thermal stability of materials. The materials are heated to degradation in a controlled atmosphere and the loss of weight in terms of temperature is recorded. The degradation of different materials varies from one another; some of the materials degrade faster than the others. The purity and composition of a material can be determined using this technique. A derivative weight loss is plotted against temperature to understand the point where the weight loss is most apparent. TGA is one of the most common and important techniques used to analyze the thermal degradation patterns of polymers and estimate the presence of solvent residues and moisture in the material.

The analyzer part of the TGA instrument has a high precision balance with a pan, generally made of platinum, to load the sample. The pan is kept in a furnace where it is heated/cooled during the analysis. The temperature is accurately measured using a thermocouple. The experiment is usually performed in an inert gas atmosphere to prevent other undesired reactions or oxidation of the sample [30].

The thermal stability of samples in the present study was determined using Q-50, TA Instruments (USA) Thermo Gravimetric Analyzer, under nitrogen atmosphere at a heating rate of 10^0C/min.

2.2.7 Scanning Electron Microscopy (SEM/FESEM)

Scanning electron microscopy is a technique used to get the magnified image of a sample using an electron beam. There are three principal electron microscopes, namely, the scanning, transmission and emission. The electron beam directed on to the sample produces an image, in the scanning and tunneling microscopes. The specimen itself is the source in the case of a field-emission microscope. An electron microscope has many advantages over an optical microscope. In an electron microscope, much higher magnifications are possible since electrons have a smaller wavelength than photons and it has a bigger depth of field. A scanning electron microscope basically consists of an electron gun (source), an electron collector, a lens system and a cathode-ray display tube. The tungsten or lanthanum hexaboride filament thermionically emits electrons which are focused by a series of lenses. The sample under investigation is scanned by the beam of focused electrons under high vacuum, and image is formed by capturing the secondary and/or backscattered electrons. Samples can be prepared very easily by coating a very thin conductive layer over the sample. The primary electron beam causes the emission of the secondary electrons from the surface of the sample which are collected by the detector [32].

The samples, in the present study, were analyzed using a field emission scanning electron microscope (Hitachi FESEM SU6600) which gives better images compared to conventional SEM. The electrons released by a field emission source are accelerated in the field gradient and pass through electromagnetic lenses which focus them on to the specimen, under high vacuum. Secondary electrons are emitted when the

primary electrons hit the surface of the specimen, and are collected by a detector to create an image of the sample surface, by comparing the intensity with that of the incident electrons. A field emission gun provides very narrow probing beams with high as well as low energies, providing an improved spatial resolution, minimal sample damage and charging. This helps to get very clear, less electrostatically distorted and high resolution images. Photograph of Hitachi SU6600 FESEM is shown in figure 2.10.

Figure 2.10: Hitachi SU6600 FESEM

2.2.8 Atomic Force Microscopy (AFM)

Atomic force microscopy is a very high resolution scanning probe microscopy tool for investigating materials at the nano-scale. It has a cantilever made of silicon or silicon nitride with a very sharp tip or probe at the end to scan the sample surface. The radius of curvature of the tip is usually of the order of a few nanometres. When the cantilever tip is brought very near to the surface of the sample, a deflection of the cantilever occurs due to the forces between the tip and the sample

surface, according to Hooke's law. The force depends on the type of sample, the surface roughness, surface contamination, the tip geometry and distance between the tip and the sample surface. A laser spot is directed to the top of the cantilever and is reflected to a two-segment or four-segment, position sensitive photodiode. The tip scans the surface by moving in raster scan, probing line by line. The PZT scanner on which the sample is kept moves and this causes the relative motion between the AFM tip and the sample. When the sample is scanned, the reflected laser, due to cantilever motion, falls on different regions on the photodiode array and is directed to the detector. A feedback mechanism functions to adjust the tip-to-sample distance, maintaining a constant force between the tip and the sample surface to avoid any collision of tip with the surface of the sample.

AFM operates mainly in two modes, the static (contact) and the dynamic (non-contact) modes. In the static mode, the tip is drawn across the sample surface and the deflection of the cantilever directly gives an image of the topographical map of the sample surface. In this method, sample and tip can get damaged due to the dragging motion together with the attractive forces between the tip and the sample surface. The cantilever is oscillated at or close to its fundamental frequency, in the dynamic mode. The tip-sample interaction force modifies the oscillation frequency, amplitude and phase which provide the information about the sample surface [32].

In the present study, with polymer thin film samples, Park systems XE 100 AFM in non-contact mode was employed for the analysis. AFM is suitable for analyzing both insulating as well as conducting samples

unlike the scanning tunneling microscope (STM) which can image conducting samples only. Schematic diagram of an AFM and photograph of the Park XC100 AFM are shown in figures 2.11(a) and (b).

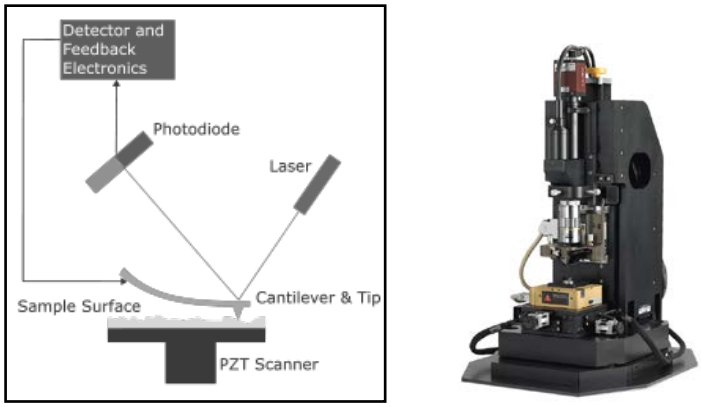

Figure 2.11: (a) Schematic diagram of an AFM and (b) Park Systems XE100 AFM

2.2.9 DC Electrical Conductivity: 2-point probe and 4-point probe techniques

In the present study, 4-point probe method was adopted to measure the dc electrical conductivity of polyaniline samples synthesized using various methods. The 4-wire sensing was carried out using Keithley 2400 source meter and 2001 multi-meter interfaced to a computer, using a dedicated program developed in LabVIEW. For measuring the DC electrical conductivity of high resistance samples, and analysing the diode characteristics of the fabricated polymer LED device prototypes and pressure sensing capabilities of polyaniline samples, the standard 2-point probe method using Keithley 2400 source meter integrated to a computer was employed. One of the main disadvantages of the 2-point probe method is that it cannot be used to measure the electrical conductivity of materials with moderate or high conductivity, with

resistance comparable to that of the probe resistance, spreading resistance and contact resistance. In a 2-point probe technique, each wire acts as the current and voltage probe.

If 'R_{mat}' is the resistance of the material under test, the total resistance 'R_T'is given by,

$$R_T = V/I = 2\,R_p + 2\,R_c + R_{mat} \text{ ----------(1)}$$

where R_p is the probe/wire resistance and R_c is the contact resistance. Even though it is an easier method, it is difficult to determine 'R_{mat}' using the 2-point probe method due to the reason mentioned above. This difficulty can be overcome by using the 4-probe method in which there are 4 terminals. Current is applied through 2 outer probes and voltage is measured across the other two probes. Schematic diagrams of 2-probe and 4-probe techniques are shown in figures 2.12(a) and 2.12(b).

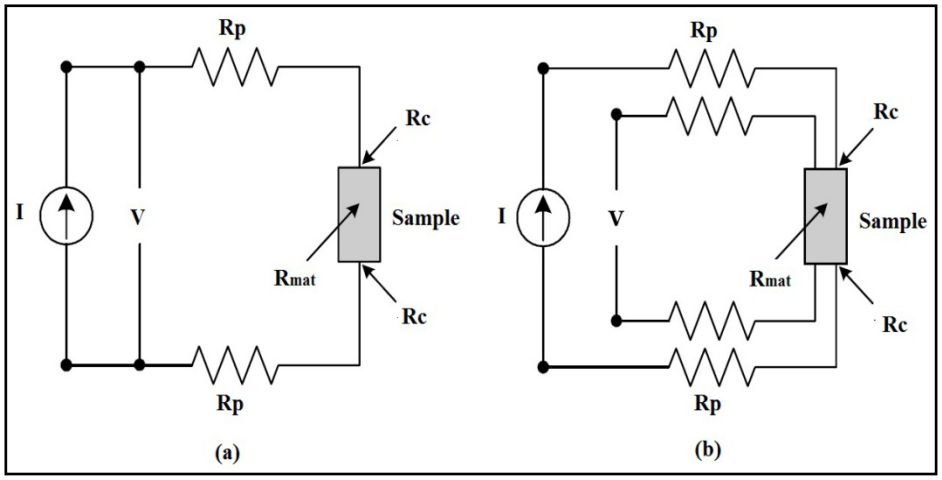

Figure 2.12: Schematic diagrams of (a) 2-point and (b) 4-point probe techniques

In the 4-terminal method, only a very small amount of current flows through the voltage path and although it contains both R_p and R_c, the voltage drop across R_p and R_c can be neglected due to this reason. This is a consequence of the very high value of the input impedance which is more than 10^{12} ohms. Thus, the measured voltage is just the voltage drop across the sample under investigation. The 4-probe configuration with collinear probes (probes arranged in a line) with the same probe spacing of approximately 2.5 mm was used in the present study. Current was applied through the two outer probes (force wires, 1st and 4th) and voltage was measured across the inner probes (sense wires, 2nd and 3rd) [32]. The schematic diagram of the 4-probe arrangement is shown in figure 2.12(c).

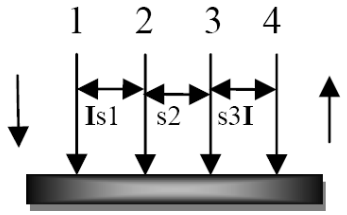

Figure 2.12(c): Schematic diagram of the 4-probe arrangement

The resistivity '***ρ***' is given by,

$$\rho = \left(\frac{2\pi}{\frac{1}{s1} - \frac{1}{s1+s2} - \frac{1}{s2+s3}\frac{1}{s3}} \left(\frac{V}{1} \right) \right) \text{----------(2)}$$

Since the probe spacings are equal (s=s1=s2=s3),

$$\rho = 2\pi s \frac{V}{1} \text{----------(3)}$$

When the probe spacing s=0.1588, 2πs is unity and the equation for resistivity reduces to,

$$\rho = \frac{V}{1} \text{ ----------(4)}$$

For an arbitrary shaped sample, a correction factor (F) is introduced. Then the resistivity becomes,

$$\rho = 2\pi sF\frac{V}{1} \text{ ----------(5)}$$

where 'F' is introduced as a correction for the thickness and diameter of the sample, probe placement, sample temperature and location of the probes near the sample edges. The sample thickness should be thinner or comparable with the probe spacing. 'F' is a product of three independent correction factors in the case of collinear probes.

$$F = F1.F2.F3 \text{ ----------(6)}$$

where F1, F2 and F3 are correction factors for sample thickness, lateral sample dimensions and placement of probes relative to the sample edges, respectively.

For thin samples (with non-conducting bottom boundaries) with thickness, 't' for which, $s \le \frac{t}{2}$, F1 reduces to

$$F1 = \frac{\left(\frac{t}{s}\right)}{21n(2)} \text{ ----------(7)}$$

For very thin samples, for which, F2 and F3 approach unity,

$$\rho = \frac{\pi}{1n(2)} t \frac{V}{1} 4.532 t \frac{V}{1} \quad \text{----------(8)}$$

2.3 Spin coating

Spin coating is a technique used to deposit homogeneous films from solutions on flat substrates. Solutions of the materials under investigation are dropped or dispensed onto a rotating substrate placed inside the spin coater. The platform, above which the substrate is placed, is rotated at very high speeds and the solution spreads homogeneously over the substrate due to centrifugal force, evaporating the volatile solvent. A vacuum pump provides the required force to pull the substrate towards the platform while spinning. The thickness of the film thus deposited is determined by the concentration of solution and the solvent, nature of material and the spin speed with which the substrate is rotated. The spin speed, acceleration and the spinning time can be precisely controlled, in a spin coater. Higher the spin speed, thinner will be the films deposited. All these parameters have to be optimized to obtain films of desired thickness. Spin coating can be used to obtain homogeneous thin films with thickness ranging from a few nanometres to micrometres [33].

For the present studies, an SPS Spin 150 wafer spinner (figures 2.13(a) and (b)) and a Laurell WS-400B-8NPP/LITE spinner were used to deposit polymer films on glass and ITO substrates.

Figure 2.13: (a) SPS Spin 150 wafer spinner and (b) different chucks (substrate holders) used in the spin-coater

2.4 Thermal Evaporation

Thermal evaporation or resistive thermal evaporation is one of the most common and easiest thin film metal deposition techniques. It involves thermal evaporation of a solid material (usually metals like Al, Ca, Au, Ag, etc.) by resistive heating and re-condensing onto a cooler substrate to form a thin film of the material. The material is heated to evaporation by placing it inside a container (filament, crucible or a boat) that has a fixed electrical resistance. The container is heated by passing a current sufficient to evaporate the material inside it. The chamber is evacuated to very low pressures below 10^{-5}mbar, to avoid metal vapour-air molecule collisions which deviate the path of evaporated material. The mean free path of the metal vapours will be larger under a high vacuum environment. A very high vacuum environment is necessary for depositing contamination-free, high quality metal films of desired thickness [34].

A rotary and diffusion pump driven (Indovision BJK 300) vacuum system was used to deposit the cathode material (aluminium film) for fabricating ITO/polymer/Al structures. Prototype PLEDs were fabricated using Doosan cluster tool which consists of a metal coating unit in which very thin films of lithium fluoride and aluminium were deposited. The vacuum required for the evaporation chamber associated with the cluster tool is provided by a cryogenic pump which can go down to pressures of the order of 10^{-8} mbar. Schematic diagram of the resistive thermal evaporation system is shown in figure 2.14.

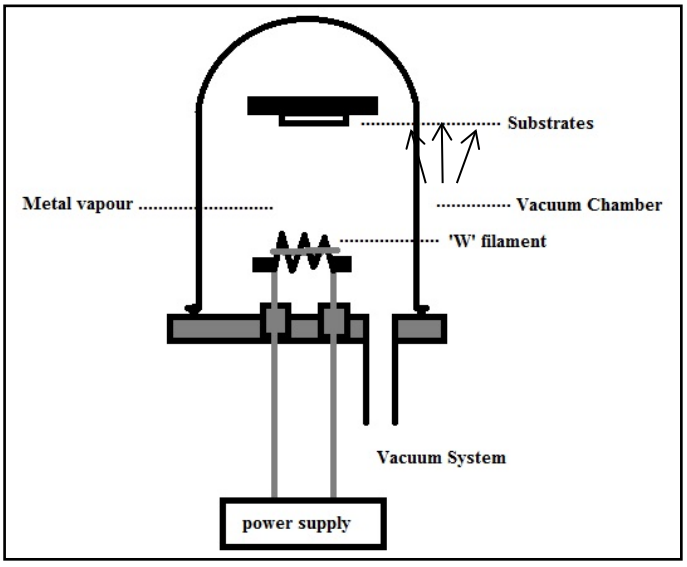

Figure 2.14: Schematic diagram of the resistive thermal evaporation system

2.5 Indium tin oxide (ITO) Etching and Patterning Procedure

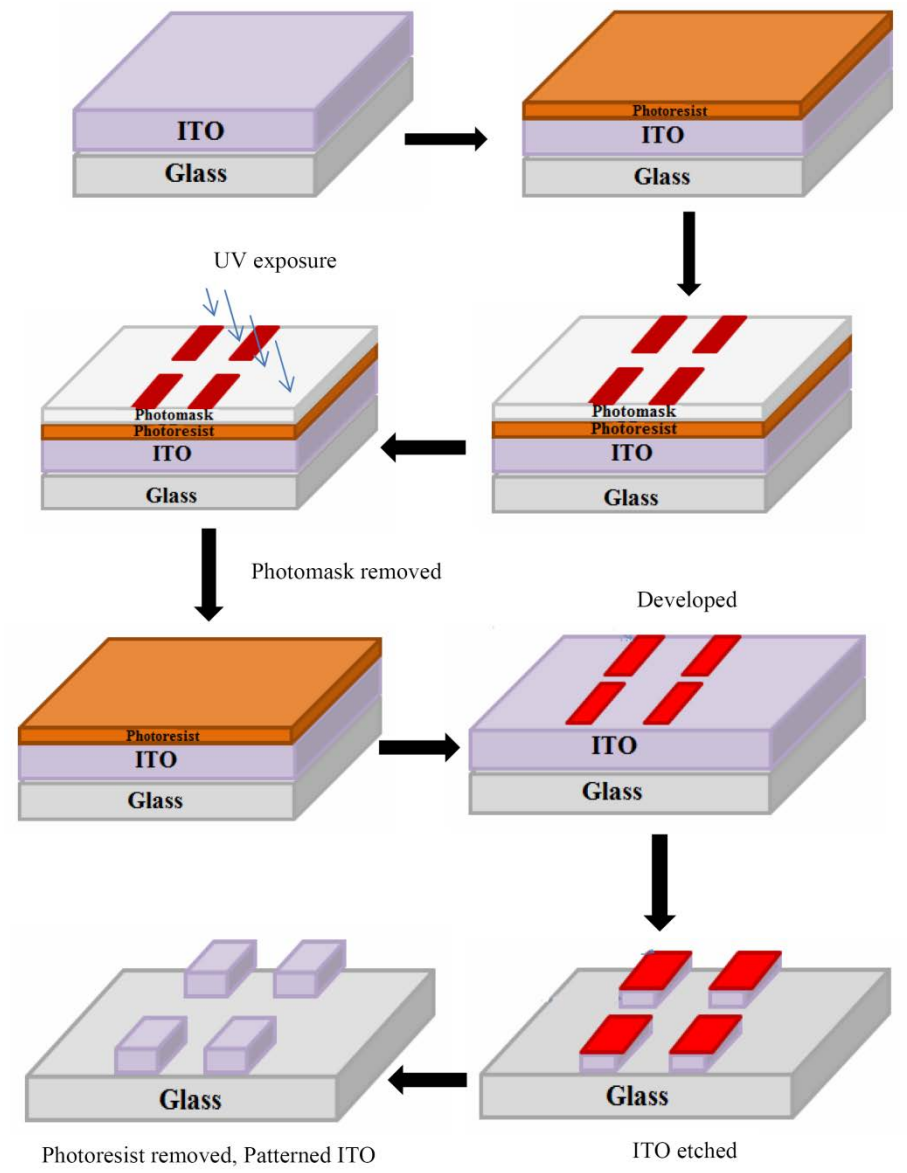

Figure 2.15: Various steps involved in patterning ITO coated substrates

Patterning ITO is the first and the most critical step, while fabricating devices on an ITO coated substrate. There are several steps involved in patterning ITO in the required manner. The various steps

involved in patterning the ITO on the substrates are shown in figure 2.15. Initially, a thin film of positive photoresist is spin-coated on the cleaned ITO substrate. It is then covered with a photo-mask (chromium mask) and exposed to UV radiation for a fixed time. The photo-mask is removed and the photo resist is developed. The developer is generally, a solution of KOH (4g) in distilled water (400mL). A strip of photo resist remains over the UV un-exposed regions. The substrates are then dipped in ITO etchant to remove ITO from those regions devoid of the photo resist. The photo resist is then removed from the ITO substrates using acetone. The final substrates have patterned ITO layers which are cleaned thoroughly with soap solution and de-ionised water.

2.6 Fabrication of Polymer Light Emitting Diodes (PLED)

Prototype PLED devices are generally assembled in a sandwich structure where the emissive layer is coated between the anode and cathode layers. Both single layer and multi-layer structures can be fabricated depending on the HOMO-LUMO energy levels of the emissive polymer. The single layer architecture consists of a spin-coated polymer film sandwiched between the indium tin oxide (anode) and aluminium (cathode) layers. The patterned ITO coated glass slides are cleaned in soap solution, rinsed in distilled water and dried prior to usage. The light emitting polymers dissolved in dichloromethane (DCM) are spin-coated on the cleaned and suitably masked ITO surfaces to get homogeneous thin films. A thin layer of aluminium is thermally evaporated on top of the polymer layer. Proper electrical contacts are taken from the ITO and aluminium layers to carry out the I-V characterization of the fabricated structure.

Schematic diagrams illustrating the various steps involved in a single-layer device fabrication are shown in figure 2.16

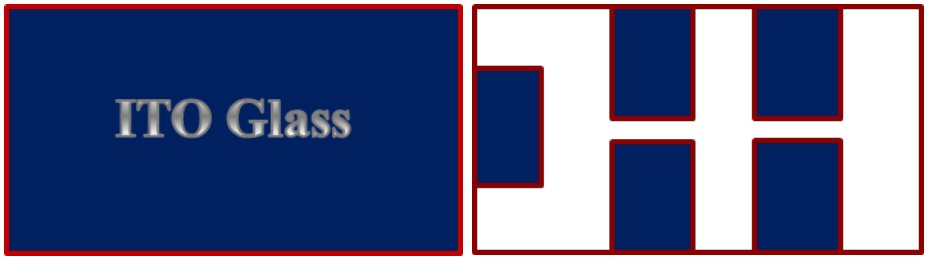

(a) ITO coated glass slide **(b) After Etching**

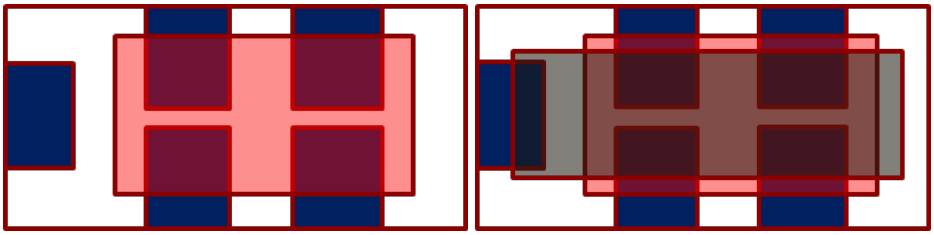

(c) After polymer coating **(d) After cathode deposition**

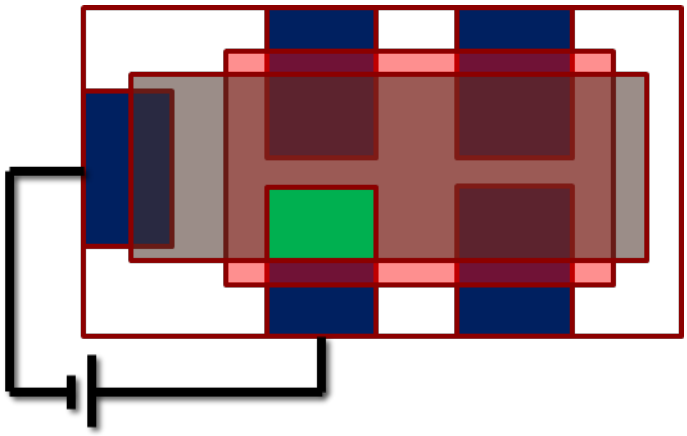

(e) Biasing and lighting up the pixel

Figure 2.16: Schematic diagrams of various steps involved in single layer PLED fabrication

Multi-layered structures are fabricated for realizing efficient electroluminescence from the devices, when the electrode work functions

have a mismatch with the HOMO-LUMO energy levels of the light emitting polymer. In multi-layered structures, an additional layer of PEDOT:PSS is spin coated on cleaned and patterned ITO glass plates to reduce the mismatch mentioned above. The light emitting polymers are spin cast on PEDOT:PSS layers and the cathode layer is thermally evaporated. The devices are sealed using a UV-curable epoxy to protect them from environmental degradation.

In the present work, both single and multi-layer devices were fabricated for studying the diode characteristics and the electroluminescence, to assess the suitability of a few, novel, light emitting polymers as emissive layers in PLED applications. ITO/emissive polymer/ Al single layer structures and ITO/PEDOT:PSS/emissive polymer/ LiF-Al multi-layer structures were assembled. For the multi-layer structures, the cathode layers were deposited using a cluster tool (Doosan DND, Korea). Precise control over the thickness of the cathode layer could be achieved by using a fully automated cluster tool. A very thin layer of LiF (1.5 nm) with a top aluminium layer (200 nm) was used as the cathode layer. Contacts were taken from the anode (ITO) and cathode for I-V and electroluminescence measurements. A forward bias was given across the electrodes using Keithley 2400 source meter adopting the 2-point probe method. The electroluminescence was measured in terms of relative spectral distribution using Konica Minolta CS1000 spectroradiometer. Spectral radiance is the quantity of light emitted from a surface and collected within a particular solid angle, which is generally measured in $W.sr^{-1}.m^{-2}.nm^{-1}$with surface area and wavelength or frequency.

The photograph of the cluster tool used for PLED fabrication is shown in figure 2.17.

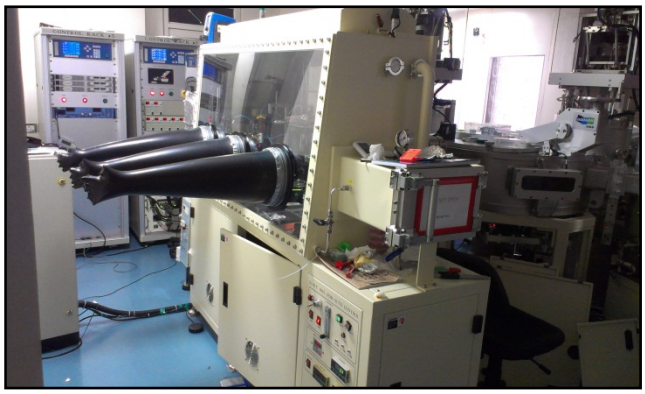

Figure 2.17: Doosan Cluster tool for PLED fabrication

2.7 Electroluminescence

Electroluminescence is a phenomenon in which light is emitted in response to the application of a current or electric field, usually seen in semiconductors. In this process, a forward bias is applied through the electrodes coated on the material. In the forward bias condition, electrons from the cathode and holes from the anode migrate towards the intermediate emissive layer where they form excitons. Excitons are short-lived electron-hole pairs which decay radiatively, releasing the characteristic energy related to the band gap of the material [35, 36].

The light emitted by the device can be analyzed using a spectroradiometer by determining luminance, spectral radiance, colour, colour temperature, CIE coordinates, etc. In the present study, Konica Minolta CS1000 spectroradiaometer shown in figure 2.18(a) was utilized to measure the spectral radiance against different wavelengths, for the

fabricated devices. Green light emission from an organic light emitting diode is shown in figure 2.18(b).

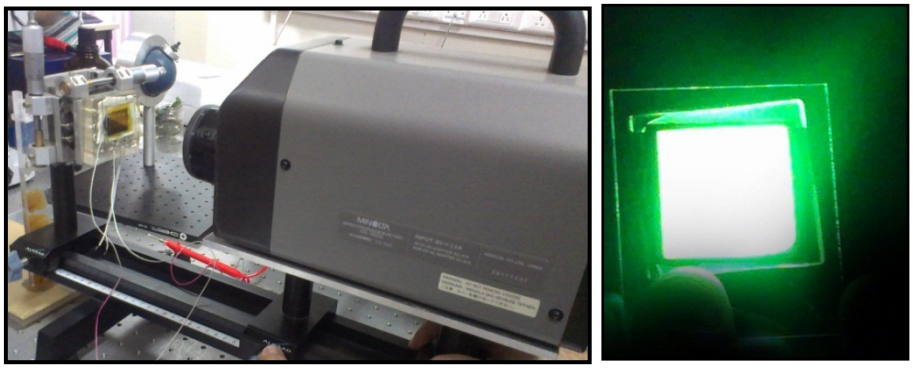

Figure 2.18: (a) Electroluminescence measurement set-up using Konica Minolta CS 1000 and (b) electroluminescence from a green light emitting device

2.8 CIE Coordinates and Chromaticity

To define a particular colour in the study of colour perception, The International Commission on Illumination (CIE) introduced a colour space termed the CIE 1931 XYZ colour space. XYZ are the tristimulus values. X and Z correspond to human eye perception of blue and red colours respectively, and Y corresponds to luminance. Human eye has cone cells which are photoreceptors for medium and high brightness colour vision with sensitivity peaks in the wavelength regions 420-440nm (short), 530-540nm (medium) and 560-580nm (long). Thus a colour perception can be described by three parameters, called the tristimulus values. The combinations of these three values thus constitute the whole CIE colour space. Since the human eye has three different kinds of colour receptors that respond to different wavelengths, the plot of all visible colours is a three dimensional-figure. Colour can be defined by two terms, chromaticity and brightness. The CIE colour space is

designed to visualize all colours in terms of brightness and chromaticity. The two normalised parameters, x and y are functions of the tristimulus values X, Y and Z and can be expressed as,

$$x = \frac{X}{X+Y+Z} \ldots\ldots\ldots (9)$$

$$y = \frac{Y}{X+Y+Z} \ldots\ldots\ldots (10)$$

$$z = \frac{Z}{X+Y+Z} = 1 - x - y \ldots\ldots\ldots (11)$$

Thus, a resultant colour space, termed CIE xyY colour space, derived from x, y and Y values, is usually used to specify colours. The CIE colour space (figure 2.19)is a plot with the shape of horse-shoe or a tongue, in which any colour is expressed by the x and y values and is called the gamut of human vision. If any two colours are chosen from the colour space designated by their corresponding x and y values, the colours that come on a straight line joining these two points can be formed by mixing these two colours in appropriate ratios [37, 38, 39].

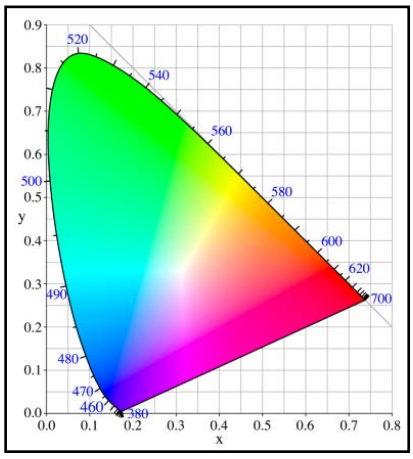

Figure 2.19: CIE 1931 colour space

References:

[1] Prasanna Chandrasekhar, *Conducting Polymers: Fundamentals and Applications*, Kluwer Academic Publishers, London (1999) pp 16-21, 101-124

[2] S. J. Varma, S. Jayalekshmi, *J. Appl. Polym. Sci.*, **117**, 138–142 (2010)

[3] S.J.Varma, Jerin George, Jeeju.P.P, S.Jayalekshmi, *Journal of Luminescence*, **132**, 801-805 (2012)

[4] Sreekanth J Varma et al, *Polym. Int.*, (2012), DOI 10.1002/pi.4131

[5] Hari Singh Nalwa, *Handbook of Organic Conducting Molecules and Polymers: Vol. 2*, John Wiley & Sons, New York (1997), pp 505-566

[6] Donald L.Wise et al (Editors), *Electrical and Optical Polymer Systems*, Marcel Dekker, Inc., New York, (1998), pp 362-363

[7] S.Thomas and G.E.Zaikov, *Polymer Nanocomposites Research Advances*, Nova Science Publishers, Inc. (2008), pp 317

[8] K.Lee et al, *Nature Letters*, **441**, 65-68 (2008)

[9] S.H.Lee et al, *Adv. Funct. Mater.*, **15**, 1495-1500 (2005)

[10] W.R.Salaneck, I Lundström, B Rånby (Editors), *Conjugated Polymers and Related Materials*, , Oxford University Press, London (1993), pp 73-98

[11] Meixiang Wan, *Conducting Polymers with Micro and Nanometer Structure*, Springer-Verlag, New York (2008), pp 22

[12] K.S.Lee, T.Hino and N.Kuramoto, *Chem.Lett.*, **36**, 340-341 (2007)

[13] J. Huang and M.Wan, *J. Polym. Sci. Part A, Polymer Chemistry*, **37**, 131-157, (1999)

[14] T.Taka, J.Laakso and K.Levon. *Solid State Communications*, **92**, 393-396, (1994)

[15] Surajit Sinha, Sambhu Bhadra, Dipak Khastgir, *J. Appl. Polym. Sci*.,**112**, 3135–3140 (2009)

[16] J. Yue, A. J. Epstein, *J. Am. Chem. Soc*., **112,** 2800 (1990)

[17] J. Yue, Z. F. Wang, K.R. Cromack, A. J. Epstein, A. G. MacDiarmid. *J. Am. Chem. Soc.*,**113,** 2665 (1991)

[18] S. A. Chen, G. W. Hwang, *J. Am. Chem. Soc*., **116**, 7939 (1994)

[19] H. S. O. Chan, L. M. Gan, C. H. Chew, L. Ma, S. H. Seow. *J. Muter. Chem*., **3,** 1109 (1993)

[20] Y. Cao, P. Smith, A. J. Heeger, *Synth. Met.*, **48,** 91 (1992)

[21] J. Yue, G. Gordon, A. J. Epstein, *Polymer*, **33,** 4409 (1992)

[22] R. E. Cameron, S. K. Clement. *U.S. Patent* 5,008,041, (1991)

[23] Banwell and McCash, *Fundamentals of Molecular Spectroscopy*, Tata McGraw Hill Publishing Company Ltd., 4th edn., New Delhi (1995), pp 93-94, 100-125

[24] E.A.Davis, N.F.Mott, *Phil.Mag*, **22** (1970) 903

[25] J.Bardeen, F.J.Blatt, L.M.hall, *Proc. Photoconductivity Cong.*, Wiley, New York (1956), pp 146

[26] H.B.Bebb, E.W.Williams, *Semiconductors and Semimetals*, (R.K.Willardson and A.C.Beer (Eds)), Academic Press, New York (1972) pp 181-320

[27] P.J.Dean, *Prog. Crystal Growth Charact*.**59**, 2453 (1985)

[28] T.A.Skotheim, R.L.Elsenbauner, J.R.Reynolds (Eds), *Handbook of Conducting Polymers(II edn.)*, Marcel Dekker Inc., New York (1998)

[29] V R Gowariker et al, Polymer Science, *New Age International*, India (1986), pp 173-192

[30] Paul Gabbott, *Principles and Applications of Thermal Analysis*, John Wiley & Sons, USA (2008) pp 87-118

[31] M.P.Sepe, *Thermal Analysis of Polymers*, Rapra Publishing, UK (1997), pp 13-18

[32] Dieter K. Schroder, *Semiconductor Material and Device Characterization*, 3rd edn., John Wiley & Sons Inc., USA (2005) pp 629-634, 544-547, 1-20

[33] S. Middleman and A.K. Hochberg, *Process Engineering Analysis in Semiconductor Device Fabrication*, McGraw-Hill, New York (1993), pp 313

[34] K.L.Chopra, *Thin film Phenomena*, McGraw Hill, New York (1969), pp 11-20

[35] Zakya Kafafi, *Organic Electroluminescence*, Taylor & Francis Group, New York (2005), pp 2

[36] Jan Kalinowski, *Organic Light Emitting Diodes: Principles, Characteristics & Processes*, Marcel Dekker, New York (2005), pp 1-2

[37] CIE (1932), *Commission Internationale de l'Eclairage proceedings*, Cambridge University Press, Cambridge (1931)

[38] T.Smith and J.Guild, T Smith and J Guild, *Trans. Opt. Soc.*, **33,** 73 (1931)

[39] Hunt, R. W., *Measuring Colour* (3rd ed.), Fountain Press, England (1998), pp 39-46,54-57

…..ൟ…..

Chapter 3

POLYANILINE AND ITS COMPOSITES: POSSIBLE CANDIDATES FOR PRESSURE SENSING APPLICATIONS

Contents

The sensitive dependence of electrical conductivity on applied pressure can be utilized to design a variety of pressure sensors for a wide range of applications. The present chapter deals with the investigations carried out on the dependence of dc electrical conductivity on applied pressure of both nanostructured and microstructured forms of doped polyaniline samples and their composites. A comparison of the pressure sensitivity of the nanostructured and the microstructured samples has also been carried out.

3.1 Introduction

Polyaniline and its composites have been subjected to intense investigations for the past 40 years. Various technologically important applications have been put forward and a lot of devices fabricated based on these investigations. In all these applications, the electrical conductivity that can be achieved through doping and structural variations has been the main focus.

The electrical conductivity of doped conducting polymers such as polyaniline (PANI) shows significant dependence on many parameters including doping concentration, polymer structure ambient temperature and pressure. The influence of pressure on conductivity can be envisaged as closer packing of the material, allowing better inter-chain interactions in both fibrillar and globular conducting polymers. In most of the pressure dependence studies, the change in conductivity with smaller applied pressures is quite negligible [1]. Maddison and Unsworth, in their investigation with polypyrrole / tosylate, observed an approximately 59% increase in conductivity above a pressure range of 1.1 GPa and a hysteresis in the conductivity [2]. An apparent metal-to-insulator transition was observed in PF_6^- and K^+ doped trans-polyacetylene and CSA doped polypyrrole by the Heeger group [3]. A positive coefficient for the activation energy of conduction has been observed as an indication for this finding. The compression sensitivity and hysteresis of composites of polyaniline and a block copolymer, styrene-butadiene, was investigated by Fernando G. Souza et al [4].PANI thin films were also subjected to pressure dependence studies by Bao et.al, at pressures above 22 GPa at room temperature and they observed enhanced inter-chain charge transport due to sample compression [5]. These samples also exhibited hysteresis like behaviour and never returned to the initial conductivity.

The present work highlights the prospects of applications of doped polyaniline (PANI) and its composites (Multi-Walled Carbon Nanotube (MWNT) and polyvinylchloride) in pressure sensing devices. PANI and its composite samples in the form of pressed pellets show orders of

change in electrical conductivity with applied pressure in the range 0 to 30 MPa. The percentage variation of electrical conductivity with applied pressure is strikingly large for PANI and its composite samples.

This chapter is divided into two major sections. The first section deals with the investigations on the pressure sensitivity of dc electrical conductivity of nanostructured, doped PANI samples and their composites with MWNT. The second section involves similar studies on microstructured, doped PANI and their composites with polyvinylchloride (PVC) and MWNT.

3.2 Materials

Aniline, Ammonium persulphate, orthophosphoric acid, d-10-camphorsulphonic acid, naphthalene-2-sulphonic acid and hydrochloric acid were procured from SD Fine Chemicals Pvt. Ltd., India. Multi-walled carbon nanotubes were purchased from Conyuan Biochem. Ltd., Taiwan.

3.3. Nanostructured Polyaniline and Polyaniline/MWNT composites

3.3.1 Synthesis of nano-structured PANI and PANI-MWNT composites

Aniline was distilled under reduced pressure prior to use. The chemical oxidative polymerization [6, 7] of monomer aniline was done in the acidic medium of 1M camphorsulphonic acid (CSA) and orthophosphoric acid (OPA) with, ammonium persulphate (APS) as oxidant. The oxidant was added immediately to the aniline-acid solution and stirred for 5 hrs. The resultant solution was filtered and washed with water and acetone. The powder thus obtained was dried in hot air oven at 50°C for 4 hrs.

To synthesize β-Naphthalene sulphonic acid (NSA) doped PANI, NSA was initially dissolved in de-ionised water to get 1M solution. The polymerization was initiated by taking a cooled 1:1 mixture of aniline-NSA solution to which the oxidant, APS dissolved in de-ionised water was added [8]. The mixture was stirred for 24hrs at 0 to 5°C. The precipitate was washed with de-ionized water, methanol and ethyl ether several times and then kept for drying at room temperature in a hot air oven for 24 hours.

PANI-MWNT composites were also synthesized by the same procedure described above, using the same dopants. MWNT was mixed with aniline in the acidic medium and then kept for in-situ polymerization.

Pressed pellets of all the samples with 13mm diameter and 2 mm thickness were made by applying 9 tons using a table-top hydraulic pellet press. The quantity of the sample taken, applied pressure and pressing time were optimized and maintained the same for all the samples.

3.3.2 Characterization

X-ray Diffraction, Fourier Transform Infrared Spectroscopy Scanning Electron Microscopy and Raman Spectroscopy were used to carry out the structural characterization of the samples. The XRD studies of the samples were done using Rigaku X-ray diffract meter using Cu-Kα radiation. FTIR and Raman spectroscopic investigations were performed using Bruker Tensor 27 spectrophotometer and Jobin Yvon Horibra LABRAM-HR micro-Raman spectrophotometer with 488nm argon laser as the source

respectively. The spectra were analyzed to assure the presence of MWNT in the composite samples and structurally characterize the samples. Scanning Electron Microscopy (SEM) images were recorded using Hitachi SU6600 FESEM. Variation of dc electrical conductivity with applied pressure was studied using a fully-automated Keithley 2400 source meter, adopting 2-point probe connections from either side of the pellets.

3.3.2.1 X-ray diffraction studies

The XRD patterns of acid doped PANI samples and their composites with MWNT are shown in Figures 3.1(a), (b) and (c).

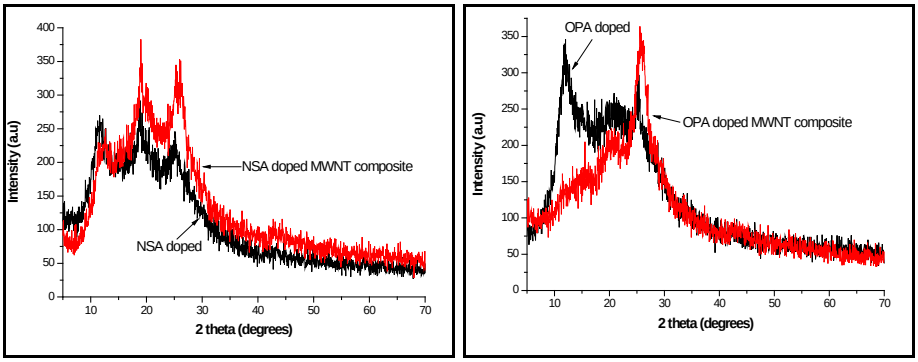

Figure 3.1: (a) XRD patterns of NSA doped PANI and its composite with MWNT (b) OPA doped PANI and the composites with MWNT

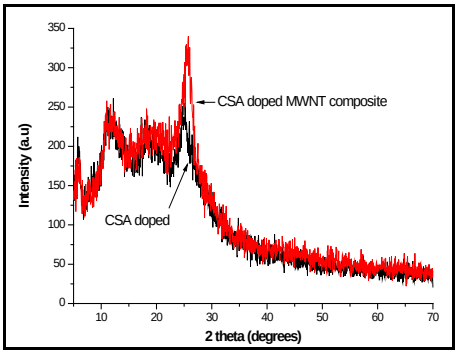

Figure 3.1(c): XRD pattern of CSA doped PANI and its composite with MWNT

PANI shows amorphous peaks at around 11^0 and 19^0 and a sharper peak at 25^0. MWNT has a highly crystalline peak at 25^0 which is much more intense and sharper than that of PANI at the same position. PANI-MWNT samples show crystalline peak of MWNT at 25^0 with high intensity and sharpness. The amorphous peaks of PANI at 11^0 and 19^0 appear sharper in the XRD spectrum of PANI-MWNT confirming the formation of the composite. The appearance of the graphite-like diffraction peak at 25^0, which is common to both PANI and MWNT, indicates the presence of long range π-conjugation, in all the samples. This peak is very much sharper in MWNT because of much enhanced π-conjugation in MWNT. These observations are common to all the three acid doped PANI samples and their composites [9].

3.3.2.2 Fourier Transform Infrared Spectroscopic Studies

The FTIR spectra of CSA, OPA and NSA doped PANI powder samples are shown in figure 3.2.

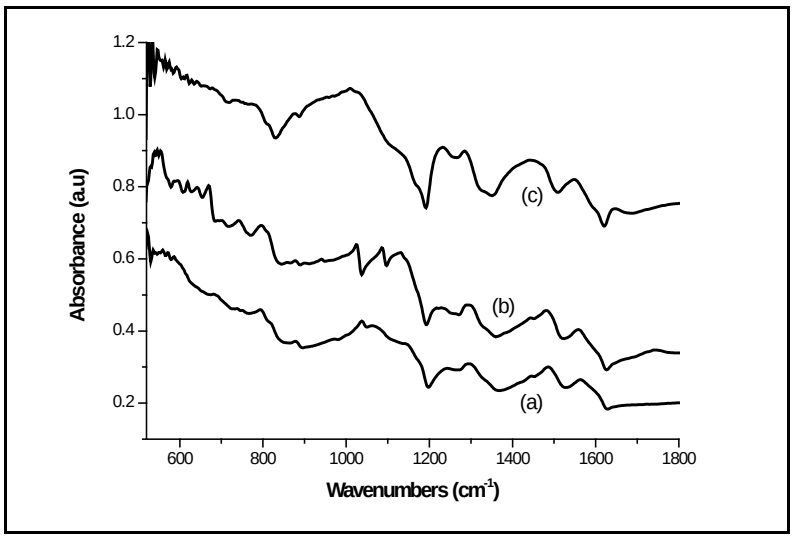

Figure 3.2: FTIR spectra of (a) CSA, (b) NSA and (c) OPA doped PANI samples

In OPA doped PANI, peaks are observed at 1473 $cm^{-1}$and at 1052 cm^{-1}corresponding to C=C stretch of the benzenoid unit of PANI and the quinoid unit vibration of doped PANI, respectively, as reported earlier [10, 11].

In CSA doped PANI, the peak at 1240cm^{-1} corresponds to the C-N stretch vibration and the one at 684cm^{-1} denotes the C-H out of plane bending [12]. The peaks at 1566cm^{-1} and 1487cm^{-1} correspond to the C=C stretching deformation of quinoid and benzenoid rings [13] respectively and the one at 1301cm^{-1} is attributed to the C-N stretching of secondary aromatic amine [14]. The vibrations of $–SO_3H$ group [15] are observed at 508cm^{-1}, 582cm^{-1}, 790$cm^{-1}$and 1039cm^{-1}, which confirms the presence of the dopant CSA.

Characteristic peaks of NSA doped PANI are observed at 1560cm^{-1}, 1481cm^{-1}, 1292cm^{-1}, 1238cm^{-1}, 1128cm^{-1}, and 800cm^{-1}[9]. When compared to the EB form of PANI, a small red shift can be observed for these bands [8, 16]. There is also broadening of the bands and change in the relative intensities. The enhancement of the oscillator strength of the backbone-related vibrations because of a vibronic coupling with the π-electron charge oscillation along the chain [8, 17] can be a possible reason for this. Similar effect has also been found in PANI–HCl, indicating that the backbone structure of PANI–NSA tubules and PANI–HCl are similar. The peaks at 1026cm^{-1} and 671cm^{-1}, which can be attributed to the absorption of $-SO_3^-$ [8,15]are absent in the FTIR spectrum of PANI-HCl. These peaks however, confirm the presence of the dopant NSA in PANI-NSA.

3.3.2.3 Raman Spectroscopic Studies

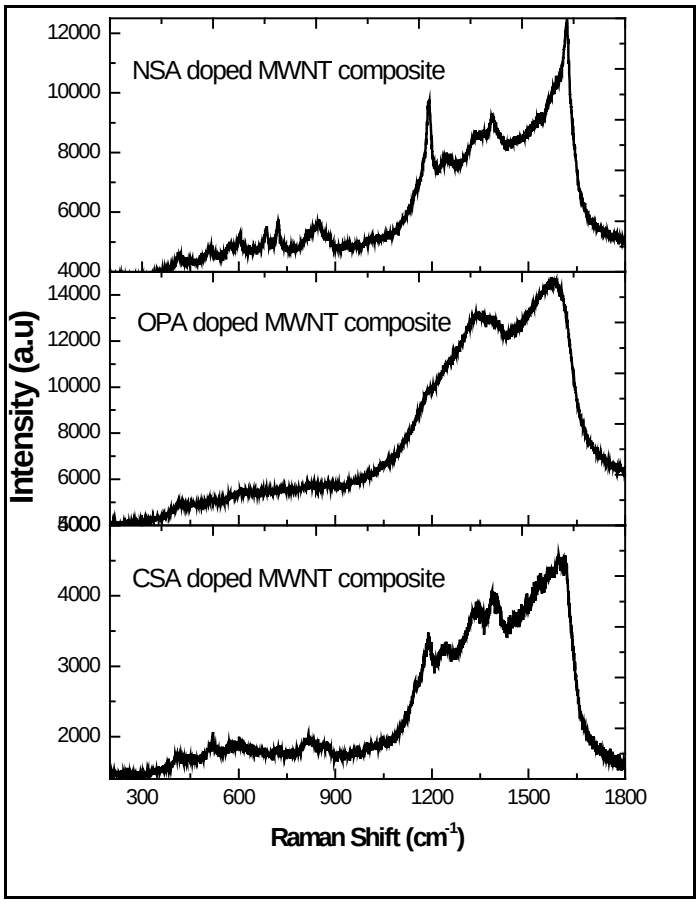

Figure 3.3: Raman spectra of PANI/MWNT composites

The presence of MWNT in the PANI/MWNT composites could not be established from the FTIR investigations. Hence Raman spectral studies were carried out on the PANI/MWNT composites and the spectra are shown in figure 3.3.The Raman spectra depict the G-mode vibrations [18] of MWNT (graphite like) at 1346cm^{-1}, 1347cm^{-1}, 1344 cm^{-1} for the NSA, OPA and CSA doped composites respectively. Similarly the D-mode vibrations of MWNT are observed at 1575cm^{-1}, 1573cm^{-1}, 1592 cm^{-1}

respectively for NSA, OPA and CSA doped composite samples. Thus the presence of MWNT in all the three composite samples has been established.

3.3.2.4 SEM Analysis

The field emission scanning electron microscopy images of doped PANI and its composite samples are shown in figures 3.4(a) to 3.4(f).

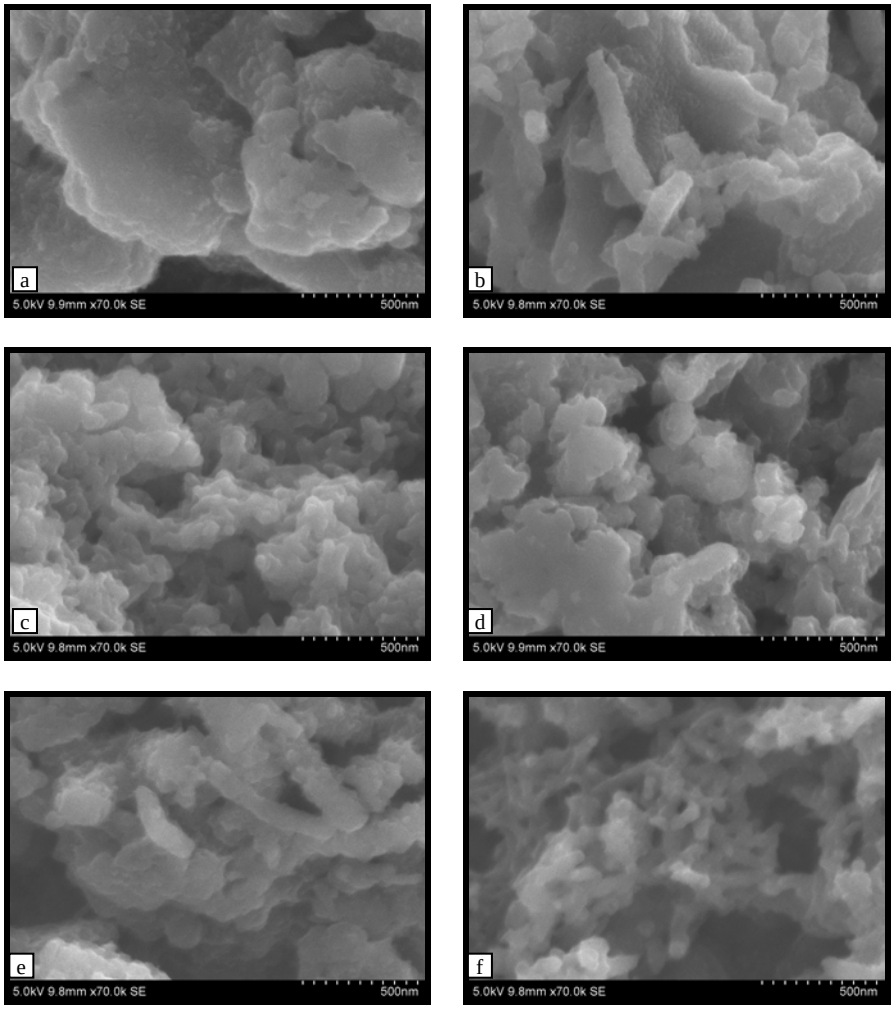

Figure 3.4: FESEM images of (a) CSA doped, (b) CSA doped MWNT composite, (c) OPA doped, (d) OPA doped MWNT composite, (e) NSA doped and(d) NSA doped MWNT composite samples of PANI

All the samples are nano-sized as evident from the FESEM images. The nanostructure of these samples is a consequence of the immediate addition of the oxidant which significantly affects the rate of reaction. It has been well-established in chemical oxidative reactions that rapid addition of the oxidant can result in the formation of nanostructures [19]. The presence of MWNT cannot be identified separately from these FESEM images, since PANI forms a layer enclosing the MWNTs.

3.3.2.5 Pressure Sensitivity Studies

The variation of DC electrical conductivity with applied pressure of the pellet samples was studied using a home-made sample holder (figure 3.5(a)), connected to Keithley 2400 source metre, automated using Lab VIEW software. Calibrated loads were applied on top of the sample holder and the change in conductivity for each sample with the loads was analyzed using a dedicated program developed in Lab VIEW. Screen shots of the program and its graphical user interface are shown in figures 3.5(b) and (c) respectively. An average of 10 conductivity values was taken as the conductivity of each of the pellets.

Figure 3.5(a): Sample holder used in the experiment to measure the change in conductivity with applied load using 2-probe method

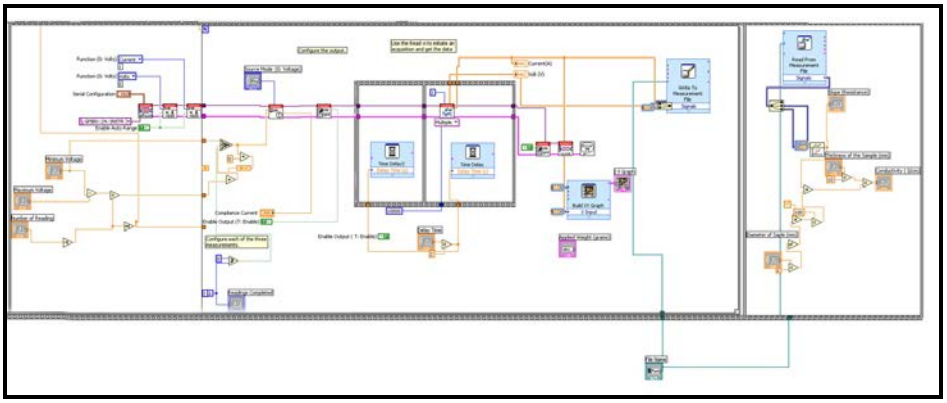

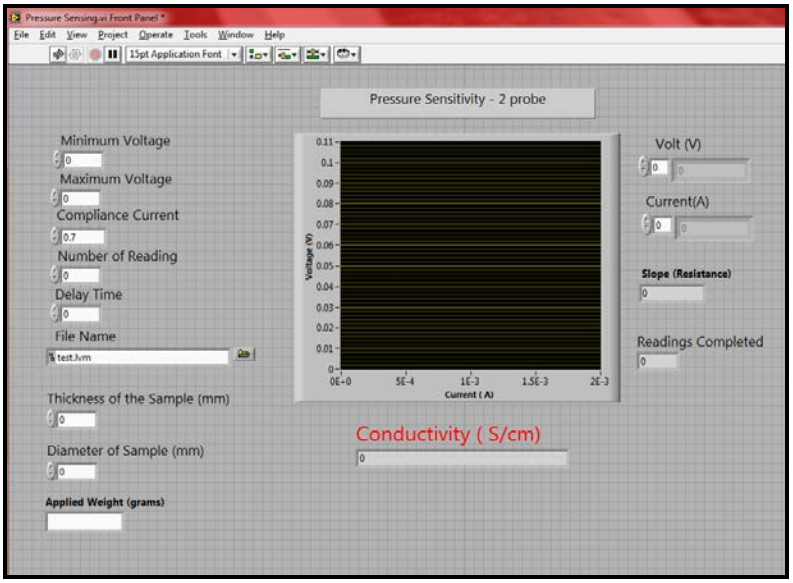

Figure 3.5: Screenshots of (b) LabVIEW program and (c) graphical user interface for 2-probe pressure sensitivity measurement

It is observed that there is appreciable change in the dc electrical conductivity of the samples with applied pressure.

The percentage variation of conductivity of each sample with applied pressure is calculated using the equation,

$$\% \text{ variation} = \frac{100 \text{ x } (\sigma_1 - \sigma_0)}{\sigma_0} \text{ ---------- (1)}$$

where σ_1 is the conductivity with maximum load and σ_0 is the conductivity with no load.

A graph drawn with applied pressure along the x-axis and % variation in conductivity along the y-axis for different samples is shown in figure 3.6.

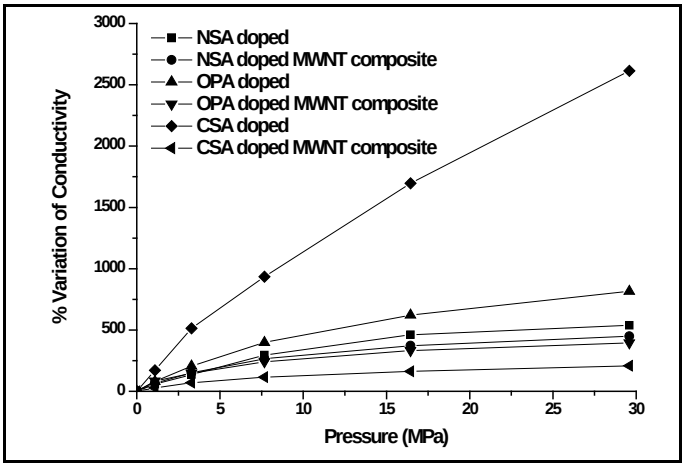

Figure 3.6: Percentage variation of conductivity with applied pressure for various PANI and its composite samples

From figure 3.6, it is clear that there is appreciable change in conductivity with applied pressure for all the samples investigated. It is also observed that with the application of pressure, there is an increase in percentage variation of dc electrical conductivity above two orders of magnitude.

The variation of conductivity with pressure for each sample depends upon the dopant used and the presence of MWNT. The highest conductivity of ~10.5 S/cm is observed for the NSA doped, MWNT composite of PANI. However, the maximum percentage variation is observed for the CSA doped PANI sample without MWNT.

The electrical conductivity in doped PANI is mainly due to (1) the ability of the charge carriers to move along the polymer backbone and (2) the ability of the charge carriers to hop between the polymer chains [20], which contribute towards the intra-chain (σ_{intra}) and inter-chain conductivity (σ_{inter}) [21] respectively.

$$\sigma = \sigma_{intra} + \sigma_{inter} \text{ ----------} (2)$$

The inter-chain conductivity is due to the expanded coil like conformation of PANI chains whereas intra-chain conductivity is due to the high extent of conjugation and better crystalline order of PANI [22].

When pressure is applied on the surface of the PANI samples, the dispersed conducting particles are forced to touch each other, resulting in the formation of conducting channels and thereby increasing the electrical conductivity [23]. It is also widely accepted that the conductivity of PANI pellets would increase with the applied pressure due to the removal of voids inside the pellets. Therefore, the observed increase in conductivity with applied pressure is mainly due to the increase in the inter-chain conductivity of PANI and PANI MWNT composite samples. The conductivity reaches a peak value when there is maximum contact which is somewhere above 30 MPa. In the present work we could not apply pressures above 30 MPa and hence could not observe any saturation in conductivity.

Table 3.1: Electrical conductivity of the samples without any load and with the maximum load applied.

PANI Sample	Conductivity without applied pressure (S/cm)	Maximum Conductivity with maximum pressure (S/cm)
CSA doped	0.020348	0.552122
OPA doped	0.119437	1.09329
NSA doped	0.487236	3.11276
CSA doped MWNT composite	0.339168	1.04144
OPA doped MWNT composite	1.082814	5.36433
NSA doped MWNT composite	1.91649	10.5094

From Table 3.1, it is clear that the conductivity is higher for the composite samples whereas the percentage variation in conductivity with applied pressure is higher for the doped PANI samples without MWNT, compared to the composite samples. MWNT is a good electrical conductor. It acts as a bridge between the isolated conducting regions in PANI matrix. It also covers the voids in the pellets on the application of even a small pressure and hence prominent changes in conductivity are not observed by applying higher pressures. That is why the percentage variation of the conductivity with applied pressure in the composite samples is not prominent when compared to that in doped PANI samples. In general, doped PANI samples consist of isolated conducting regions separated by insulating regions. On the addition of MWNT, the isolated conducting regions get connected to some extent, facilitating the formation of conducting channels. Thus there is appreciable enhancement in electrical conductivity. On the application of pressure, further enhancement in the number of connected regions occurs.

However, the formation of conducting channels gets maximized for a particular optimum pressure and hence further increase in pressure does not make any significant difference in the distribution of conducting channels. Hence there is no significant percentage variation in electrical conductivity with applied pressure in the composite samples compared to the doped PANI samples.

3.4 Microstructured polyaniline and its composites with PVC and MWNT

Particle size and morphology of PANI can be controlled by varying the reaction conditions like the rate of addition of the oxidant, type of dopant and the concentration of dopant in chemical oxidative polymerization reactions. Slower addition of the oxidant leads to the formation of micro-sized PANI particles. The following samples were investigated:1) Hydrochloric acid (HCl) and orthophosphoric acid (OPA) doped PANI, 2) HCl and OPA doped PANI-MWNT composite and 3) HCl and OPA doped PANI-MWNT composites synthesized in the presence of Polyvinylchloride (PVC). The effect of pressure on the electrical conductivity of these samples was investigated following the same procedure mentioned above.

3.4.1 Synthesis of microstructured polyaniline samples

Two different, acid doped conducting polyaniline samples were synthesized successfully by the chemical oxidative polymerization of aniline (5 ml) using ammonium persulphate (2.9 g in 50 mL, 1M acid) as initiator in the presence of (1M,75 mL) hydrochloric acid (HCl) and orthophosphoric acid (OPA) *(Sample code – PH and PO respectively)*. The addition of initiator was controlled so that complete addition was

finished in 10 minutes. The reaction was carried out at room temperature for 4 hours while stirring.

A fixed amount of MWNT was added in-situ to the aniline/acid (HCl and OPA) mixture for synthesizing PANI/MWNT composite adopting chemical oxidative polymerization *(Sample Code: PMH and PMO respectively).* The reaction conditions were maintained the same as described above. Aniline:MWNT ratio was maintained as 1:0.4 in both the samples.

The third set of samples, PANI - MWNT - PVC composites, was also synthesized by the in-situ addition of MWNT and emulsion grade PVC by adopting the same procedure without changing the reaction conditions using HCl and OPA as the acid media *(Sample Code: PMHP and PMOP respectively).* Aniline:MWNT:PVC ratio was maintained as 1:0.4:1 in both the composite samples.

The powder samples obtained were then filtered, washed and dried in dynamic vacuum at 50^0C for 4 hours. The dried samples were finely powdered and pelletized using the hydraulic table top pellet press applying 9 tons of pressure. The pressed pellets were 13mm in diameter and 2 mm thick. Electrical contacts were introduced on both faces of the samples by coating gold using vacuum evaporation technique.

3.4.2 Characterization

3.4.2.1 FTIR Analysis

The FTIR spectra of PH, PMH, PMHP, PO, PMO and PMOP samples are shown in figures 3.7(a), (b), (c) and 3.8(a), (b), (c).

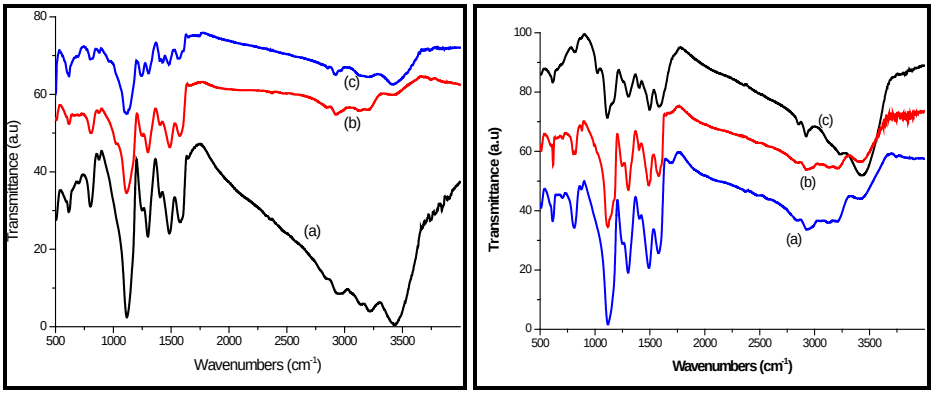

Figure 3.7: FTIR spectra of (a) PH, (b) PMH, (c) PMHP;Figure 3.8: FTIR spectra of (a) PO, (b) PMO, (c) PMOP powder samples

The characteristic peaks of doped polyaniline can be seen in the FTIR spectra all the samples shown in figures 3.7(a), (b), (c) and 3.8(a), (b), (c). From these spectra, major peaks of PANI can be seen around 1571cm^{-1}(C=N stretch of the quinoid unit of PANI), 1486cm^{-1} (C=C stretch of the benzenoid unit of PANI) and 1110cm^{-1}(quinoid unit vibration of doped PANI) for OPA doped samples and around 1567cm^{-1}, 1482cm^{-1}and 1110cm^{-1}respectively for HCl doped samples[24, 25, 26, 10]. The presence of PVC in PMHP and PMOP samples can be confirmed by the presence of peaks at 1245cm^{-1} (C-H rocking vibration) and 1016cm^{-1} (C-C stretching band of PVC backbone chain) respectively [27, 28, 29, 30, 31, 32]. A decrease in intensity of the PANI peaks can be seen in PMH and PMO samples due to the addition of MWNT and, a further decrease in intensity of the PANI peaks can be seen in PMHP and PMOP samples due to the addition of PVC. The decrease in intensity of PANI vibrational peaks upon the addition of MWNT and PVC can be attributed to the better extent of interaction between the PANI chains, MWNT and PVC [27].

3.4.2.2 X-ray diffraction Analysis

The XRD patterns of PH, PMH, PMHP, PO, PMO and PMOP powder samples are shown in figures 3.9(a), (b), (c) and 3.10(a), (b), (c).

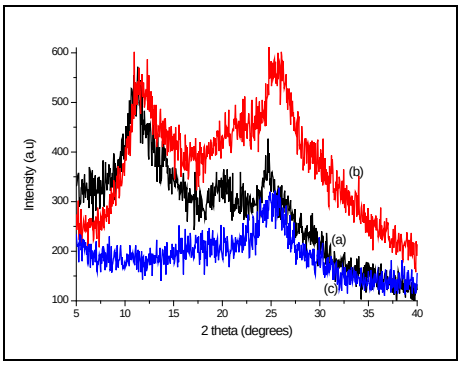

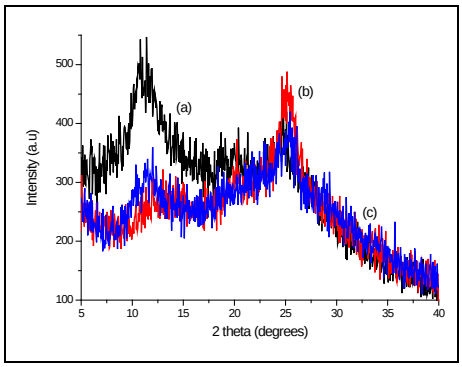

Figure 3.9: XRD patterns of (a) PH, (b) PMH, (c) PMHP, Figure 3.10: XRD patterns of (a) PO, (b) PMO, (c) PMOP powder samples

The XRD patterns of HCl (PH) and OPA (PO) doped PANI samples show semi-crystalline peaks around 11.35^{o}, 20.30^{o}, 24.75^{o}and 11.02^{o}, 20.30^{o}, 25.22^{o} respectively, as reported earlier [9]. In the PANI/MWNT composites (PMH and PMO), the peaks around 25^{o} have grown sharper, indicating the presence of MWNT [9, 25]. The intensity of XRD peaks of the PANI composite samples, PMHP and PMOP, has reduced considerably due to the presence of PVC which is an amorphous material.

3.4.2.3 Pressure Sensitivity Studies

Electrical conductivity of the pressed pellet samples of PANI and its composites was measured using Keithley 236 Source Measuring Unit (SMU) interfaced to a PC, adopting two probe technique. Pressure was applied to the samples by inserting calibrated weights on the sample holder. The variation in the electrical conductivity with applied pressure was investigated in the pressure range 0 to 140 kPa for all the six samples up to the saturation limit.

The variation in electrical conductivity with applied pressure was analyzed by plotting the percentage variation in electrical conductivity with applied pressure for the six PANI samples as shown in figures 3.11(a), (b), and (c). Since the percentage variation values are not comparable to each other, the graphs are shown as three separate figures. The same data is presented as a combined plot in figure 3.11(d).

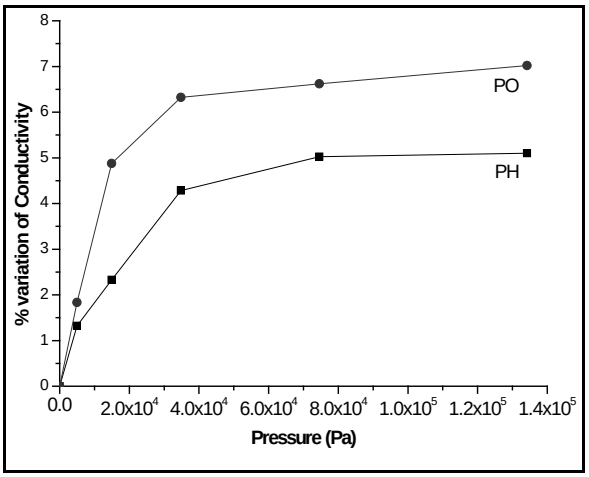

Figure 3.11(a): Percentage variation of conductivity with pressure for PO and PH pressed pellets

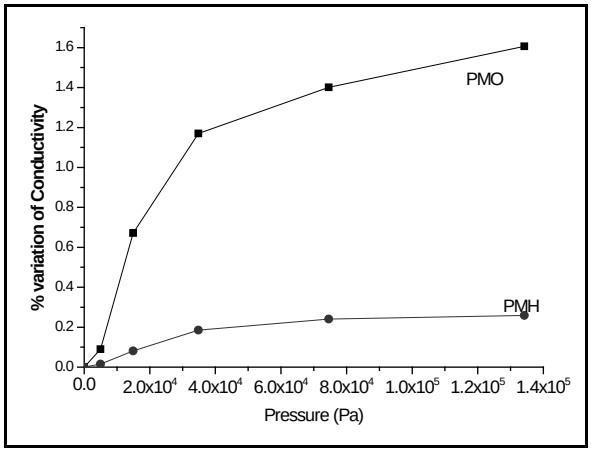

Figure 3.11(b): Percentage variation of conductivity with pressure for PMO and PMH pressed pellets

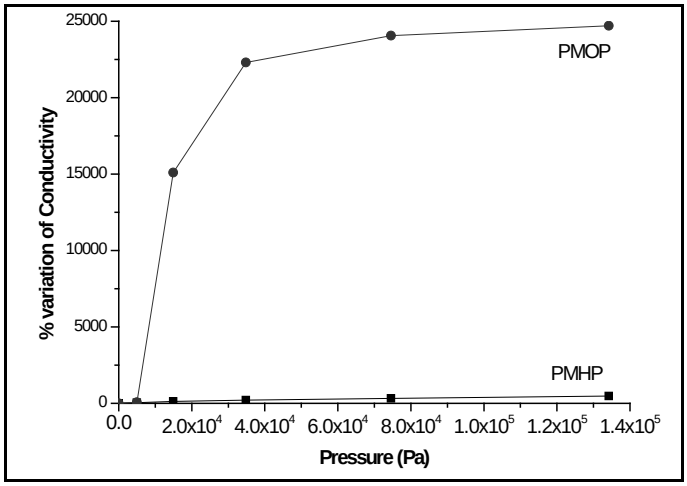

Figure3.11(c): Percentage variation of conductivity with pressure for PMOP and PMHP pressed pellets

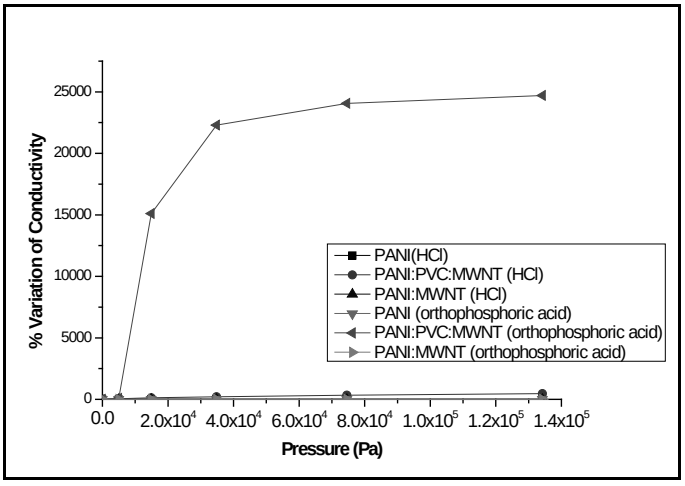

Figure3.11(d): Comparison of percentage variation of conductivity with pressure for all the six PANI samples

The dc electrical conductivity values with and without applied pressure for all the six PANI samples are shown in Table 3.2 [33].

Table 3.2: Conductivity of the samples without any load and with the maximum load applied.

Sample Code	Conductivity without applied pressure (S/cm)	Maximum Conductivity with maximum pressure (S/cm)
PH	0.9151	0.9618
PO	0.9001	0.9633
PMH	1.70053	1.72784
PMO	1.6204	1.6246
PMHP	0.015	0.0856
PMOP	$1.25x10^{-4}$	0.031

There is appreciable change in electrical conductivity with applied pressure only for the samples, PMOP and PMHP. For the rest of the samples, the change in conductivity with applied pressure is only marginal. Hence, it can be inferred that the presence of PVC and MWNT in the composite plays an important role in the sensitive dependence of conductivity on pressure.

The variation of conductivity with applied pressure and the percentage variation of conductivity are much pronounced and strikingly higher in PANI-PVC-MWNT composites. It is also found that OPA doped PANI-PVC-MWNT composite shows the highest percentage variation of conductivity when compared to other samples. PVC is an insulator and it separates the conducting PANI and MWNT islands so that any small applied pressure creates a conducting path between the separated PANI chains, MWNT or both. All the six samples reach the saturation value of conductivity at just about 80 kPa. It is also observed that PANI-PVC-MWNT composite samples do not regain its original

value of conductivity after the applied pressure is withdrawn, even after a very long time unlike the other samples which take less than 1 minute to regain the original conductivity. Although the percentage variation of electrical conductivity with applied pressure is highest for the PANI-PVC-MWNT composite samples, these samples suffer from the hysteresis effect. However, such a hysteresis effect is not observed in any of the nanostructured PANI samples.

3.5 Conclusions

In the present study, micro and nano structured PANI samples doped with different dopants and their composites have been investigated to analyze the change in electrical conductivity with applied pressure. Most of the samples respond to applied pressure with an appreciable variation of electrical conductivity. Even though PANI-MWNT-PVC composites show significant variation of conductivity with applied pressure, it cannot be categorized as an excellent pressure sensor due to the inherent hysteresis effect. For all the microstructured PANI samples and their composites, the pressure range over which the sensor application is possible is also limited. All the nanostructured samples and their composites show quite sensitive pressure dependence of electrical conductivity above 30MPa which is much higher than the saturation pressure limit possible with the microstructured samples. The highly pressure sensitive, nanostructured PANI samples and their composites offer prospects of applications as excellent pressure sensors. These pressure sensors are especially suitable for plantar foot pressure measurement systems used for designing footwear to suit the requirements of diabetic patients and sports personnel in a cost-effective way.

References

[1] Prasanna Chandrasekhar, *Conducting Polymers: Fundamentals and Applications*, Kluwer Academic Publishers, London (1999) pp 164-167

[2] Maddison D.S and Unsworth J, *Synth. Met*., **22**, 257 (1988)

[3] Reghu Menon et al, *Synth. Met*.,**69**, 329 (1978)

[4] Fernando G. Souza Jr, Ricardo C. Michel, Bluma G. Soares; *Polymer Testing*, **24,**998–1004(2005)

[5] Bao Z.X, Liu C.X, Pinto N.J, *Synth. Met.*,**87**, 147, 1997

[6] Jang, *J. Adv Polym Sci*, **199**, 189 (2006)

[7] Jang, J.; Bae, J.; Lee, K. *Polymer*, **46**, 3677 (2005)

[8] Huang, J.; Wan, M. *J Polym Science Part A: Polym Chem*.,**37**, 151 (1999)

[9] S. J. Varma, S. Jayalekshmi, *J. Appl. Polym. Sci.*, **117**, 138–142 (2010)

[10] Bellamy, A. J. *The Infra-red Spectra of Complex Molecules*(2nd ed.); Wiley: New York, (1962)

[11] Zhang, X.; Zhang, J.; Liu, Z.,*Appl Phy.A*, **80**, 1813 (2005)

[12] Zhang, L; Wan, M. *Nanotechnology*, **13**, 750 (2002)

[13] Zhang, et al, *Macromolecules*, **41**, 7671(2008)

[14] Jinsong, T.; Xiabin, J.; Baochen, W.; Fosong, W. *Synth Met*., **24**, 231 (1998)

[15] Wang, Y.; Rubner, M. F. *Synth Met.*, **47**, 255 (1992)

[16] MacDiarmid et al,*Mol Cryst Liq Cryst*, **121**, 187 (1985)

[17] Wan, M.; Li, M.; Li, J.; Liu, Z. *J Appl Polym Sci*., **53**, 131 (1994)

[18] Sapurinaet al,*Eur Polym J*, **36**, 2321 (2000)

[19] Terje A. Skotheim and John R.Reynolds, *Conjugated Polymers: Theory, Synthesis, Properties and Characterization*, CRC Press, Taylor & Francis Group, New York (2006), pp 7.6

[20] Keszler, A. M.; Nemes, L.; Ahmad, S. R.; Fang, X. *J Optoelectron Adv Mater*, **6**, 1269 (2004)

[21] Devendrappa, H.; Subba Rao, U. V.; Ambika Prasad, M. V. N.,*J Power Sources*, **155**, 368(2006)

[22] MacDiarmid, A. G. *Synth. Met.*, **125**, 11 (2001)

[23] Kim, S. G.et al,*Colloid Polym Sci*, **278**, 894 (2000)

[24] Geng Y, Li J, Sun Z, Jing X and Wang F, *Synth.Met*.**96,** 1-6 (1998)

[25] Amrithesh M, Aravind S, Jayalekshmi S and Jayasree R S , *J.Alloys Compd.*,**458,** 532-535(2008)

[26] Jang J, Bae J and Lee K, *Polymer*,**46,** 3677- 3684 (2005)

[27] Ahmed et al, *Sains Malaysiana*, **40**, 757-763 (2011)

[28] Kang et al, *Progress in Polymer Science*, **23**, 277-324 (1998)

[29] Kequing Zhagna and Xinli Jinga, *Polym. Advan. Technol*, **20**, 689-695 (2009)

[30] Sarifah Fauziah et al, *Malaysian Polymer Journal*, **4**, 7-18 (2009)

[31] S.Ramesh et al, *Spectrochimica Acta Part A*, **66**, 1237-1242 (2007)

[32] S.Ramesh et al, *Ionics*, **15**, 413-420 (2009)

[33] Sreekanth J Varma and S.Jayalekshmi, *Proc. of SPIE*,**7037**, 703716, (2008)

…..ஜ۞ஜ…..

Chapter 4

BLUE EMISSION IN POLYANILINE THIN FILMS: A QUEST FOR QUANTUM CONFINEMENT

Contents

Polyaniline (PANI) is well-known for its remarkable electrical and optical properties which find immense applications in polymer optoelectronics. Though extensive work has been reported in polyaniline samples both in bulk and thin film forms, much attention has not been paid to investigate the quantum confinement effects in ultra-thin polyaniline films. The present work is devoted to the search for quantum confinement effects in ultra-thin polyaniline films having nanometre thickness, prepared from m-cresol, through conventional and less sophisticated spectroscopic techniques. Remarkable blue-shift has been observed in the absorption spectrum of these samples. Much intense photoluminescent emission with considerable blue-shift observed in these ultra-thin films is cited as the clear evidence for confinement effects.

4.1 Introduction

Quantum confinement effects are well-known and investigated very well in metals and inorganic semiconductors in their nano dimensions. Nano sized materials exhibit entirely different properties in these length scales [1-7]. The structural, thermal, mechanical, optical and

electrical properties of nanomaterials are quite exciting and different from their bulk analogues. For example, gold appears in different colours and show modified electrical properties when the size is reduced below the confinement regime. Nanostructured inorganic semiconductors such as quantum wells and quantum dots find extensive applications in photonics and bio-photonics because of the unique characteristics they acquire in the nano regime [8-24]. Semiconducting and metal like conducting polymers have been subjected to extensive investigations during the past few decades [25] and their potential applications have been identified in many technologically advancing fields [25]. In spite of this, research on nanostructured polymers and confinement effects in polymers has not advanced much and is still in its budding state [26].

Polyaniline (PANI) is an extensively pursued conducting polymer having immense technological applications. Present work is an attempt to unravel quantum confinement effects in ultra-thin films of PANI synthesized by chemical oxidative polymerization technique. There are no reports on the quantum confinement effects in PANI films based on spectroscopic investigations. In semiconducting materials, spectroscopic investigations are widely known for identification of quantum confinement effects. Probably there is only a single paper related to confinement effects in polyaniline films in which a polyaniline based quantum well structure has been fabricated and the investigations are mainly based on sophisticated techniques such as Scanning Tunneling Microscopy (STM) and Scanning Tunneling Spectroscopy (STS) [27]. The authors also suggest that quantum well behaviour can be achieved in 40 nm sized, iodine doped PANI which is in the lower semiconducting

regime. The present work is significant since, conventional and cost effective spectroscopic techniques have been employed to confirm the quantum confinement effects in ultrathin PANI films. Polyaniline is cast as thin films from meta-cresol in nanometre and micrometre thickness scales and the quantum confinement effect is established in nanometre scale PANI through UV-VIS-NIR absorption and photoluminescence (PL) studies. Blue emission in PANI films is not reported in detail elsewhere and the intense blue emission observed in ultra-thin PANI films, in the present work, is novel in all respects.

4.2 Experimental Details

4.2.1 Synthesis of PANI films

Aniline and other reagents were bought from SD fine chemicals, India. Meta-cresol and aniline were distilled separately under reduced pressure before use. Other reagents were used as purchased. Pre-distilled aniline was polymerized in 1M HCl medium using 1M ammonium peroxydisulphate as initiator via chemical oxidative polymerization (28, 29), and the solution kept in a freezing mixture at -5^0C was stirred for 5 hours. It was then thoroughly washed and filtered using acetone and distilled water. The sample was dried in dynamic vacuum for 24 hours and ground to obtain PANI in its powder form. The obtained Emeraldine salt (ES) form of PANI was de-doped using 1M ammonia solution to obtain the Emeraldine base (EB). The obtained EB form of PANI was then washed and filtered thoroughly using plenty of distilled water and dried under dynamic vacuum for 24 hours. The EB powder (25mg) was re-doped using 1M (30mg) d-10-camphorsulphonic acid (CSA) to obtain the soluble and conducting form of PANI. The powder form of

conducting PANI was then dissolved in m-cresol (2.5mL) to obtain a good solution [29]. Homogeneous and good quality thin films in nanometre and micrometre thickness scales were obtained by spin coating (SPS Spin wafer 150) the solution at different spin speeds for different durations on ultrasonically cleaned glass substrates. The minimum thickness of PANI films spin coated on glass substrates was in the order of 50 nanometres and the maximum was about 4 micrometres. The thickness of the films thus obtained was measured using Dektak 6M stylus profiler and films with thickness 50 nm (±5 nm), 100nm (±5 nm), 150 nm (±5 nm) and 4 μm (±100 nm) were selected for the present studies. Although all micrometre thick samples (bulk) show the same properties (as it should be), the thickest film sample was selected as a representative for the bulk film sample whose properties have already been well investigated and characterized [30, 31, 32]. The film thickness could be precisely controlled by varying the viscosity of the PANI solution, spin speed and spinning time. Room temperature dc electrical conductivity of these PANI films was measured using standard 4-probe technique [33] employing Keithley 2400 source meter and Keithley 2001 multi-meter interfaced to a PC with a program developed in LabVIEW. These bulk films were found to be highly conducting with room temperature dc electrical conductivity of about 200 S/cm.

4.3 Sample Characterization

Fourier transform infrared spectra (FTIR) of PANI powder in the doped, de-doped and re-doped forms were obtained using Bruker–Tensor 27 FTIR spectrophotometer. The UV-VIS-NIR absorption studies of the samples were carried out using Jasco V-500 UV-VIS-NIR

spectrophotometer. The scan rate was fixed as 200nm/minute. The PL spectra of the PANI film samples were recorded using Fluoromax 3 fluorescence spectrophotometer.

4.3.1 FTIR Spectroscopic Studies

The FTIR spectrum of CSA re-doped PANI in powder form is shown in figure 4.1. The spectrum exhibits all the reported peaks, confirming the formation of CSA re-doped PANI. All the major peaks are listed in table 4.1 given below, with the respective vibrational assignments [34, 35, 36, 37]

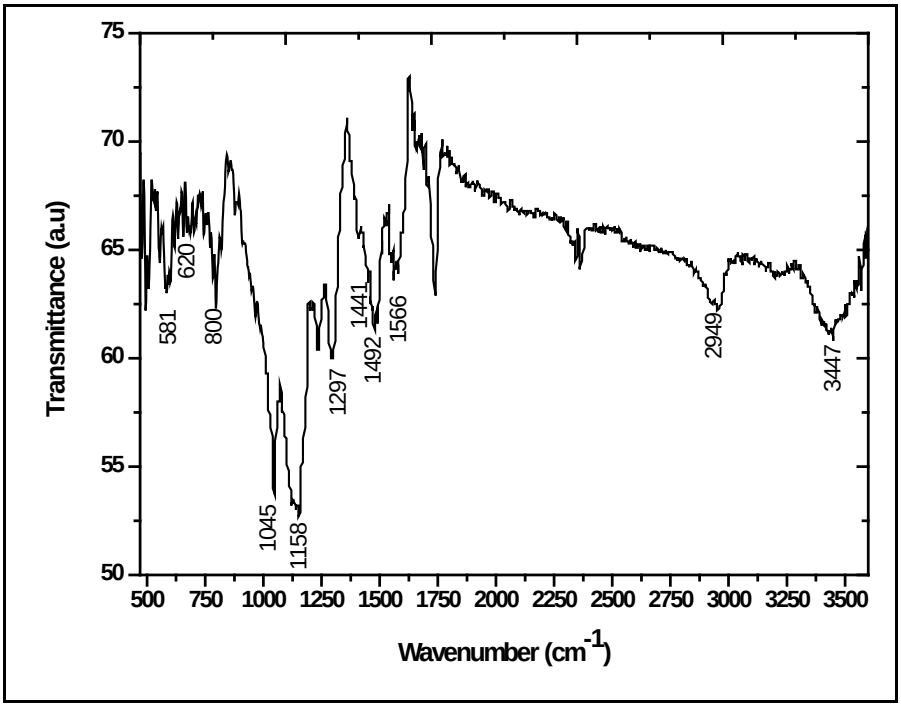

Figure 4.1: FTIR spectrum of CSA re-doped PANI

Table 4.1: FTIR data of CSA re-doped PANI

Wavenumber (cm^{-1})	Assignment
581	S=O stretching mode
800	aromatic C-H out of plane bending
1045	NH^+….SO_3- interaction
1158	vibrational mode of –NH^+= structure which occurs due to protonation of PANI
1297	C-N^+ stretching vibration in the polaron structure (characteristic of conducting protonated form
1441	C=C benzenoid ring vibration
1492	N-benzenoid ring stretching vibration
1566	N-quinoid ring stretching vibration
3447	ssN-H stretching

4.3.2 UV-VIS-NIR Spectroscopic Studies

Figures 4.2(a) and 4.2(b) show the UV-VIS-NIR absorption spectra of PANI films having thickness 4μm and, 50 nm, 100 nm and 150 nm. From the figures, one can see that the major absorption peak at 390 nm corresponding to the π to π^* transition in the 4μm thick PANI film has been blue-shifted to 294 nm in the case of ultra-thin PANI films with thickness 50 nm, 100 nm and 150 nm. A free-carrier absorption tail extending to the NIR region can also be seen in the absorption spectrum of the 4μm PANI thin film sample which indicates the metallic nature and the corresponding higher electrical conductivity of this sample [29]. However, such a free-carrier absorption tail is absent in the spectra of ultra-thin PANI films. The blue shift of about 100 nm observed in the

optical absorption spectra of ultrathin PANI films, compared to the micrometre thick PANI film provides the first indication of quantum confinement effects in ultrathin PANI films having thickness in the 50nm to 150 nm range. Figure 4.3(a) illustrates the estimation of the band gap energy of the 4 μm thick PANI sample which comes to about 2.37 eV (±0.1 eV). The band gap energy estimation of the ultra-thin PANI films (thickness - 50 nm, 100 nm and 150nm) is illustrated in figure 4.3(b). It is observed that all the three ultra-thin PANI samples have the same band gap energy of about 3 eV (±0.1 eV). The increase in band gap energy of the ultrathin PANI films provides another indication of the confinement effects in these samples.

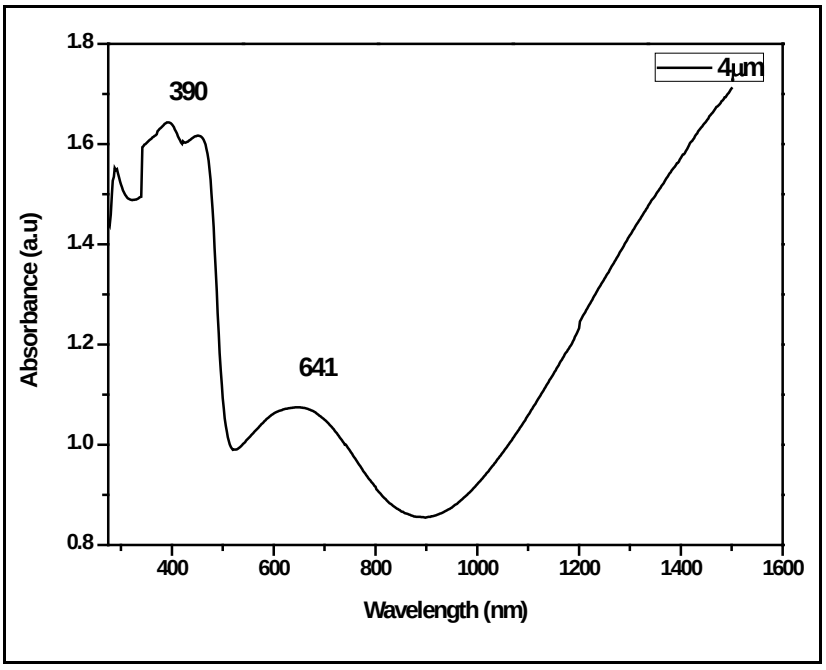

Figure 4.2 (a): UV-VIS-NIR absorption spectrum of 4μm PANI thin film

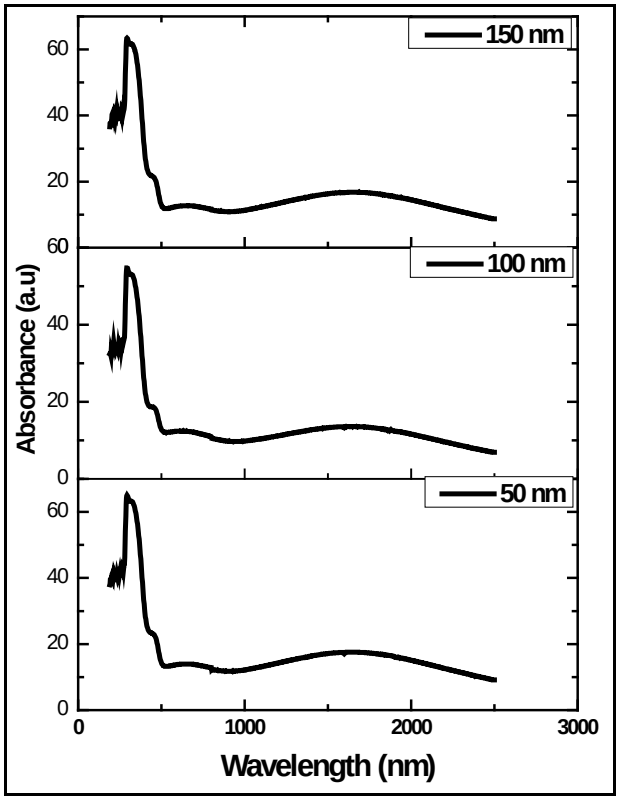

Figure 4.2(b): UV-VIS-NIR absorption spectra of ultrathin PANI films

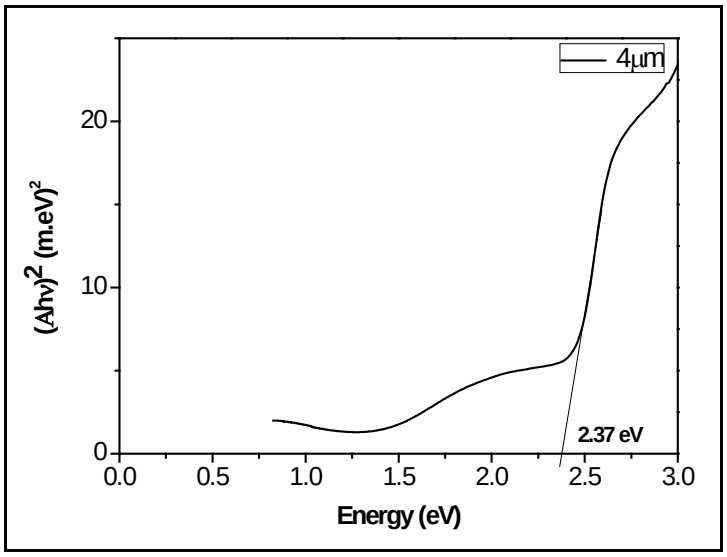

Figure 4.3(a): Band-gap estimation of 4μm thick PANI film

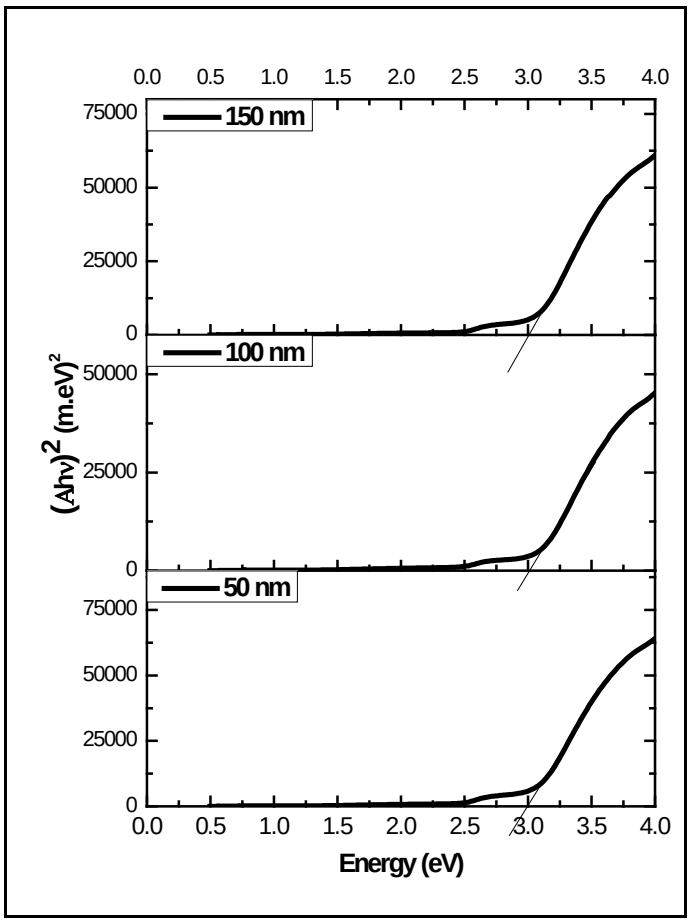

Figure 4.3(b): Band-gap estimation of ultrathin PANI films

4.3.3 Photoluminescence (PL) studies

Figure 4.4(a) depicts the PL spectrum of PANI film sample having 4 μm thickness, under an excitation wavelength of 350 nm. The corresponding PL spectra of ultra-thin PANI films having thickness 50 nm, 100 nm and 150 nm are shown in figure 4.4(b), for the excitation at 290 nm. All the nanometre sized thin film samples of PANI show intense emission around 419nm. The peak emission for the 4 μm thick PANI sample is at 519 nm. A blue shift of about 100 nm in the emission

peak in the PL spectrum of ultrathin PANI samples is observed when compared to that of the 4 μm thick PANI sample. This observation is another important evidence for the quantum confinement effects in nanometre sized ultrathin PANI films. The PL intensity of the nanometre sized thin films of PANI has increased 100 times compared to that of 4 μm sized PANI film. An intense violet-blue emission has been observed for all the nanometre sized PANI samples as shown in figure 4.5. The intense PL emission can be attributed to the larger oscillator strength and lesser polymer chain aggregation in ultrathin films of PANI [38]. The lifetime of excited state charge carriers is lesser in the case of ultrathin films, when compared to that in micrometre sized film of PANI. As a result, radiative transition predominates, resulting in an enhanced intensity in the PL emission.

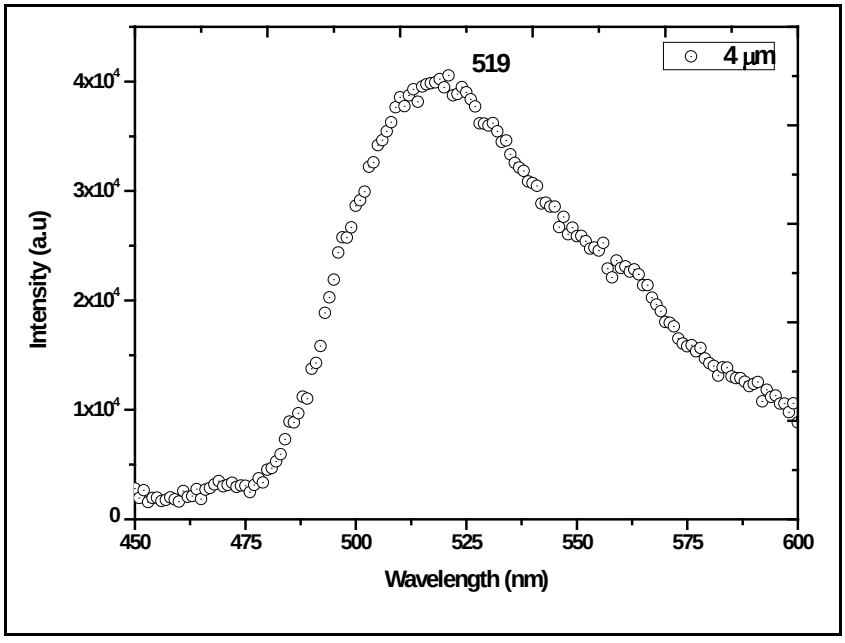

Figure 4.4(a): PL spectrum of 4μm PANI thin film

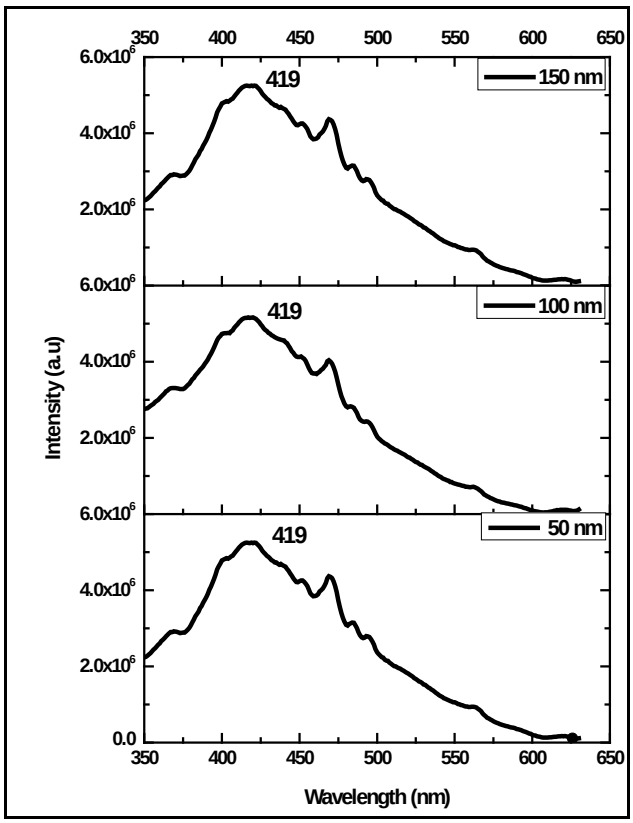

Figure 4.4(b): PL spectra of nanometre sized PANI thin films

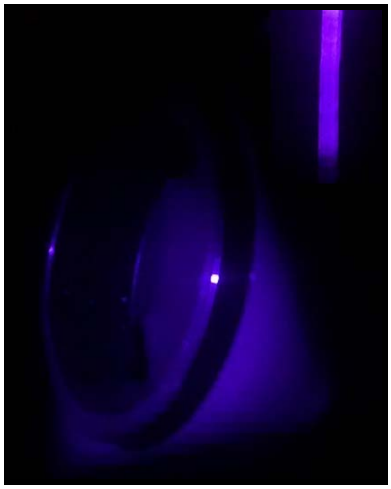

Fig 4.5: Photograph of intense violet-blue PL emission from ultrathin films of PANI (In-set is the light emerging through the slit and the main image is the reflected light from the interior of the spectrometer)

4.3.4 Atomic Force Microscopy

Conducting PANI has crystalline islands embedded in an amorphous sea. The crystalline islands are responsible for electrical conduction in PANI [39]. Confinement of charge carriers occurs inside these islands. In micrometre sized PANI films, the crystallites will be of micrometre size. But in ultra-thin films of PANI, the crystalline islands are of a few nanometers in size. This difference in crystallite sizes is a consequence of the various spin speeds used for film coating. For coating the micrometre sized PANI film, the solution was spun at lower speeds, whereas, much higher speeds were employed for the spin coating of ultrathin PANI films. On high speed spinning, the micrometre sized crystallites get broken down to smaller crystallites and are distributed homogeneously in the resulting film. AFM images of PANI films coated at lower and higher spin-speeds respectively are shown in figures 4.6(a) and 4.6(b).

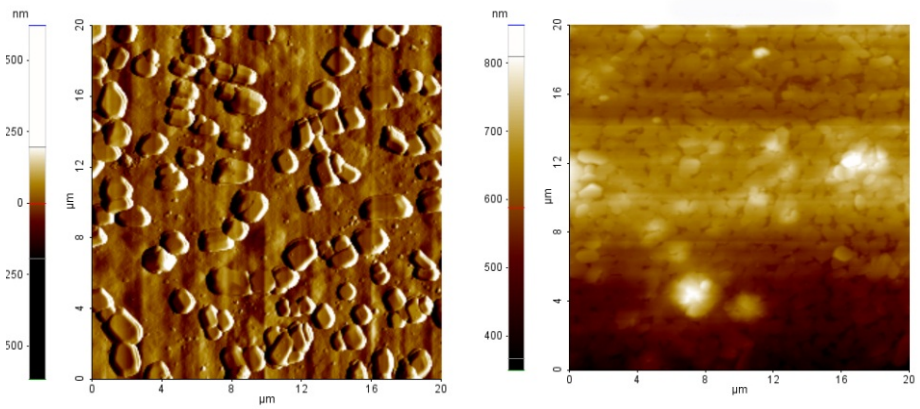

Figure4.6: AFM imagesof PANI films coated at (a) lower spin-speeds; (b)higher spin-speeds

As one can see from the above figures, the crystallite size has reduced on higher spin speeds on the formation of ultrathin films of PANI. Thus, increased spin speed has created smaller crystallites inside ultrathin films of PANI which is one of the prime factors responsible for quantum confinement in these films and the associated intense blue emission.

The effects of solution concentration and spin speed on polymer morphology have been thoroughly investigated in many polymer systems [40]. There is a strong correlation between the polymer morphology and the concentration of the polymer solution used to spin-coat the films. The morphology of the spin-coated polymer films also depends on the spin speed with which the films are coated. In higher concentrations, it is observed that the polymer tends to form aggregates as a result of the inter-chain attraction forces. But in dilute solutions, the chains are rather isolated. The forces of inter-chain (polymer-polymer) interactions are short ranged and hence can be neglected in very dilute solutions. The probability of entanglement of the polymer chains is quite insignificant in dilute solutions. When the concentration gets higher, the polymer-polymer interactions become more significant, which increase the probability of entanglement. The significant entanglement of the polymer chains results in strong chain aggregation in highly concentrated polymer solutions. These ideas are illustrated in figure 4.7.

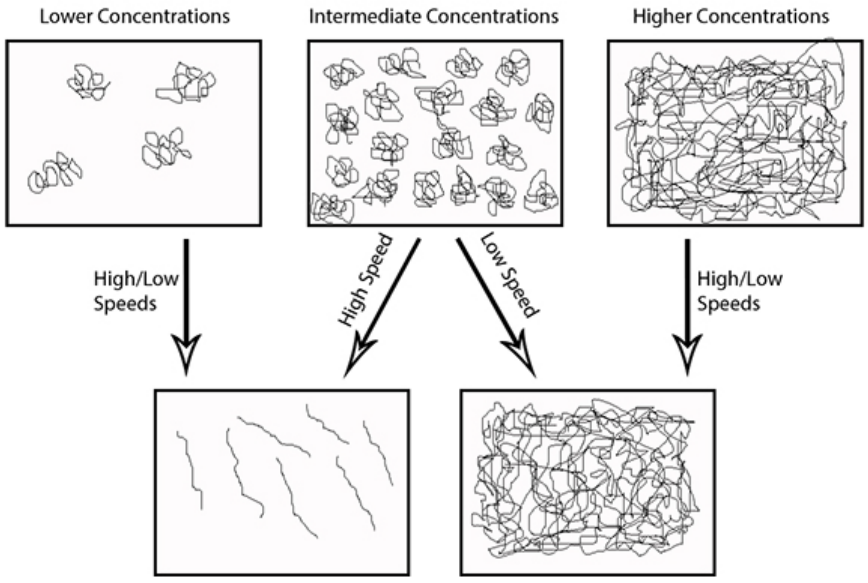

Figure4.7: Schematic diagram of polymer chains in spin-coated films deposited from polymer solutions of different concentrations with different spin speeds

A few methods [41, 42] have been suggested to understand the concentration dependence of polymer morphology based on these details. Ina method suggested by Shi et. al, the concentration regions can be characterized based on reduced viscocity (η/η^*), where η is the viscosity of the polymer solution and η^* that of the solvent. Three different regions have been found in the plot of η/η^* versus the concentration of the polymer solution. There is a linear region at lower concentrations, a curved region at intermediate concentrations and another linear region at higher concentrations. The plot suggests that the polymer chains are not entangled at lower concentrations but heavily entangled at very high concentrations. The intermediate region represented by the curved portion has been defined as that corresponding to the concentration of loose aggregation (CLA).The morphology of the

spin-coated polymer films strongly depends on the spin speed, in this region. In this region, lower speeds are not sufficient enough to break apart the polymer chains. As the spin speed increases, the aggregates break apart to form separate entities reducing the inter-chain interactions.

In the present work, higher spin speeds were used to make ultrathin films in which the polymer chains are separated. This separation blocks inter-chain hopping of charge carriers, thereby reducing the conductivity and isolating the conducting islands inside the polymer chains. These isolated, ordered regions inside the chains are too small in dimension, which is typically below 5nm [39, 43]. The dimensions of the conducting regions are thus compatible with the size requirements for confinement effects and bring about the observed blue shift in the absorption and PL spectra.

Similar spectroscopic investigations were also carried out in thin films of Polyvinyl alcohol (PVA) and Poly (methylmethacrylate) (PMMA) having the same thickness range as that of PANI films. There was absolutely no shift either in the absorption edge or in the PL emission peak of the ultrathin films of PVA and PMMA compared to those of the respective films having micrometre thickness. Both PMMA and PVA are good insulating polymers with practically very low charge carrier density and hence the concept of carrier confinement effects cannot be applied to these polymers. These observations provide additional confirmation for quantum confinement effects of charge carriers in ultrathin films of highly conducting PANI samples of the present work, based on spectroscopic investigations.

4.4 Conclusions

In the present work, quantum confinement effects in nanometre sized PANI thin films have been established based on the UV-VIS-NIR absorption and photoluminescence studies. The present work extends ample scope for developing nanostructures such as quantum wells of these polymer samples. The intense PL emission exhibited by the nanometre sized PANI films in the violet-blue region highlights the prospects of applications of these films as emissive layers in polymer light emitting diodes.

References

[1] Charles P.Poole and Frank J.Owens, *Introduction to Nanotechnology*, John Wiley & Sons,

[2] Inc., New Jersey (2003) pp8

[3] E. M. Kazaryan, L. S. Petrosyan and H. A. Sarkisyan, *Physica E*, **16**, 174 (2003)

[4] M. S. Gudiksen, J. Wang, C. M. Liber, *J. Phys. Chem. B*, **106**, 4036 (2002)

[5] H. Ajiki, *Journal of Luminescence*, **94**, 173 (2001)

[6] C. Piermarocchi, R. Ambigapathy, D. Y. Oberli, E. Kapon, B. Deveaud and F. Tassone, *Solid State Communications*, **112**, 433 (1999)

[7] W. Xie and C. Chen, *Physica B*, **266**, 373 (1999)

[8] G. A. Hughes, *Nanomedicine: Nanotechnology, Biology and Medicine*, **1**, 22 (2005)

[9] D. Alexson, H. Chen, M. Cho, M. Dutta, Y. Li, P. Shi, A. Raichura, D. Ramadurai, S. Parikh, M. A. Stroscio and M. Vasudev, *J. Phys.: Condens. Matter*,**17**, 637 (2005)

[10] R. E. Bailey, A. M. Smith and S. Nie, *Physica E*,**25**, 1 (2004)

[11] Y. Wang, Z. Tang and N. A. Kotov, *Materials Today*, **8**, 20 (2005)

[12] A.Hoshino, K.Hanaki, K. Suzuki and K. Yamamoto, *Biochemical and Biophysical Research Communications*, **314**, 46 (2004)

[13] Y. Cui, Q. Wei, H. Park and C. M. Lieber, *Science*, **293**, 1289 (2001)

[14] M. BruchezJr, M.Moronne, P. Gin, S. Weiss and A. P. Alivisatos, *Science*, **281**, 2013 (1998)

[15] D. Bimberget al,*Thin Solid Films*, **367**, 235 (2000)

[16] S. Iwamoto, J. Tatebayashi, S. Kako, S. Ishida and Y. Arkawa, *Physica E*, **21**, 814(2004)

[17] S. Lu, R. Jia, D. Jiang and S. Li, *Physica E*, **17**, 453 (2003)

[18] L. V. Asryan and S. Luryi, *Solid-State Electronics*, **47**, 205 (2003)

[19] C. Gmachl, A. Tredicucci, D. L. Sivco, A. L. Hutchinson, F. Capasso and A. Y. Cho, *Science*, **286**, 749 (1999)

[20] A. Tredicucci, C. Gmachl, F. Capasso, D. L. Sivco, A. L. Hutchinson and A. Y. Cho, *Nature*, **396**, 350 (1998)

[21] V. K. Kononenko, I. S. Manak and S. V. Nalivko, *SpectrochimicaActa Part A: Molecular and Biomolecular Spectroscopy*, **55**, 2091 (1999)

[22] W. H. Seo and B. H. Han, *Solid State Communications*, **119**, 367 (2001)

[23] L. Sirigu, L. Degiorgi, D. Y. Oberli, A. Rudra and E. Kapon, *Physica E*, **7**, 513 (2000)

[24] M. Asada, Y. Miyamoto, Y. Suematsu, *IEEE J. Quantum Electron.*,**22**, 1915 (1986)

[25] F. Klopf, J. P. Reithmaier, A. Forchel, *Appl. Phys. Lett.***77**, 1419 (2000)

[26] Ali Eftekhari (Editor), *Nanosrtuctured Conducting Polymers*, John Wiley & Sons, Inc., UK (2010), pp 60-74

[27] S.J.Varma, Jerin George, Jeeju.P.P, S.Jayalekshmi, *Journal of Luminescence*, **132**, 801-805(2012)

[28] Narayanan T N, et al,*J. Phys. D: Appl. Phys*.**42,**165309 (2009)

[29] Wang Y and Rubner M F, *Synth Met*. **47,**255-66**(**1992)

[30] MacDiarmid AG and Epstein A J, *Synth Met*. **69**, 85-92 (1995)

[31] L.H.Huo et al, Thin Solid Films, **350**, 5-9 (1999)

[32] Younan Xia and Alan G**.** MacDiarmid, *Macromolecules*, **27,** 7212-7214 (1994)

[33] Donald L Wise et al, *Electrical and optical Polymer Systems*, Marcel Dekker, Inc., New York, (1998) pp 365-376

[34] F.M.Smits, *The Bell System Technical Journal***37**, 711-718 (1958)

[35] KeqingZhanga and XinliJinga, *Polym. Adv. Technol*.**20**, 689–695 (2009)

[36] ChetnaDhand, Maumita Das, GajjalaSumana, Avanish Kumar Srivastava, Manoj Kumar Pandey, CheolGi Kim, Monika Datta and Bansi Dhar Malhotra, *Nanoscale*, **2,**747–754(2010)

[37] S.F.S. Draman, R. Daik, and A. Musa, *International Journal of Chemical and Biological Engineering*, **2** 112-119(2009**)**

[38] SarifahFauziah Syed Draman, RusliDaik and Musa Ahmad, *Malaysian Polymer Journal* **4,** 7-18(2009)

[39] Alexei Nabok, *Organic and Inorganic Nanostructures*, Artech House Inc., London (2005)pp.120

[40] Leite F L, Alves W F, Mir M, Mascarenhas Y P, Herrmann P S P, Luiz H C, Osvaldo M, Oliveira N, *Appl. Phys. A*, **93,** 537–542(2008)

[41] Joseph Shinar, *Organic Light Emitting Devices: A Survey*, Springer, AIP Press, USA, (2004) pp 157-166

[42] R.Simha and L.Ultrachi, *J.Polym.Sci. A*, **2**, 853 (1967)

[43] Y.Shi, J.Liu, and Y.Yang, *J.Appl.Phys.*,**87**, 4254 (2000)

[44] F. Lux et al, *Synth. Met.*, **55**,347-352 (1993)

…..ஜ۞ஜ…..

Chapter 5

HIGHLY CRYSTALLINE POLYANILINE FILMS

Contents

Polyaniline is one of the most promising conducting polymers ever studied owing to its tunable electrical, optical and structural properties. The conductivity values of polyaniline have reached optimum values that can be achieved by doping. A further enhancement is possible only by improving the order within and among the polymer chains. In this study, films doped with CSA and NSA made from m-cresol via ultrasonication is reported to achieve very high extent of crystalline order. This has been established through X-ray diffraction experiments conducted on these polyaniline films. Simple chemical methods like chemical oxidative polymerization and dispersion polymerization have been adopted to synthesize PANI films of excellent crystallinity and very high conductivity values. Further increase in conductivity can be achieved by suitably adjusting the dopant concentration. The XRD spectra corresponding to the crystalline PANI were index accordingly and crystal systems similar to cubic, monoclinic and triclinic could be identified. Such exceptional crystallinity and corresponding crystal systems in polyaniline is novel in all respects.

5.1 Introduction

Polyaniline is one of the most promising conducting polymers ever studied owing to its tunable electrical, optical and structural properties [1, 2]. The highest electrical conductivity of polyaniline that can be achieved through suitable doping has already reached its saturation limits [3-5]. Any further enhancement in conductivity is possible only through an intelligent manipulation of the order within and among the polymer chains [6, 7].

Crystallinity in conducting polymers, especially in polyaniline, is determined by the extent of conjugation and order in the material. Enhancement in conductivity is one of the chief consequences of improving the order and the extent of conjugation in polyaniline [1]. Highly conducting polyaniline can hence be realized by the appropriate choice of the synthesis techniques followed by the skilful modifications wherever necessary. The extent of conjugation cannot be increased infinitely [8]. The other option is to adopt methods to enhance the crystallinity which in turn will result in a drastic improvement in conductivity [2, 9-12].

Only a few papers have been published, related to the synthesis of highly crystalline PANI films with ordered structure and high electrical conductivity [13, 14]. The reported conductivity values range from 200-400 S/cm in chemical oxidative polymerized PANI samples [5] and from 1000-1200 S/cm in those samples prepared using self-stabilized dispersion polymerization [3, 15]. There is a strong relation between dc electrical conductivity and crystallinity of polyaniline and the conductivity gets enhanced with increase in crystallinity [16].

In the present work, polyaniline films with high crystallinity and electrical conductivity were synthesized adopting chemical oxidative polymerization and dispersion polymerization methods. Co-doped polyaniline using hydrochloric acid (HCl) and dodecyl benzene sulphonic acid (DBSA) was also investigated to study the role of dopants in the crystalline structure in polyaniline films. Spin coated thin films of these polyaniline samples were cast on glass substrates from the de-protonated and re-doped sample solutions in suitable solvents. Detailed investigations on the crystalline structure of these PANI films were carried out mainly using X-ray diffraction. The extent of crystallinity, crystal structure and morphology observed in all these samples are novel, as far as PANI films are concerned.

5.2 Materials for Synthesis

Aniline, ammonium persulphate, HCl, *m*-cresol, N-methylpyrrolidone (NMP) chloroform, orthophosphoric acid, *β*-naphthalene sulphonic acid (NSA) and *d-10*-camphorsulphonic acid (CSA) were purchased from SD fine chemicals. Dodecyl benzene sulphonic acid (DBSA) was purchased from Sigma Aldrich. Aniline and *m*-cresol were distilled under reduced pressure prior to usage.

5.3 Highly crystalline polyaniline films by chemical oxidative polymerization

5.3.1 Synthesis of highly crystalline PANI films

Conducting form of polyaniline (PANI) in powder form was synthesized by chemical oxidative polymerization of aniline in 1M HCl using 1M ammonium peroxydisulphate as initiator [17]. The reaction

was carried out for 4 hours in an ice bath (rock salt mixture) while stirring. The resultant polymerized sample was washed and filtered using acetone and water thoroughly for removing oligomers and excess acid. The filtered product was then dried under dynamic vacuum for 24 hours and then powdered to obtain polyaniline in the form of fine particles. The PANI powder thus obtained was de-doped using 1M ammonia solution and then re-doped using 1M *d-10*-camphorsulphonic acid (CSA). The re-doped sample was dissolved in NMP and *m*-cresol separately to study the role of solvents on the crystallinity of the films prepared. The sample solutions were ultrasonicated for several hours to obtain good solutions. The solutions were filtered using 0.45 micron PTFE filter. Films were then coated on glass substrates by spin coating process (SPS Spin wafer 150) at 500 rpm for 15s and dried under dynamic vacuum to get homogeneous and good quality films of about 1.5μm thickness. The thickness of the films was determined using Veeco Dektak 6M stylus profiler.

5.3.2 Characterization

The PANI powder and film samples were structurally characterized using X-ray diffraction (Rigaku X-ray diffractometer with Cu-Kα radiation (1.542Å)), Fourier Transform Infrared Spectroscopy (Bruker–Tensor 27), Scanning Electron Microscopy (Hitachi SU 6600 FESEM) and Atomic Force Microscopy (Park XC100). Thermo-gravimetric analysis (Q50, TA Instruments) was carried out to assess the temperature stability of PANI samples. The UV-VIS-NIR absorption studies of the samples were also done using Jasco V-500 UV-VIS-NIR spectrophotometer.

The dc electrical conductivity of the samples was measured using the standard 4-probe technique [18] employing Keithley 2400 source

meter and Keithley 2001 multi-meter interfaced to a PC with a program developed in LabVIEW. The whole electrode set-up with sample was kept in a conductivity cell under dynamic vacuum conditions of pressure about 10^{-3} mbar in which the sample temperature could be varied using a PID controller.

5.3.2.1 XRD analysis of HCl doped and CSA re-doped PANI

The XRD spectra of HCl doped and CSA re-doped PANI in powder form are shown in figure 5.1. The characteristic peaks of PANI are observed around 12^o, 21^o and 25^o. The crystalline peak of PANI at 25^o has grown sharper in the CSA re-doped PANI compared to that in HCl doped PANI. It is reported that in highly conducting metal like PANI powder samples, the peak at 25^o dominates and those at 12^o and 20^obecome less intense and almost vanish [3]. In the present work, the XRD spectrum of CSA re-doped PANI exhibits these features prominently compared to that of HCl doped PANI. Thus, re-doping with CSA has improved the conducting properties of PANI.

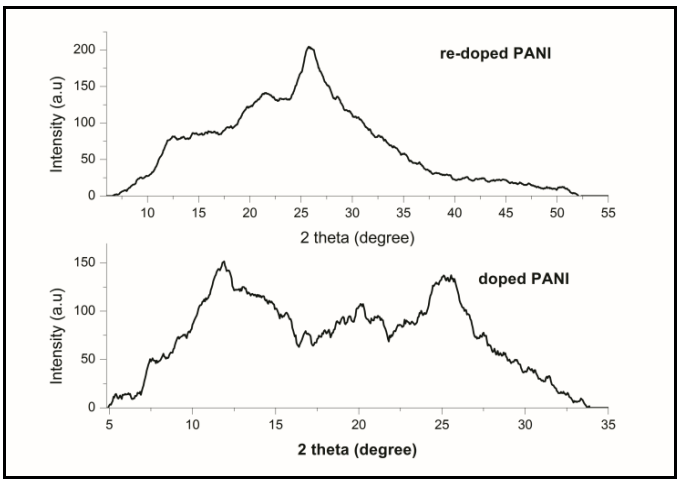

Figure 5.1: XRD spectra of (a) HCl doped and (b) CSA re-doped PANI.

5.3.2.2 Analysis of FTIR studies of powder and film forms of PANI

The FTIR spectra of the HCl doped, de-doped and CSA re-doped forms of PANI are shown in figure 5.2. In figure 5.2(a), the major peaks observed at 1589cm^{-1},1495cm^{-1},1309cm^{-1},1163cm^{-1}and 831cm^{-1} are in good agreement with the already reported peaks of PANI (Emeraldine Base) confirming the formation of de-doped PANI [19, 20]. In figures 5.2(b) and 5.2(c), the major peaks are at around 1570cm^{-1}(C=N stretch of the quinoid unit of PANI), 1479cm^{-1} (C=C stretch of the benzenoid unit of PANI) and 1106cm^{-1}(quinoid unit vibration of doped PANI) which agree with the peaks reported earlier [19, 21-23]. In the FTIR spectrum of HCl doped PANI, the intensity of 1309cm^{-1} peak has increased, which confirms the effect of HCl doping [17]. The presence of the peak at 610cm^{-1} which corresponds to C-Cl stretching mode, also confirms the formation of HCl doped PANI [24]. In figure 5.2(c), the vibrations of -SO_3H group are observed at 790cm^{-1} and 1045cm^{-1}, which confirm the presence of the dopant CSA [7, 25], in CSA doped PANI.

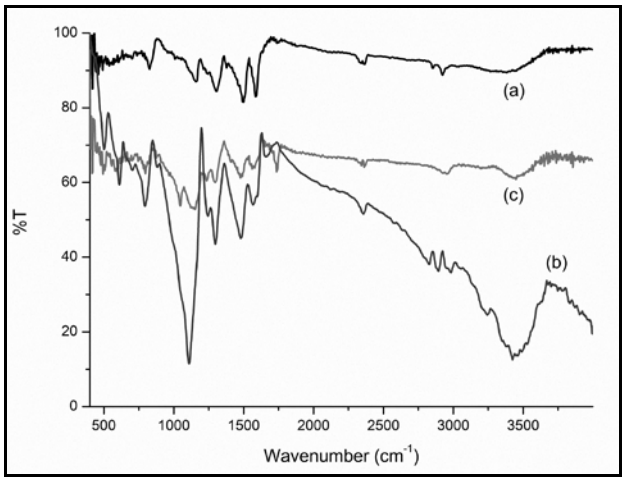

Figure 5.2: FTIR spectra of (a) de-doped, (b) HCl doped, and (c) CSA re-doped PANI

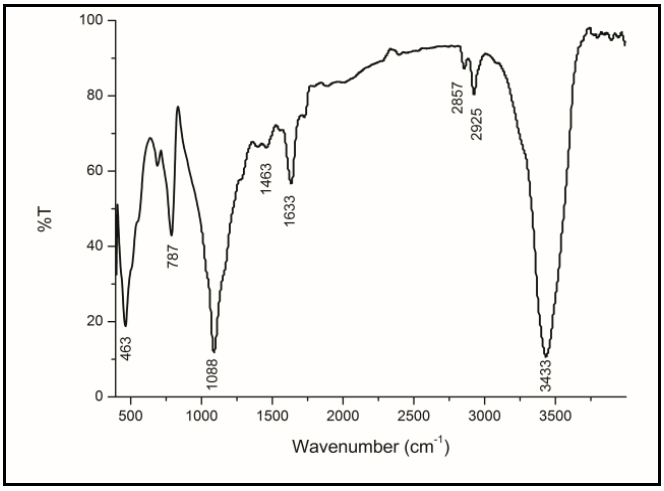

Figure 5.3: FTIR spectrum of CSA re-doped PANI film, from m-cresol

The FTIR spectrum of CSA re-doped PANI film cast from *m*-cresol is shown in figure 5.3. Major peaks can be seen at 787cm^{-1} (sulphonic acid group), 1088cm^{-1} (C-C stretching), 1463cm^{-1}(aromatic ring retained), 2857cm^{-1}, 2925cm^{-1} and 3433cm^{-1}(N-H stretching) [26-28]. The peaks at 2857cm^{-1}, 2925cm^{-1} are due to traces of m-cresol present even after drying the film. It is observed that in the FTIR spectrum of CSA re-doped PANI film, the peaks appear more well-defined and sharper. This is a consequence of the formation of a more ordered polymer structure in the CSA re-doped PANI film.

5.3.2.3 TGA of doped, de-doped and re-doped PANI

The thermograms of HCl doped, de-doped and CSA re-doped PANI, are shown in figure 5.4. From the figure, it is clear that the thermal stability of all the samples is quite high. The CSA re-doped sample has higher stability compared to HCl doped sample, up to 300^{0}C. The de-doped EB sample is very stable up to 525^{0}C. In the CSA re-doped PANI, the first mass loss at 100^{o}C is due to the elimination of

humidity in the sample. The second mass loss at 232^0C can be attributed to the degradation of CSA and the third at 375^0C can be recognized as the beginning of polymer backbone degradation [13, 29]. Thermal analysis of CSA re-doped PANI is in good agreement with the earlier reports [30].

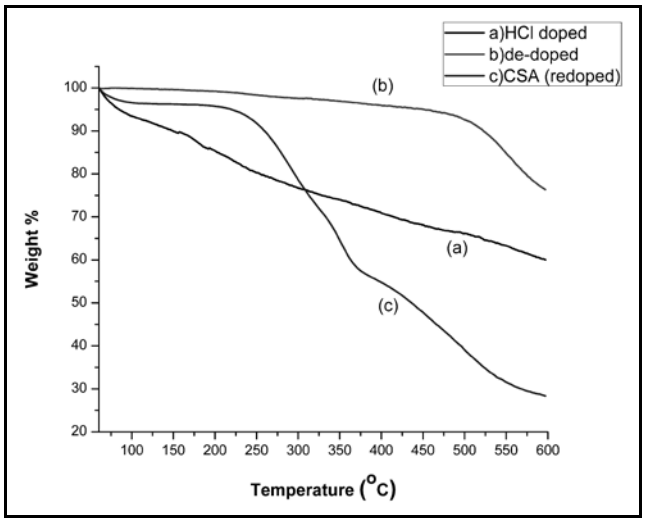

Figure 5.4: Thermograms of (a) HCl doped, (b) de-doped and (c) CSA re-doped PANI

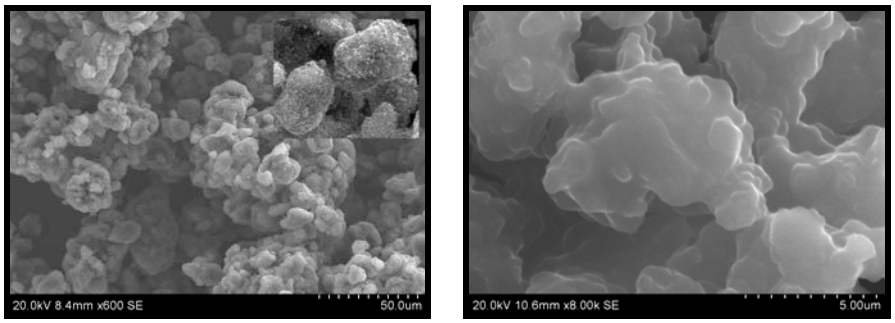

Figure 5.5: SEM images of (a) HCl doped PANI and (b) CSA re-doped PANI

HCl doped PANI powder is insoluble in most of the conventional solvents, whereas the CSA re-doped PANI shows better solubility. Figures 5.5(a) and 5.5(b) show the SEM images of HCl doped PANI and

CSA re-doped PANI samples. From these images, it is clear that the morphology has changed while re-doping the sample using CSA [26, 31]. HCl doped PANI has a morphology resembling closed globules whereas the CSA re-doped PANI exhibits open and flake like morphology. The morphology change might have improved the solubility of the CSA re-doped PANI which is found to be highly soluble in both *m*-cresol and NMP.

5.3.2.5 UV-VIS-NIR Spectroscopic Studies of PANI films

The optical absorption spectra of PANI films cast from NMP and *m*-cresol are shown in figure 5.6.In the optical absorption spectrum given in figure 5.6(a), the free carrier absorption tail extending to the NIR region, in the case of PANI films prepared from *m*-cresol can be clearly seen. It shows the metallic nature of PANI films [5] with *m*-cresol as the solvent. *M*-cresol in these films acts as a secondary dopant to enhance the conductivity of the films in addition to CSA [32]. The higher electrical conductivity observed for these films of PANI can thus be attributed to the effects of both *m*-cresol and CSA dopants. The absorption peak corresponding to π- π^* transition in *m*-cresol cast films of PANI can be seen at 440nm and that in NMP films of PANI, at 350nm [5]. Another broader absorption observed in NMP cast films of PANI at 850nm can be attributed to π to polaron transition [29].

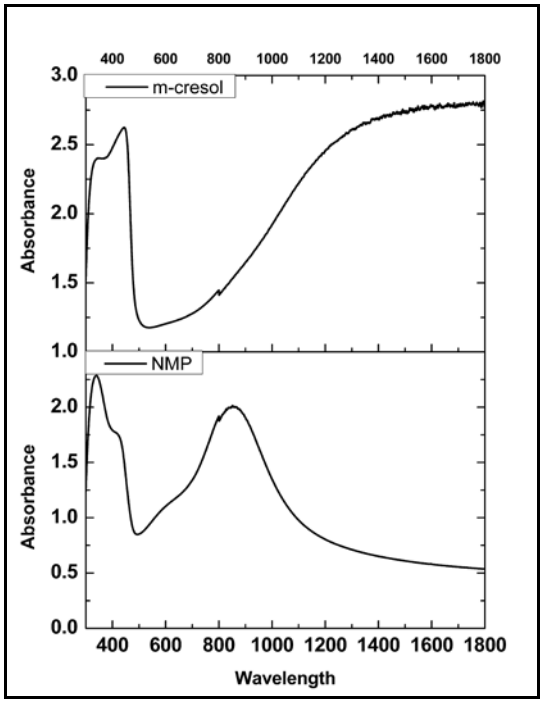

Figure 5.6: UV-VIS absorption spectra of (a) *m*-cresol and (b) NMP dissolved films of PANI

5.3.2.6 XRD analysis of highly crystalline PANI films

The XRD spectrum of CSA re-doped PANI film prepared from *m*-cresol is shown in figure 5.7 (a). The XRD spectrum confirms the presence of exceptionally high crystallinity/ordering in the film sample. Highly intense and sharp crystalline peaks can be observed at 5.5^{o}, 15.8^{o} and 20.8^{o}. Additional smaller crystalline peaks can be seen at 7.8^{o} and 36.7^{o}. An amorphous peak can be observed at 25^{o}. High extent of crystallinity has recently been reported in PANI films [33] where the synthesis method used is different from the method used in the present work. The excellent crystallinity observed in the XRD spectrum of the CSA re-doped PANI films of the present investigations has not been reported in any of the previous studies. It has already been reported that ultrasound

irradiation can bring about improved crystallinity in PANI samples [34]. In the present work, PANI solutions have been ultrasonically irradiated for several hours to obtain homogeneous solutions. The combined effects of ultrasonic irradiation and the secondary doping of *m*-cresol can be the prime factors contributing towards the high extent of crystallinity observed in the PANI films prepared from *m*-cresol [34].

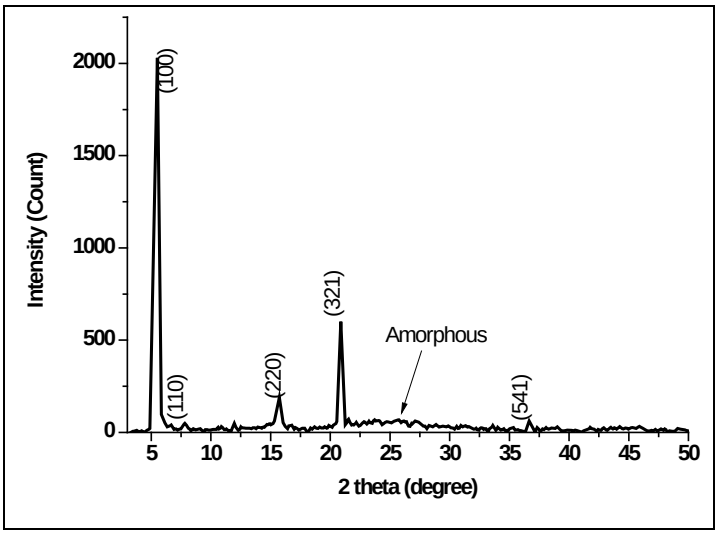

Fig 5.7(a): XRD pattern of PANI film from *m*-cresol

The XRD spectrum of PANI film prepared from NMP is depicted in figure 5.7(b), which agrees with the reported spectrum, with a crystalline peak at 19^{o} [35]. The presence of this broad crystalline peak can also be attributed to the effect of ultrasonic irradiation of PANI samples in NMP solution. Unlike the powder forms of PANI, NMP cast PANI film shows better crystallinity as a consequence of re-doping using CSA and ultrasonication.

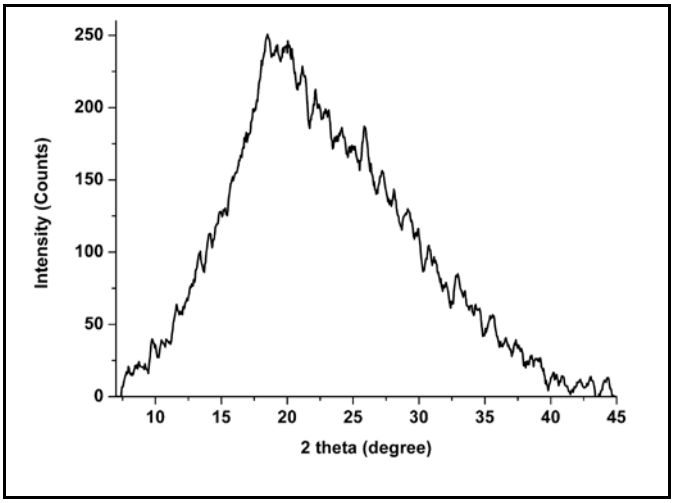

Fig 5.7(b): XRD pattern of PANI film from NMP

It can be deduced that ultra-sonication allows the proper ordering of PANI molecules in the films and contributes to the higher order of crystallinity than the powder forms of PANI. From the XRD spectrum of PANI film prepared from *m*-cresol, the d-spacing values corresponding to the peaks at 5.5^{o}, 15.8^{o} and 20.8^{o} can be calculated as 16Å, 5.6Å and 4.2Å respectively. The d-value of 5.6Å suggests an intra-chain ordering within the PANI molecules. The d-spacing of 4.2Å associated with the diffraction peak at 21^{o} corresponds to the face-to-face inter-chain stacking distance between phenyl rings which improves π–π inter-chain stacking. In effect, a more planar chain conformation with reduced torsion angles between the phenyl rings and the plane of the backbone, resulting in elongation of the effective conjugation length can be observed. This results in an improved carrier transport and a longer mean free path [3]. In addition, the d-value of 16Å corresponding to the highly intense and sharp peak at 5.5^{o} is an indication of the order closely associated with the dopant ions between the polymer chains [4, 17].

The percentage crystallinity of this highly crystalline PANI film is deduced from the XRD spectrum using the relation [36, 37],

Percentage crystallinity, $A_p = (A_c/(A_c+A_a))x100$ ----------(1)

where A_c=area under the crystalline peak, A_a= amorphous peak area and A_c+ A_a= total area including crystalline and amorphous peak regions. The area under the crystalline peaks and amorphous peaks has been calculated using multiple-peak fit programme in Origin 8.

The percentage crystallinity is found to be 79.8% which confirms the existence of exceptional order in these PANI films prepared from *m*-cresol. The average crystallite size is found to be 27 nm, using the Scherrer formula [36].

The peaks are indexed by calculating hkl indices according to available literature [38] and the details are shown in table 5.1. The hkl indices suggest a simple cubic crystal structure, and the lattice parameter is found to be 1.59nm. For indexing the peaks in the XRD spectrum, the lower intensity crystalline peaks (7.83^0 and 36.66^0), in addition to the highly crystalline peaks have also been considered.

Table 5.1: Indexed peaks of CSA re-doped PANI film (Cubic system)

$Sin^2\theta$	$h^2+k^2+l^2$	hkl	Sinθ	a (nm)
0.995	1	100	0.04	1.59
2	2	110	0.06	1.59
8.107	8	220	0.13	1.58
13.982	14	321	0.18	1.59
42.146	42	541	0.31	1.58

5.3.2.7 AFM analysis of highly crystalline PANI film

Conducting PANI consists of islands of ordered/crystalline regions embedded in a sea of amorphous region [39]. These regularly arranged regions are the prime factors responsible for the high electrical conductivity of PANI. Conduction can occur due to inter-chain hopping in addition to intra-chain hopping. Tunneling of charge carriers from crystalline to crystalline regions through the amorphous regions is also a possible conduction process in PANI. Thus, electrical conduction in PANI is due to the collective effects of inter-chain hopping, intra-chain hopping and tunneling of charge carriers. AFM is regarded as a standard technique to study the topography of thin films in a high resolution scale [40]. Figure 5.8 shows the AFM image of the thin film of CSA re-doped PANI dissolved in *m*-cresol. From the figure, one can see the distribution of micrometre and nanometre sized regular shaped crystalline regions on the surface of the film.

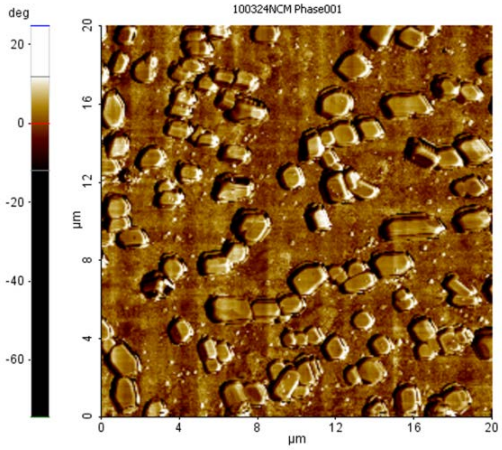

Figure 5.8: AFM phase image of the thin film of CSA re-doped PANI from *m*-cresol

The distance between the crystalline regions is too small so that the intra crystalline hopping or tunneling of charge carries is possible in addition to inter-crystalline hopping which enhances the overall conductivity of the thin film. The AFM image together with the XRD spectrum of PANI film prepared from *m*-cresol gives a clear picture of the regular arrangement of PANI molecules inside each crystallite.

5.3.2.8 DC electrical conductivity studies of PANI films

The room temperature dc electrical conductivity of PANI films has been measured under dynamic vacuum conditions, using the 4-probe technique. The conductivity of the *m*-cresol film of PANI is found to be 473S/cm which is much higher compared to that of NMP film of PANI which is only 16.6S/cm. DC electrical conductivity values suggest a high extent of order in PANI films prepared from *m*-cresol.

The variation of dc electrical conductivity of the PANI films prepared from m-cresol with temperature is shown in figure 5.9. The experiment was conducted using standard 4-probe set-up where the sample film was kept inside a conductivity cell in which a pressure of 10^{-3} mbar was maintained and the temperature was varied from room temperature to 425 K. It is observed that the dc electrical conductivity decreases with increasing temperature. However, the variation with temperature is not very significant (about 18% decrease in conductivity for an increase of 150^0C in temperature). As the temperature increases, the molecules are set into vibrations resulting in a decrease in the mobility of the charge carriers due to scattering. The vibrating molecules slightly distort the ordering/crystallinity of the polymer system. The slight distortion in the ordering is the prime factor for the observed decrease in

electrical conductivity. It is observed that on cooling to room temperature, the same film retains its room temperature conductivity. This is an indication that the decrease in conductivity with increase in temperature, in the temperature range used in the present work, is not due to any permanent change in the polymer structure or the escape of the dopants. In other words, no permanent distortion happens to the polymer in the temperature range studied, which is below the glass transition temperature of PANI. Hence it can be concluded that the polymer films cast from *m*-cresol possess good temperature stability up to around 425K.

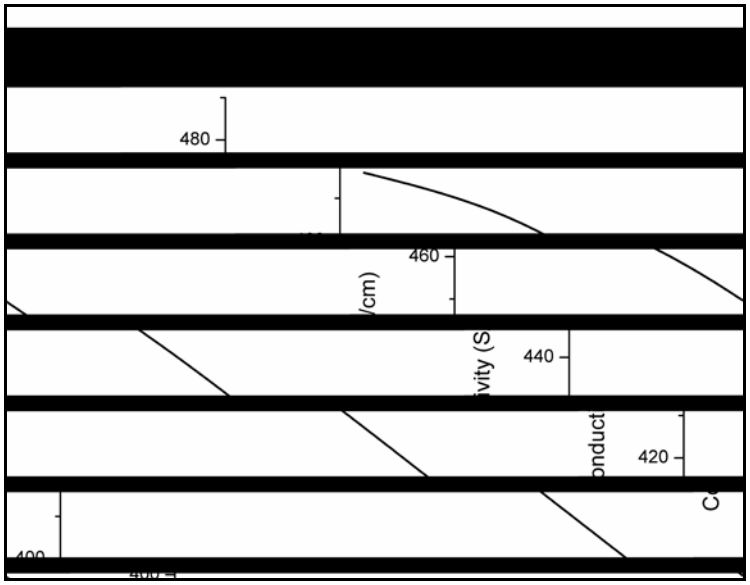

Figure 5.9: Variation of dc electrical conductivity with temperature of PANI films prepared from *m*-cresol

5.4 Crystallinity in HCl and DBSA co-doped PANI films, synthesized by chemical oxidative polymerization

5.4.1 Synthesis of highly crystalline, co-doped polyaniline films

Co-doped polyaniline was synthesized using HCl and DBSA as dopants. 1M HCl and DBSA were taken in 1:1 proportion (50 mL each).

Distilled aniline (5mL) was stirred in HCl-DBSA solution in an ice bath [41]. Green PANI powder was obtained following the procedures described earlier. PANI powder was de-doped using 1M ammonia solution. De-doped PANI was then re-doped using CSA and NSA separately and dissolved in m-cresol to obtain good solutions. The solutions were ultrasonicated for several hours. Good quality thin films of polyaniline, re-doped with NSA (***PA-NS***) and CSA (***PA-CS***) were spin-cast on glass slides using these solutions.

5.4.2 Characterization

5.4.2.1 FTIR studies of PA-NS and PA-CS films

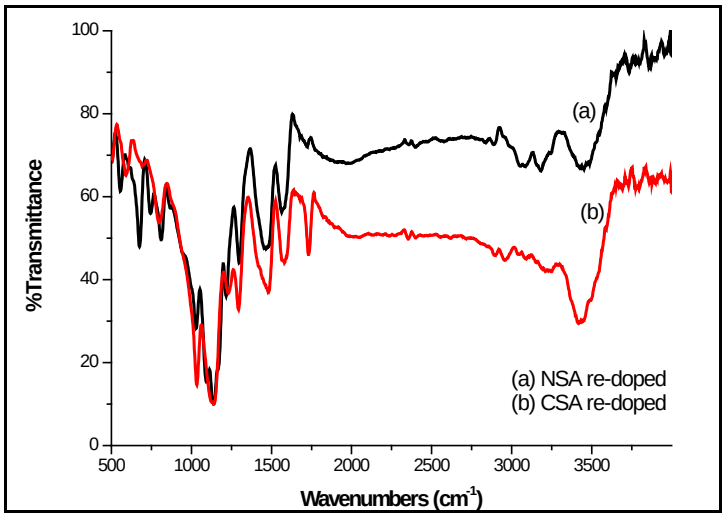

Figure 5.10: FTIR spectra of (a) PA-NS and (b) PA-CS films

The FTIR spectra of NSA and CSA re-doped PANI film samples (PA-NS and PA-CS respectively) are shown in figure 5.10. FTIR spectra show all the characteristic peaks of doped PANI along with those of $-SO_3H$ groups, indicating the presence of NSA and CSA dopants. The wavenumbers and the corresponding vibrational assignments are tabulated in table 5.2 [42-45].

Table 5.2: FTIR data of PA-NS and PA-CS films

Wavenumber (cm^{-1})		Assignments/Comments
PA-NS	PA-CS	
556, 486	590, 506	aromatic ring deformation
744		C-H op on 1,2 ring
1030	1033	$-SO_3H$ group vibrations
1138	1139	characteristic of doped PANI derived from an ordered organization indicating longer effective conjugation length
1216	1230	C-N str of BBB
1298	1293	C-N str
1468	1479	str of benzene ring
1563	1581	str of N-Q-N
1723	1730	C=N str of Q
3451	3429	NH_2 asym str

Abbreviations: op = out-of-plane, str = stretching, B = benzenoid unit, Q = quinoid unit, asym = asymmetric

5.4.2.2 TGA of PA-NS and PA-CS films

The thermal degradation of the film samples of the polymer under study was investigated using Q50 thermo gravimetric analyzer, TA Instruments. Figures 5.11(a) and (b) show the thermograms of PA-NS and PA-CS films prepared from co-doped PANI. The thermal stability of these films is found to be quite high. The degradation starts only above 250^0C in both the film samples.

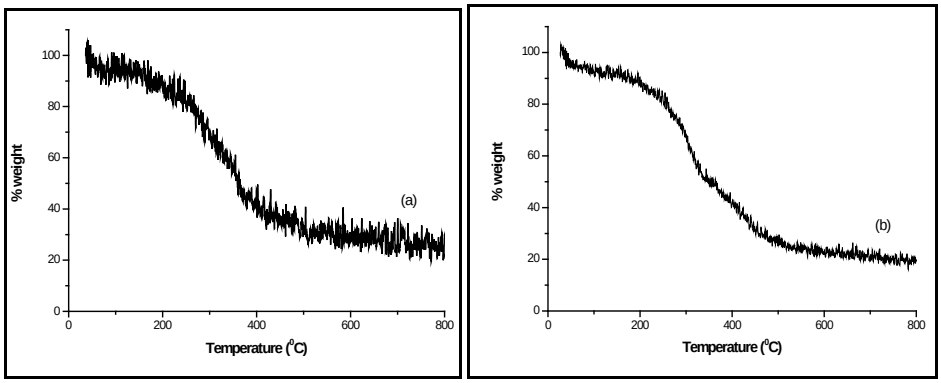

Figure 5.11: TGA of (a) PA-NS and (b) PA-CS films

5.4.2.3 SEM analysis of PA-NS and PA-CS films

The FESEM images of PA-NS and PA-CS films are shown in figures 5.12 (a) and (b). A significant variation in their morphology can be observed in these SEM images. Highly ordered regions can be seen in both these films. These images show the highly crystalline nature of these films.

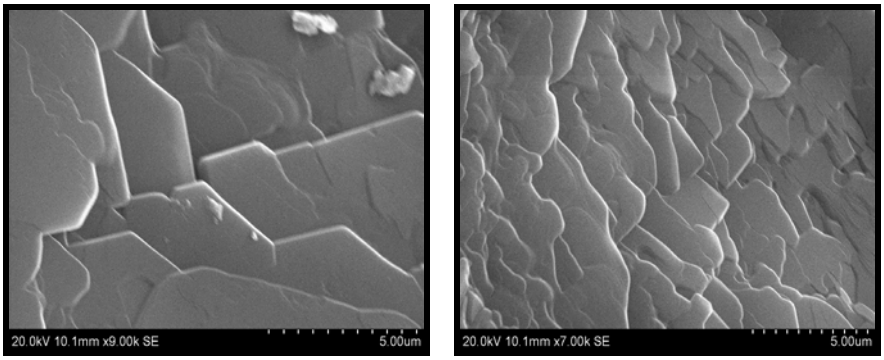

Figure 5.12 (a) FESEM images of PA-NS films

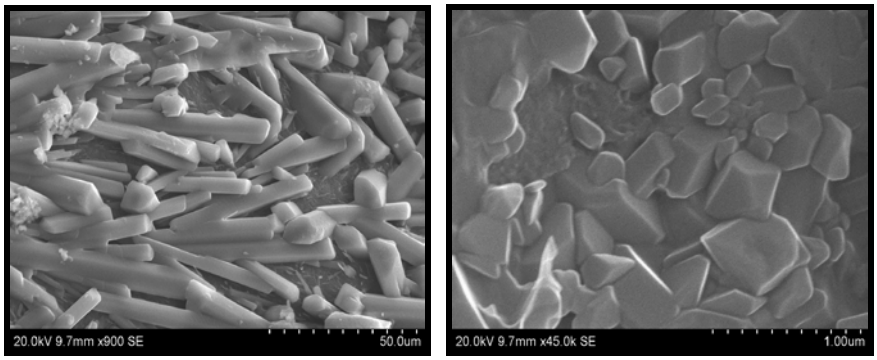

Figure 5.12(b): FESEM images of PA-CS films

5.4.2.4 XRD analysis of PA-NS and PA-CS films

The XRD spectra of PA-NS and PA-CS films are shown in figures 5.13(a) and 5.13(b) respectively. Both films appear to be highly crystalline in the XRD spectra. The films were indexed using Fullprof Suite and DICVOL software packages. PA-NS films show crystalline structure similar to monoclinic system and PA-CS films show crystalline structure similar to triclinic system.

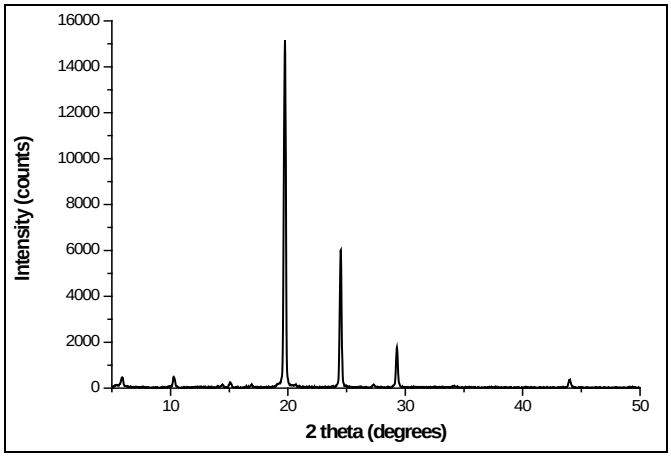

Figure 5.13(a): XRD pattern of PA-NS film

The difference in morphologies can be attributed to the two different dopants, NSA and CSA. The indexed peaks and related details are tabulated in tables 5.3 and 5.4. As explained earlier, the higher extent of crystallinity in these films can also be attributed to the effects of dopants, *m*-cresol and ultrasonication.

Table 5.3: Indexed peaks of PA-NS film (Monoclinic system)

h	k	l	d (Å)	2 θ (degree)
1	0	0	15.00949	5.884
0	0	1	8.61887	10.255
2	0	-1	5.88009	15.055
2	1	0	4.49860	19.719
2	0	2	3.63588	24.463
2	1	2	3.05188	29.239
4	1	3	2.05963	43.925
a =15.1238 Å, b = 5.6174 Å, c = 8.6635 Å				
$\alpha = 90, \beta = 94.034, \gamma = 90$, Volume = 734.19(Å)^3				

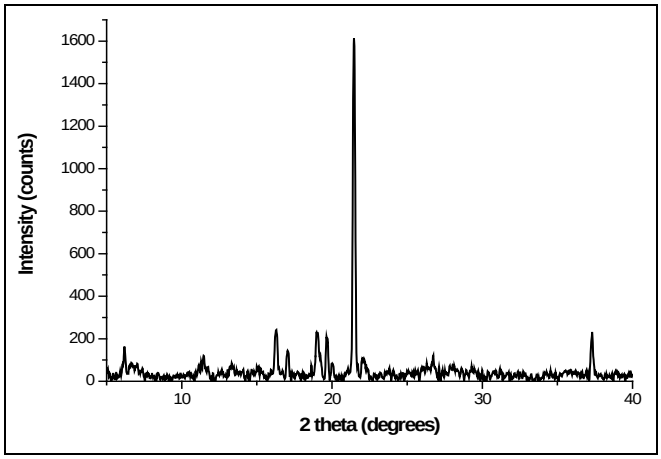

Fig 5.13(b): XRD pattern of PA-CS film

Table 5.4:Indexed peaks of PA-CS film (Triclinic System)

h	k	l	d (Å)	2 θ (degree)
1	0	0	14.29045	6.18
0	1	0	5.44722	16.259
0	0	1	5.20233	17.03
1	0	1	4.67727	18.958
2	-1	0	4.52292	19.612
2	0	-1	4.50381	19.696
2	1	0	4.14272	21.432
0	2	1	2.41217	37.246
a =14.3629Å, b= 5.4523 Å, c= 5.2364 Å				
$\alpha = 89.048, \beta = 98.040, \gamma = 95.271$, Volume = 404.32 $(Å)^3$				

5.5 Crystallinity in highly conducting PANI films, synthesized by dispersion polymerization

5.5.1 Synthesis of highly conducting and crystalline polyaniline films by dispersion polymerization

Polyaniline was synthesized using dispersion polymerization under two different temperature conditions, i.e., using ice bath (0^0C, sample name - DHI) and dryice-acetone mixture (-30^0C, sample name - DHD). Distilled aniline (5mL) was stirred in HCl (1M, 50mL) and chloroform (2 times the volume of aniline-HCl mixture) was added while stirring. Ammonium persulphate (11 g in 50mL of 1M HCl) was added drop-wise. The solution was stirred for 24 hours. The product was washed with acetone and water, and then dried in a vacuum oven for 24 hours to obtain green PANI powder. The same procedure was repeated with orthophosphoric acid (OPA) as dopant at -30^0C (sample name - DOD).

HCl and OPA doped PANI powder samples, synthesized at -30^0C (DHD and DOD respectively) were de-doped using 1M ammonia solution. The de-doped PANI samples were then re-doped using CSA

(1:1 ratio) and dissolved in *m*-cresol to obtain good solutions. The solutions were ultrasonicated for several hours and then spin cast on glass slides to get good quality PANI films, DHDC (HCl doped, CSA re-doped) and DODC (OPA doped, CSA re-doped). Another set of PANI film samples were synthesized using twice the quantity of CSA (1:2 ratio).

5.5.2 Characterization

5.5.2.1 FTIR spectral studies of dispersion polymerized PANI film samples

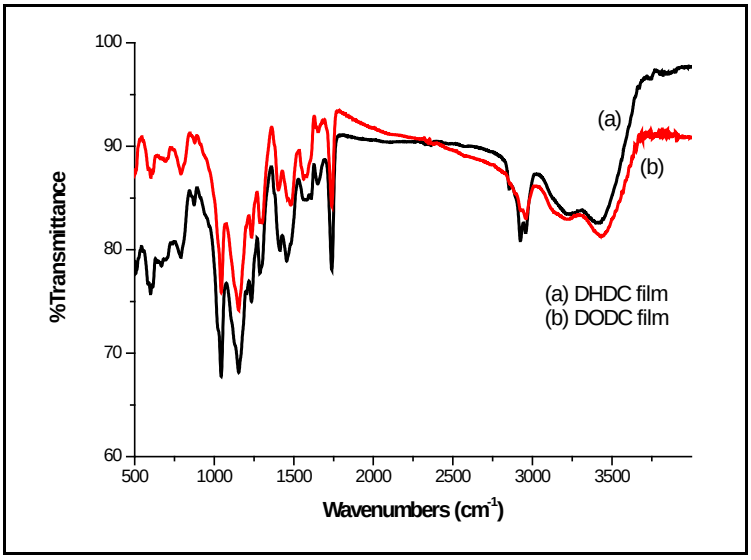

Figure 5.14: FTIR spectra of (a) DHDC and (b) DODC films from m-cresol

The FTIR spectra of DHDC and DODC film samples prepared from *m*-cresol are shown in figures 5.14(a) and (b). All the reported peaks can be seen in the spectra confirming the formation of doped polyaniline. The wavenumbers and their corresponding vibrational assignments are tabulated in table 5.5 [42-45].

Table 5.5: FTIR data of DHDC and DODC films

Wavenumber (cm-1)		Assignments/Comments
PANI (HCl) film	**PANI (OPA) film**	
788	788	-SO_3H group vibrations
873	877	C-H op on 1,2,4 ring
1044	1044	-SO_3H group vibrations
1153	1150	characteristic of doped PANI derived from an ordered organization indicating longer effective conjugation length
1232	1235	C-N str of BBB
1288		C-N str
1455	1468	str of benzene ring
1571	1572	str of N-Q-N
1647	1652	quinoid ring vibration
1740	1739	C=N str of Q
3420	3429	NH_2 asym str

Abbreviations: op=out-of-plane, str=stretching, B=benzenoid unit, Q=quinoid unit, asym=asymmetric

5.5.2.2 UV-Vis-NIR absorption studies of dispersion polymerized PANI film samples

The UV-Vis-NIR absorption spectra of DHDC (1:1 and 1:2) and DODC (1:1 and 1:2) films are shown in figures 5.15 (a), 5.15(b), 5.16(a) and 5.16(b) respectively. A band tail extending to the NIR region can be seen in all the spectra. The band tail is more prominent in doubly re-doped (1:2) samples, which confirms a more expanded conformation of PANI chains, in these samples. This can bring about a considerable extent of order among the PANI chains which in turn enhances the inter-chain hopping of charge carriers. This is the main reason for the enhanced electrical conductivity when the dopant (CSA) concentration is increased. However, there is definitely a limiting concentration of the dopant up to which the conductivity increases and after which it decreases [5].

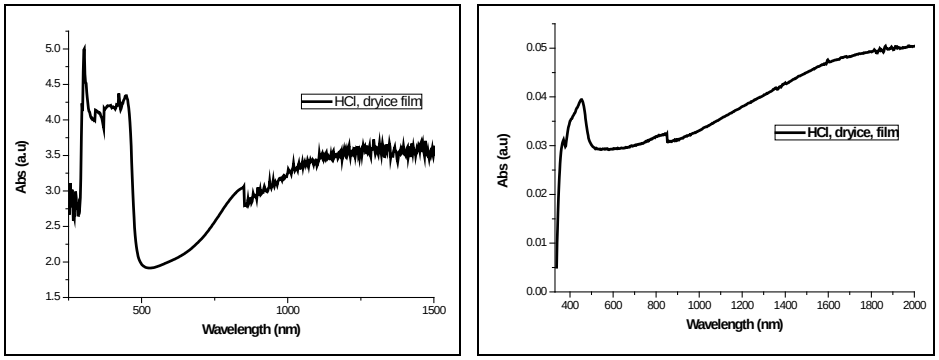

Fig. 5.15Optical absorption spectra of (a) DHDC [1:1], (b) DHDC [1:2] films

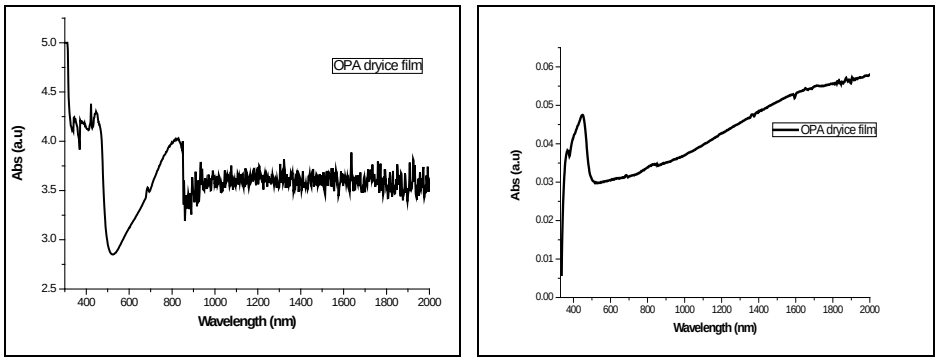

Fig. 5.16: Optical absorption spectra of (a) DODC [1:1], (b) DODC [1:2] films

5.5.2.3 XRD studies of dispersion polymerized PANI samples

The XRD spectra of powder and film forms of PANI are shown in figures 5.17(a), (b), (c) (d) and (e). The powder forms of PANI show semi-crystalline peaks around 11^0, 21^0 and 25^0 which can be seen in figures 5.17(a), (b) and (c).

Polymers being amorphous, generally do not give rise to sharp peaks in the XRD spectra, unless there is a good extent of crystallinity [46]. In the present work, PANI films show sharp crystalline peaks denoting a higher extent of order as seen in figures 5.17(d) and (e). These sharp and intense peaks arise from the expanded coil conformation which

results in well-packed PANI chains. This kind of arrangement of PANI chains improves inter-chain hopping of charge carriers, enhancing the conductivity of the films as a whole.

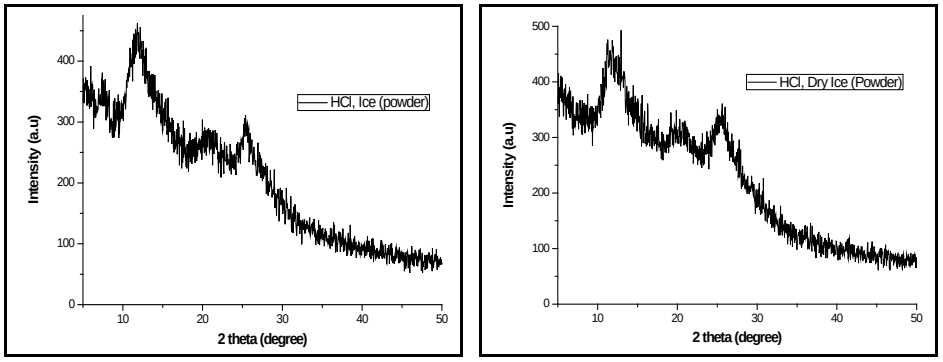

Fig.5.17: XRD patterns of (a) DHI (b) DHD PANI powder samples

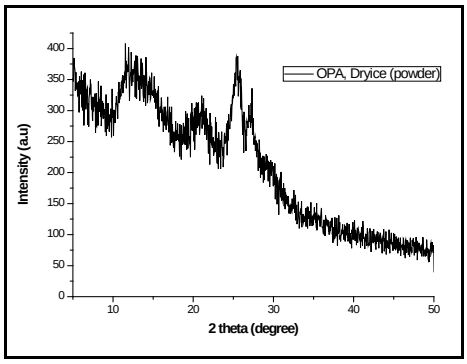

Fig.5.17(c): XRD pattern of DOD PANI powder sample

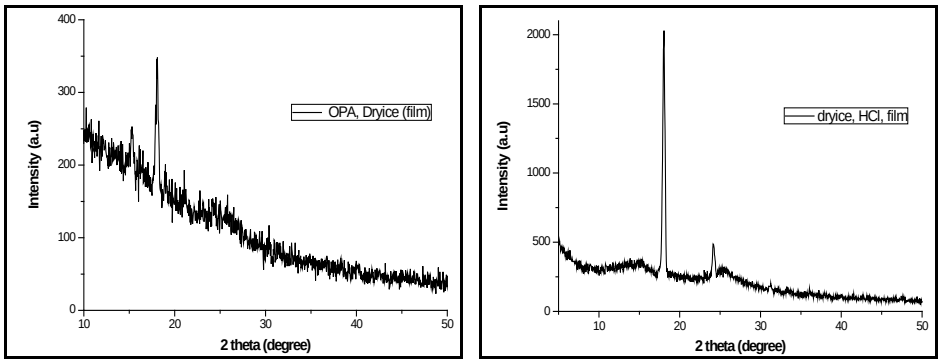

Fig.5.17: XRD patterns of (d) DODC and (e) DHDC film samples

5.5.2.4 DC Electrical Conductivity Studies

The powder samples were pelletized using a table-top hydraulic pellet press at 9 tons. The dc electrical conductivity of all the pellet and film samples was measured using Keithley 2400 source meter and 2001 multi-meter adopting the standard 4-point probe technique. The dc electrical conductivity of PANI depends on several parameters like the nature of dopants, reaction temperature, synthesis method, extent of order in PANI chains, etc. Dispersion polymerization is well known for the synthesis of highly conducting polyaniline films. Lower the reaction temperature, higher is the conductivity due to the increase in the extent of conjugation and order in the polyaniline formed. The electrical conductivity data of various polyaniline samples synthesized under different conditions is shown in table 5.6.

Table 5.6: DC electrical conductivity values of dispersion polymerised PANI samples

Sample	Conductivity
DHI pellet	0.14 S/cm
DHD pellet	4.21 S/cm
DOD pellet	3.82 S/cm
DHDC [1:1] film	**243.93 S/cm**
DODC [1:1] film	24.09 S/cm
DODC[1:2] film	52.09 S/cm
DHDC[1:2] film	**1079.99 S/cm**

Films prepared from dispersion polymerized PANI (DHDC), synthesized at lower temperature (dry ice medium) are found to possess the highest electrical conductivity. The highest extent of crystallinity, as

evident from XRD studies, is observed in these films. This is a clear indication of the fact that in conducting polymers, crystallinity/order of the polymer system is crucial in defining the electrical transport properties.

5.6 Conclusions

Quality films of PANI with excellent crystallinity have been synthesized using two different solvents, *m*-cresol and NMP via chemical oxidative polymerization method. XRD spectrum of PANI films prepared from *m*-cresol reveals highly crystalline peaks with exceptionally high intensity. The dc electrical conductivity of these films is also found to be very high. Films of PANI from *m*-cresol show higher extent of crystallinity, higher conductivity and better thermal stability compared to NMP films of PANI. The AFM study shows that the CSA re-doped, *m*-cresol film of PANI has crystalline islands distributed on the film surface which enhances the conductivity of the film. Both inter-chain and intra-chain regular arrangements introduced as a result of CSA doping, secondary doping effect of *m*-cresol and ultra-sonication are suggested to be the prime factors responsible for the excellent crystallinity of PANI thin film samples as evident from XRD and AFM studies. The *m*-cresol film of CSA re-doped PANI shows the free carrier absorption tail extending to the near IR region in the optical absorption spectrum, which is a true signature of metallic nature. The excellent order/crystallinity and the good thermal stability of the m-cresol film of PANI have been established from the temperature variation of electrical conductivity, and further confirmed by the thermal analysis. The high value of dc electrical conductivity of about 473 S/cm, excellent crystallinity and the good thermal stability up to 250^{o}C, observed in

CSA re-doped *m*-cresol film of PANI offer prospects of applications of these highly crystalline and conducting polymer films in various thin film devices.

Excellent crystallinity was achieved in HCl-DBSA co-doped films of polyaniline which were re-doped using CSA and NSA when the films were prepared by dissolving in *m*-cresol and ultrasonicated. Such films in *m*-cresol exhibited triclinic and monoclinic structure like arrangements. The peaks were indexed and the corresponding cell-parameters were evaluated. These films also exhibited excellent thermal stability.

Highly conducting polyaniline synthesized via dispersion polymerization displayed very high crystallinity in their film forms when prepared from *m*-cresol via ultrasonication. Very high conductivity values were obtained for the polyaniline thin films owing to the excellent order due to secondary doping and ultrasonication. Following the above method, dispersion polymerized PANI films prepared with HCl as the primary dopant exhibited a very high conductivity in the range of 1.08×10^3 S/cm.

Thus, polyaniline films of very high crystallinity and conductivity can be prepared by adopting de-protonation and then re-doping with CSA or NSA followed by dissolving in *m*-cresol via ultrasonication.

References

[1] Alan G.MacDiarmid and Arthur J. Epstein, *Faraday Discuss. Chem. Soc*., **88**, 317-332 (1989)

[2] Zhiming Zhang, Meixiang Wan, and Yen Wei, *Adv. Funct. Mater*., **16**, 1100–1104 (2006)

[3] Lee K, Cho S, Park SH, Heeger AJ, Lee CW and Lee SH, *Nature Lett.*, **441,** 65–68 (2006)

[4] Lee K-H,Park BJ,Song DH,Chin I-JandChoi HJ, *Polymer*,**50,** 4372–4377(2009)

[5] Donald L Wise et al, *Electrical and Optical Polymer Systems*, Marcel Dekker, Inc., New York, (1998), pp 366-370

[6] Biscaroa RS, Rezendeb MC and Faezc R, *Polym Adv Technol.*,**20,** 28–34 (2009)

[7] Bhadra S and Khastgir D, *Polym Test*,**27,** 851–857 (2008)

[8] Bansi D.Malhotra, *Handbook of Polymers in Electronics*, Rapra Technology Limited, UK (2002), pp 376

[9] H. K. Chaudhari, D. S. Kelkar, *J. Appl. Polym. Sci.*, **62**, 15 (1996)

[10] A. Gok, H. K. Can, B. Sari, M. Talu, *Mater. Lett.*, **59**, 80 (2005)

[11] P. Hourquebie, L. Olmedo, *Synth. Met.*, **65**, 19 (1994)

[12] W. J. Bae, W. H. Jo, Y. H. Park, *Synth. Met.*, **132**, 239 (2003)

[13] Biscaroa R S, Rezendeb M C and R. Faezc, *Polym. Adv. Technol.*, **20,** 28–34 (2009)

[14] Sambhu Bhadra, Dipak Khastgir, *Polym. Test.*,**27,** 851–857 (2008)

[15] Ki-Ho Lee, Bong Jun Park , Dong Hyun Song , In-Joo Chin , Hyoung Jin Choi

[16] *Polymer*,**50,** 4372–4377 (2009)

[17] Luzny.W and Banka.E, *Macromolecules*, **33,** 425-29 (2000)

[18] Wang Y and Rubner MF, *Synth Met*.,**47,** 255-266 (1992)

[19] Smits F.M, *The Bell System Technical Journal*, **37,** 711-718 (1958)

[20] Geng Y, Li J, Sun Z, Jing X and Wang F, *Synth.Met.*,**96,** 1-6 (1998)

[21] Tang J, Jing X, Wang B and Wang F, *Synth.Met.*,**24,**231-38 (1988)

[22] Amrithesh M, Aravind S, Jayalekshmi S and Jayasree R S , *J.Alloys Compd.*,**458,** 532-535 (2008)

[23] Jang J, Bae J and Lee K, *Polymer*,**46,** 3677- 3684 (2005)

[24] Bellamy A J, *The Infra-red spectra of Complex Molecules*, 2nd edn. John Wiley & Sons, New York, (1962)

[25] Pharhad Hussain A M and Kumar A, *Bull. Mater. Sci.*, **26,**329–334 (2003)

[26] S J Varma and S Jayalekshmi, *J. Appl. Polym. Sci.*,**117,** 138-42 (2010)

[27] S. Saravanan et al,*J. Phys. Chem. Solids*,**67,** 1496–1501 (2006)

[28] Pharhad Hussain A M and Kumar A, *Bull. Mater. Sci.*,**26,**329–334 (2003)

[29] A. Yelil Arasi et al,*Spectrochim. Acta* Part A,**74,** 1229–1234 (2009)

[30] Gajendran P and Saraswathi R, *Pure Appl. Chem.*,**80,**2377–2395 (2008)

[31] Cardoso M J R, Lima M F S, Lenz D M, *Mater. Res.*,**10,** 425-429 (2007)

[32] Sreekanth J Varma et al, *Polym. Int.*, (2012), DOI 10.1002/pi.4131

[33] MacDiarmid AG and Epstein AJ, *Synth Met*.,**69,** 85-92 (1995)

[34] Shukla S.K. et al, *Adv. Mat. Lett*.,**1**, 129-134 (2010)

[35] Liu H., Hu X. B., Wang J. Y. and Boughton R. I., *Macromolecules,* **35,** 9414-9419 (2002)

[36] Pouget J. P. et al,*Macromolecules*,**24,** 779-789 (1991)

[37] Sinha S, Bhadra S, Khastgir D,*J. Appl. Polym. Sci.*,**112,** 3135–3140 (2009)

[38] Castellan G W, *Physical Chemistry*, 3rd edn., Narosa publishing house, New Delhi, India (1996)pp 701

[39] Suryanarayana C., Grant Norton M., *X-Ray Diffraction: A Practical Approach*, 1st edn., Plenum Publishing Corporation, Newyork (1998)pp 97

[40] Leite F L et al,*Appl. Phys. A*,**93,** 537–542 (2008)

[41] Cheng H Y, Weng C J, Liou S J, Yeh J M, Liu S P, *Polym. Compos.*,**31,** 2049–2056 (2010)

[42] Wusheng Yin, Eli Ruckenstein, *Synth. Met.*,**108**, 39–46 (2000)

[43] J.Tang et al, *Synth. Met*., **24**, 231-238(1988)

[44] Deepak Verma and V.Dutta, *Sensorsand Actuators B*, **134**, 373-376 (2008)

[45] L.H.Huo et al, *Thin Solid Films*, **350**, 5-9(1999)

[46] Honey John, *PhD Thesis*, CUSAT (2004)

[47] V R Gowariker et al, Polymer Science, *New Age International*, India (1986), pp 173-192

…..ꕥ…..

Chapter 6

TOWARDS POLYMER LIGHT EMITTING DIODES BASED ON NOVEL HYBRID-POLYMERS AS EMISSIVE LAYERS

Contents

In this chapter, the suitability of two novel, light-emitting, hybrid polymers as emissive layers for polymer light emitting diodes have been investigated through optical, electrical and structural characterization of these thermally stable and highly soluble materials. Sandwich structures comprising Indium Tin Oxide/hybrid polymer/aluminium were fabricated to analyze the current-voltage characteristics. Prototype multi-layered devices were fabricated with these hybrids as emissive layers and electroluminescence emission demonstrated and plotted as a function of wavelength.

6.1 Introduction

Conjugated light emitting polymers are known for their extensive applications in the field of optoelectronics [1, 2, 3, 4, 5]. One of the most important applications is as emissive layers in polymer light emitting diodes (PLED) [2, 3]. Till date, numerous light emitting polymers and their copolymers with interesting electrical and optical properties have been synthesized and utilized for electro-optic device applications. Of these, polymers based on phenylenevinylenes and thiophenes which emit light in the blue-green regions and orange-red regions respectively, have been studied extensively [6]. Biphenylenes are excellent blue emitting polymers with a wide band-gap and excellent solubility whereas thienylenes are narrow band-gap polymers with poor solubility. The film forming properties of biphenylenes [7, 8, 9] are remarkable and polymers based on thienylenes have very good charge carrier mobility [10, 11]. The advantageous properties of biphenylenes and thienylenes can be suitably blended to realize superior copolymers with excellent solubility, modified emission characteristics, intermediate to both the entities and good charge carrier mobility.

In the present work, the prospects of using two novel, thermally stable, highly soluble and intense light-emitting, semi-conducting polymers as emissive layers in polymer light emitting diodes have been investigated. Detailed investigations were carried out on the structural, optical and electrical characteristics of these polymers. The initial diode characteristics were investigated by studying the current-voltage characteristics of the ITO/emissive polymer/aluminium structures. The suitability of these emissive polymers for fabricating polymer LEDs was

confirmed on the basis of the ideal diode characteristics. Prototype multi-layer polymer light emitting diodes were fabricated having ITO/PEDOT: PSS/ emissive polymer/LiF-Al architecture (PEDOT:PSS–Poly(3,4-ethylenedioxythiophene) poly(styrenesulfonate)). The diode characteristics and electroluminescence characteristics of the fabricated devices were analyzed in detail. There are no previous reports on the successful fabrication of light emitting diodes based on these hybrid polymers and the present work is novel in all respects.

6.2 The Light Emitting hybrid polymers

The hybrid polymers of biphenylenes and thienylenes named as TBPV1 and TBPV2 were synthesized via Stille coupling reaction (figure 6.1(a)). The respective monomers, M1 and M2 for these polymers were designed by Wittig-Horner reaction. The details of the monomer and polymer synthesis and their basic characteristics are given in [12][*]. The structures of TBPV1 and TBPV2 are shown in figures 6.1(b) and 6.1(c) respectively. A small change in the position of alkoxy substituents is the reason for the changes in various properties of these hybrid polymers.

[*] *Most part of the synthesis and basic characterizations of these hybrid-polymers were done, in collaboration with The Department of Polymer Science & Rubber Technology and The Department of Applied Chemistry, Cochin University of Science and Technology*

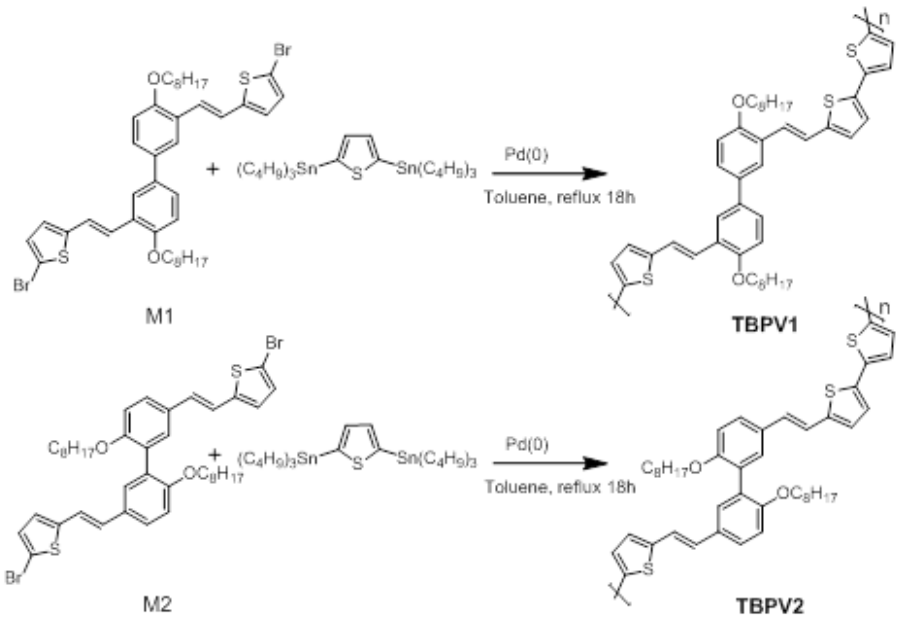

Figure 6.1(a): Reaction scheme of the synthesis of TBPV1 and TBPV2

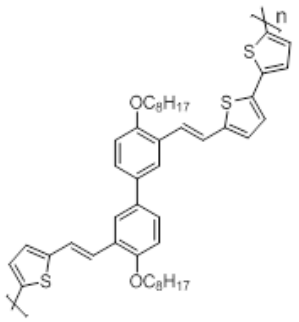

Figure 6.1(b):TBPV1

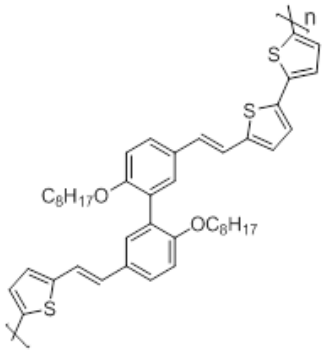

Figure 6.1(c):TBPV2

The characteristics of these hybrid polymers as obtained from gel-permeation chromatography, thermo gravimetric analysis and differential scanning calorimetric studies are tabulated below in table 6.1. Polydispersity index determines the purity of the polymers. The TGA

and DSC curves of TBPV1 and TBPV2 are shown in figures 6.2 and 6.3 respectively. The polymers are readily soluble in common organic solvents and possess high thermal stability [12].

Table 6.1: Physical and thermal properties of TBPV1 and TBPV2

Properties	TBPV1	TBPV2
Molecular weight (Mw)	4928 g mol^{-1}	4549 g mol^{-1}
Polydispersity Index (PDI)	1.66	1.82
Degradation temperature (Td)	443.56^0C	452.76^0C
Glass transition temperature (Tg)	54^0C	55^0C

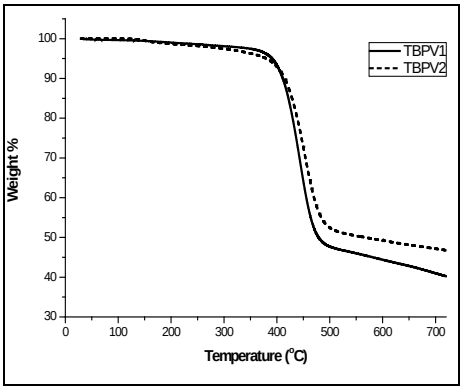

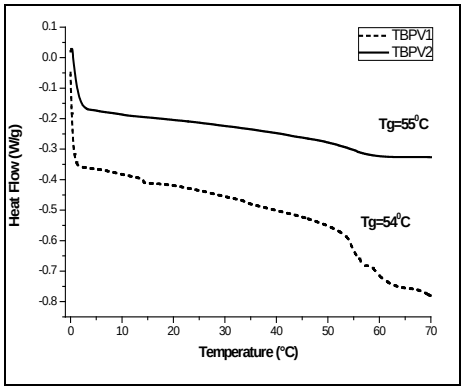

Figure6.2: TGA of TBPV1 and TBPV2 **Figure 6.3: DSC of TBPV1 and TBPV2**

6.3 Characterization

The optical absorption spectra and photoluminescence spectra of the hybrid polymers in solution and film forms were recorded using Jasco V-500 UV-VIS-NIR spectrophotometer and Fluoromax 3 fluorescence spectrophotometer respectively. Rigaku X-ray diffractometer with Cu-Kα radiation (λ=1.542 Å) was used for analyzing the extent of crystallinity in these hybrid polymers. The morphology of these polymers in the powder form and roughness in the film form were

analyzed using Hitachi SU6600 FESEM and Park XC100 AFM respectively. The electrical characterization studies were conducted using the fully-automated Keithley 2400 source meter and the electroluminescence studies were done using Konica Minolta CS1000 spectroradiometer.

6.3.1 X-ray Diffraction Studies

The XRD patterns of TBPV1 and TBPV2 in the powder form are shown in figure 6.4. The XRD spectra of TBPV1 and TBPV2 reveal the semi-crystalline nature of these polymers showing a partially crystalline peak at d-values of 7.64 and 7.53A^0 respectively for TBPV1 and TBPV2. Amorphous peaks at 4.02A^0 and 4.17A^0 can also be seen for TBPV1 and TBPV2 respectively.

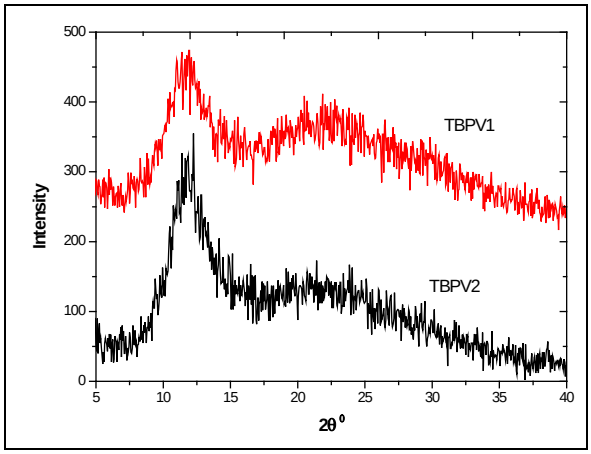

Figure 6.4: XRD patterns of TBPV1 and TBPV2 powder samples

The semi-crystalline peaks corresponding to the d-values 7.64 A^0 and 7.53 A^0 appear as a result of the polymer chain separation due to the presence of alkoxy groups attached to the backbone. The amorphous diffraction peaks at 2θ values of TBPV1 at 22.6^0 (d = 4.02 A^0) and

TBPV2 at 21^0 (d = 4.17 A^0) correspond to the interlayer distance between the π-π stacks of the polymer [12, 13, 14].

6.3.2 Scanning Electron Microscopy

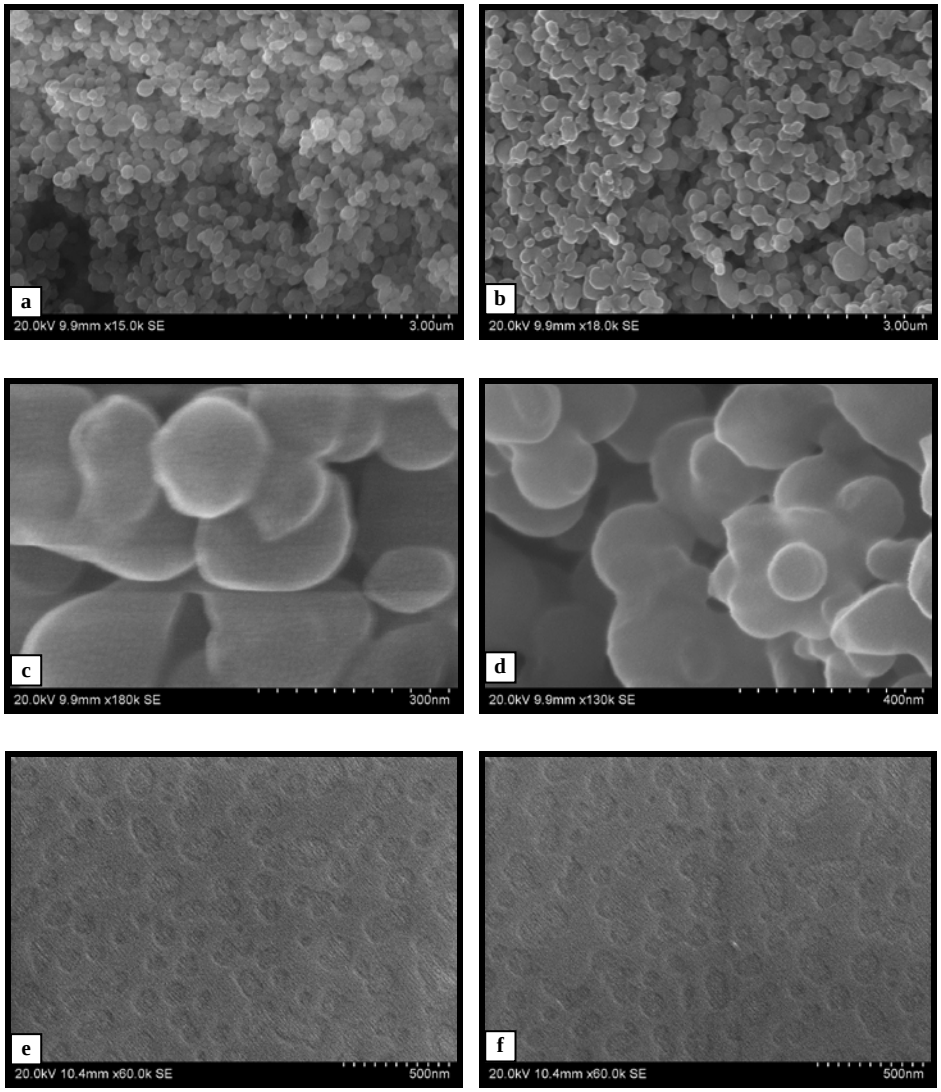

Figure 6.5: FESEM images of (e) TBPV1 and (f) TBPV2 thin films

The FESEM images of TBPV1 and TBPV2 powder samples are shown in figures 6.5(a), (b) and 6.5 (c), (d) respectively and those of respective spin-coated thin films in figures 6.5(e) and 6.5(f). Both polymers appear to be nanostructured having circular plate like morphology of ~100nm in size.TBPV1 and TBPV2 form good quality continuous films with appreciable smoothness as evident from the FESEM images.

6.3.3 Optical absorption and Photoluminescence studies

The polymers TBPV1 and TBPV2 were dissolved in dichloromethane (5mg in 2mL DCM) to obtain good solutions. The solutions were spin-coated (SPS Spin 150 wafer spinner) at 2000 rpm for 30s on clean glass slides to obtain 100 nm thick films. Thickness of the films was determined using Dektak stylus profiler. Optical absorption spectra of the respective solutions and films of TBPV1 and TBPV2 were recorded using Jasco V500 UV-Vis-NIR spectrophotometer. The photoluminescence spectra of solutions and films of TBPV1 and TBPV2, were recorded using Fluoromax 3 fluorescence spectrophotometer.

Solutions of TBPV1 and TBPV2 for optical absorption and photoluminescence studies were prepared as detailed below:

- The dilution of the polymers in DCM was fixed so as to get an absorbance less than 0.1
- The PL spectra of the same solutions with absorbance less than 0.1 were recorded immediately

The optical absorption and photoluminescence spectra of TBPV1 and TBPV2 solutions and thin films are shown in figures 6.6(a) and 6.6(b) respectively.

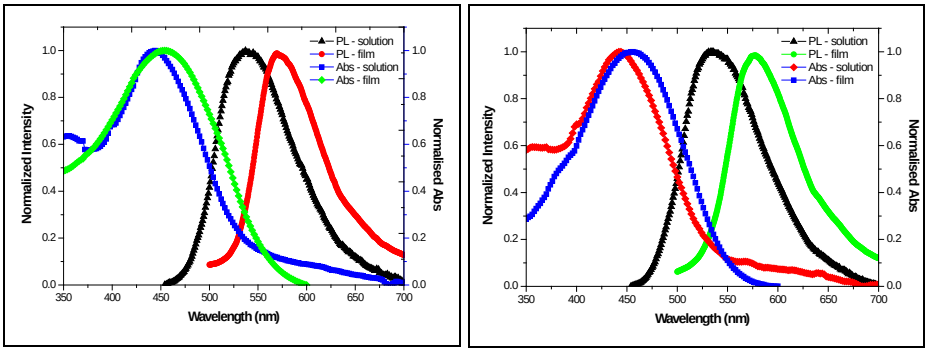

Figure 6.6: Optical absorption and PL spectra of (a) TBPV1 (solution and film) and (b) TBPV2 (solution and film)

The solutions of TBPV1 and TBPV2 show major absorption peaks at 444 nm and 442 nm respectively corresponding to π-π* transitions [12]. The films of these polymers show major absorption peaks at 456 nm and 455 nm, respectively, with a slight red-shift, due to aggregation effects in the thin film samples. The solutions of TBPV1 and TBPV2 show intense PL emission at 536 nm and 538 nm, respectively [12]. A slight red-shift can be seen in the respective PL emission peaks of the thin film samples, due tothe aggregation effects. Both polymers show intense green light emission in the solution forms and intense yellow emission in the respective film forms. The observed slight variation in the emission wavelengths of these polymers is due to the difference in the positional substitution of long alkyloxy side chains present in the polymer backbone. Photographs of TBPV1 and TBPV2 solutions in dichloromethane are shown in figure 6.7(a). Intense green light emission from the same solutions when exposed to UV-light is shown in figure 6.7(b).

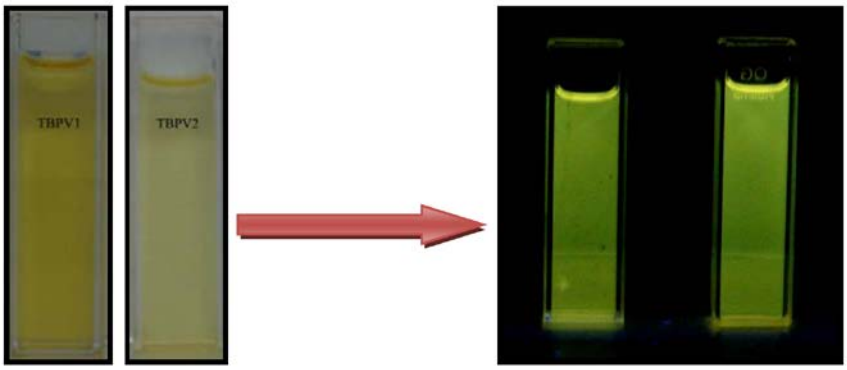

Figure 6.7(a): Dilute solutions of TBPV1 and TBPV2 in dichloromethane

Figure 6.7(b): Intense green emission in UV-light

6.3.4 Highest Occupied Molecular Orbital (HOMO)- Lowest Unoccupied Molecular Orbital (LUMO)energy levels and Band-gap

The HOMO and LUMO energy values of both the polymers were determined from cyclic voltammetry [12]. The band-gap energies of TBPV1 and TBPV2 were estimated using cyclic voltammetry and compared with the results obtained from UV-Vis spectroscopy. The band gap and HOMO-LUMO energy values are tabulated in table 6.2.

Table 6.2: Band-gap and HOMO-LUMO energy values of TBPV1 and TBPV2

Hybrid Polymers	TBPV1	TBPV2
HOMO (eV)	4.869	4.844
LUMO (eV)	2.841	2.616
Band gap (cyclic voltammetry) (eV)	2.21	2.22
Band gap (UV-Vis absorption) (eV)	2.31	2.32

6.3.5 Estimation of the CIE Coordinates

The CIE coordinates of the light emitted from TBPV1 and TBPV2 solutions and films were determined using a program in Matlab. The x, y, tristimulus (X,Y,Z) values and the emitted colours are shown in

figures 6.8(a) to 6.8(d). The (x,y) position shows the exact colour of the emitted light as perceived by the human eye. The screenshots also show the PL plot of the corresponding hybrid polymer and the exact position of the emitted colour in the chromaticity diagram.

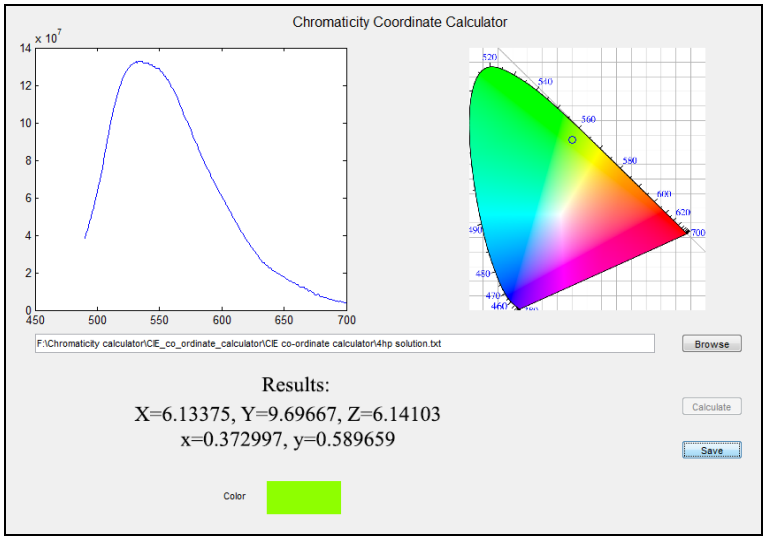

Figure 6.8(a): TBPV1 solution

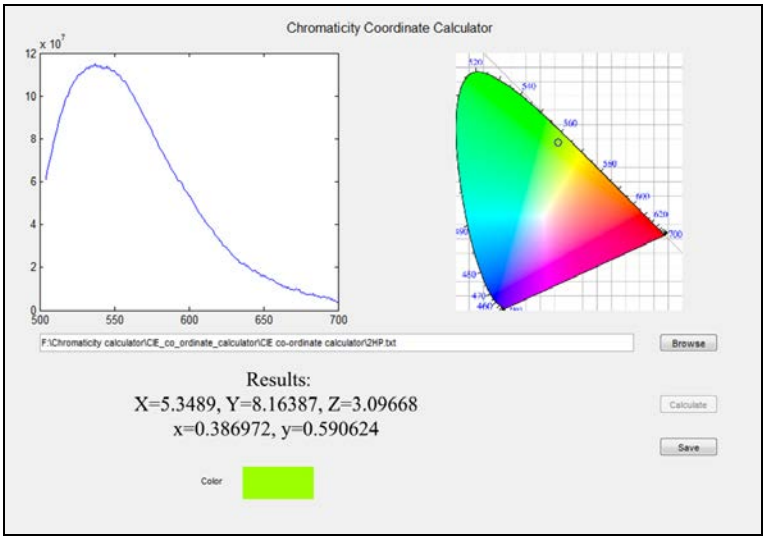

Figure 6.8(b): TBPV2 solution

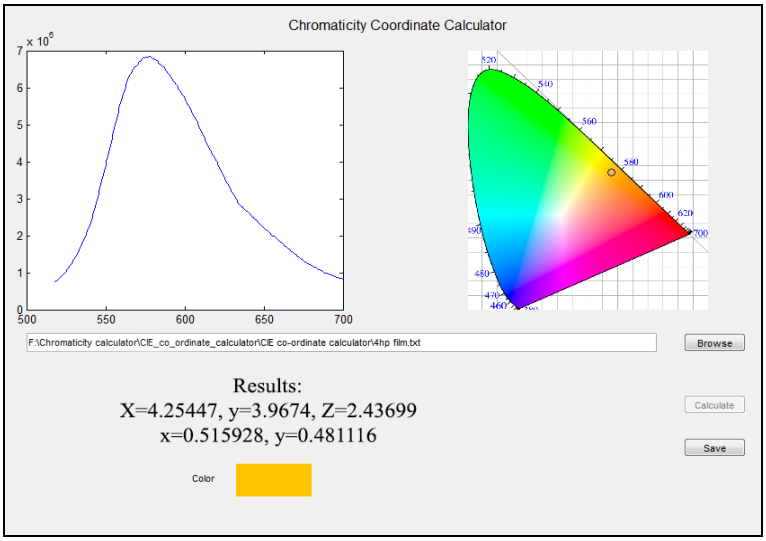

Figure 6.8(c): TBPV1 film

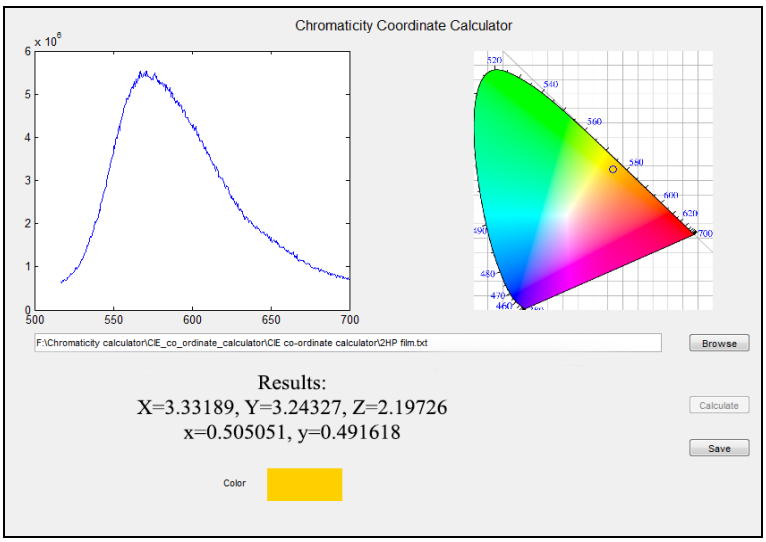

Figure 6.8(d): TBPV2 film

6.3.6 Atomic Force Microscopy Studies

The AFM images of both the polymers were obtained in non-contact mode using Park Systems XE 100 atomic force microscope. The AFM topography images of TBPV1 and TBPV2 thin films are shown in

figures 6.9(a) and (b) respectively. The images indicate quite smooth surfaces of roughness below 1.83 nm and 1.45 nm respectively, for TBPV1 and TBPV2 films.

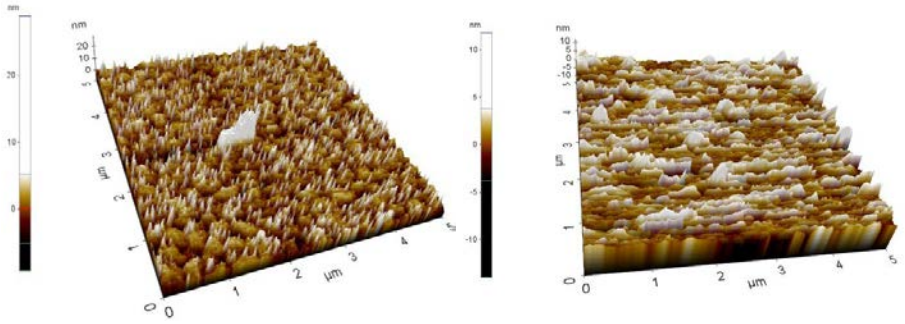

Figure 6.9: AFM images of (a) TBPV1 and (b) TBPV2 films

6.4 Current-Voltage (I-V) characteristics of ITO/hybrid-polymer/Al structures

The current-voltage characteristics of both the hybrid polymers were investigated using Keithley 2400 source meter adopting the standard 2-probe method. Thoroughly cleaned Indium Tin Oxide (ITO) coated glass slides were used as one of the electrodes. Good quality thin films of TBPV1 and TBPV2 of about 50 nm thickness were spin coated on ITO (anode) coated glass slides (SPS Spin 150wafer spinner). Aluminium layer (cathode) of thickness about 100 nm was thermally evaporated on top of the polymer layers separately. Contacts were taken from ITO and aluminium for I-V measurements.

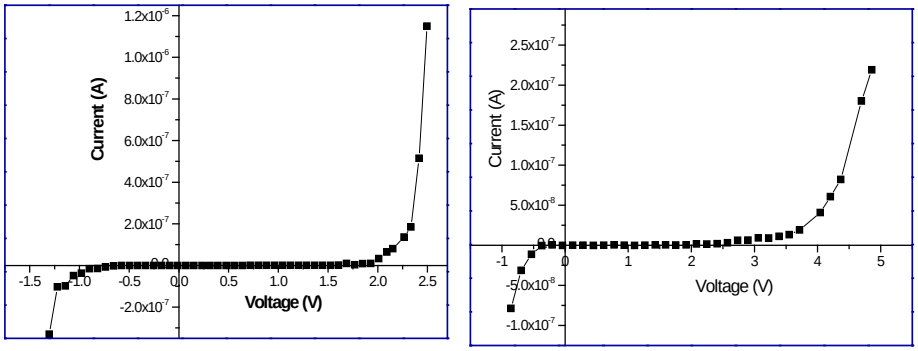

Figure 6.10: I-V characteristics of (a) ITO/TBPV1/Al and (b) ITO/TBPV2/Al structures

The forward and reverse bias characteristics of both the devices in ITO/polymer/Al configuration were analyzed. Both the devices show very good forward and reverse bias characteristics, confirming the formation of Schottkey diode like structure, which is mandatory for polymer LED applications. From figures 6.10(a) and (b), it can be seen that the on-set voltages for the devices based on TBPV1 and TBPV2 are quite small (below 3V).

The band structures of ITO/hybrid-polymer/Al(or Ca)devices are shown in figure 6.10(c) for the fabrication of efficient polymer LEDs based TBPV1 and TBPV2.

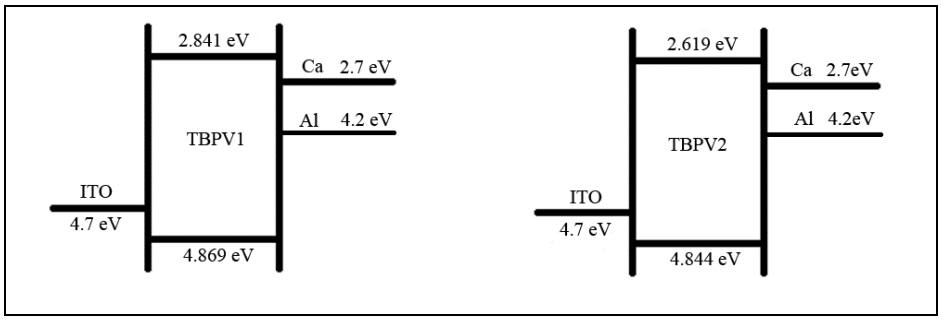

Figure 6.10(c): Band structures of ITO/hybrid-polymer/Al or Ca devices

The HOMO levels of TBPV1 and TBPV2 lie very close to the work function of ITO. Hence, an intermediate layer for efficient hole injection is not required. The LUMO levels of both polymers match very well with the work function of calcium. Thus, an intermediate layer in between calcium and the polymer is also not required. Calcium being highly reactive should be protected from immediate degradation by means of aluminium or silver coating on top. A complete, long-term degradation protection can be effected only by suitable encapsulation.

6.5 PLED fabrication using TBPV1 and TBPV2 as emissive layers

It was observed that the devices having ITO/hybrid-polymer/ aluminium architecture did not exhibit any electroluminescence emission, though intense photoluminescence emission could be observed from the hybrid polymers, TBPV1 and TBPV2. One of the prime factors inhibiting electroluminescence emission was identified as the mismatch between the HOMO-LUMO levels of the polymers and the work function of the electrodes. The device architecture was hence modified as ITO/ PEDOT: PSS/hybrid-polymer/LiF-Al with the intension of lowering the cathode work function closer to the LUMO energy level of the hybrid polymers and making the HOMO levels of the hybrid polymer compatible with the work function of the processed ITO surface. The fabrication of the devices with the modified architecture involves the following steps:

- ITO etching and patterning
- Base patterning or pixelization
- PEDOT:PSS layer deposition
- Emissive layer deposition
- Cathode deposition
- Encapsulation

6.5.1 I TO etching and patterning, Base patterning

ITO coated glass plates (50x50 mm, 150 nm, 10Ω/square, 10-15Å r.m.s roughness, above 90% transparency) were first washed in distilled water, cleaned in soap solution and then rinsed with distilled water. The cleaned glass plates were ultrasonicated in millipore water and dried in an oven at 130^0C for 1 hour.

The ITO substrates were baked for 15 minutes at 160^0C on a hot plate and kept on class 100 clean bench. A positive photoresist (CLARIENT AZ-TFP 310K (6CP)) was spin-coated (Laurell WS-400B-8NPP/LITE) on the substrates at 1000 rpm for 30 seconds. The substrates were pre-baked for 5 minutes at 100^0C and exposed to UV for 25 seconds using a mask aligner (MA 1066) with a chromium mask (50x50 mm) on top. They were kept in a developer (TMA – Tetramethyl ammonium hydroxide 2.38%) for 55 seconds, rinsed with millipore water and dried using a blower. Photoresist remains in the masked regions (figure 6.11(a)). The substrates were post-baked at 140^0C for 3 minutes on top of a hot plate. ITO was etched from the substrates using the etchant heated at 55^0C for 5 minutes. The etchant is a combination of distilled water, HCl and concentrated nitric acid in the ratio 15:4:1. The etched substrates were washed again with millipore water and dried using a blower. Photoresist was removed from the glass plates using acetone. The glass plates were thoroughly checked under a microscope for any shorts or continuity.

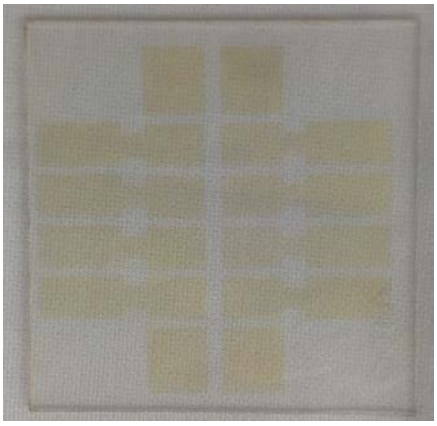

Figure 6.11(a): The patterned ITO coated glass plate with photoresist

The substrates were again cleaned in soap solution, warm water (55^0C), de-ionised water and baked on a hot plate at 165^0C for 15 minutes. The positive photoresist was again spin-coated (500 rpm for 1 minute) on the patterned ITO surfaces, pre-baked for 2 minutes 30 seconds at 100^0C and exposed under UV with a new mask for 25 seconds. The glass plates were dipped in developer for 55 seconds, rinsed with de-ionised water and post-baked for 1 hour at 200^0C to de-gas the photoresist (figure 6.11(b)). Eight pixel windows of 4 mm x 4 mm size were hence created on the substrates.

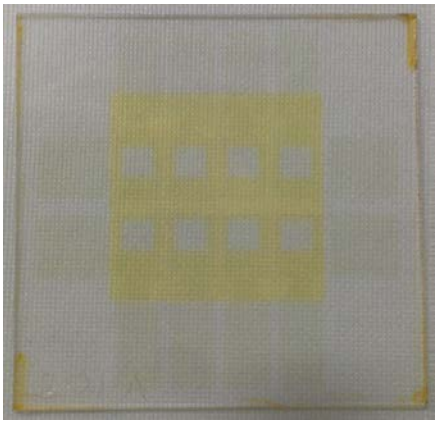

Figure 6.11(b): Patterned ITO coated glass plates after pixelization

The patterned glass plates were pre-treated with UV (UVO Cleaner – Model No.42-220, Jelight Company, USA) for 15 minutes, exposed to UV-ozone for 30 minutes and post-treated with oxygen for 10 minutes in the absence of UV. This was done to improve the hydrophilicity of ITO so that PEDOT:PSS adheres well on top of the ITO coating. UV-ozone treatment slightly increases the work function of ITO to 5.2 eV which can be compensated using PEDOT:PSS layer.

6.5.2 PEDOT:PSS layer deposition

PEDOT:PSS (Clevious P VPCH 8000 – dispersion in water) was spin-coated on the ITO substrates at a spin speed of 1000 rpm for 1 minute to get 30-40 nm thick films. The substrates were dried in an oven under dynamic vacuum of 10^{-5}mbar at 120^{0}C for 2 hours to confirm the removal of water. The layer of PEDOT:PSS helps to avoid any shorts in between the anode and the cathode as well as reduces the gap between the work function of UV-ozone treated ITO (5.2 eV) and the emissive, hybrid polymer. There is always a better interface between the PEDOT:PSS layer and the emissive polymer layer which also helps in the efficient hole injection.

6.5.3 Emissive layer deposition

The hybrid-polymers TBPV1 and TBPV2 were dissolved in dichloromethane (20 mg in 2 mL DCM). Both polymers are found to dissolve readily in DCM to give golden brown coloured solutions. The solutions were sonicated for 5 minutes to confirm the absence of any un-dissolved polymer. The polymers were spin-coated on the PEDOT:PSS coated ITO substrates at 1000 rpm for 1 minute to get approximately 300nm thick films. The substrates with polymer coating were dried in

dynamic vacuum (10^{-3} mbar) for 24 hours at room temperature to remove excess solvent trapped inside the polymer films. The thickness of the polymer layers was sufficient to avoid any shorts between the anode and cathode layers.

6.5.4 Cathode layer deposition

Cathode is normally a low work function material such as Ca, Mg, Ba, Al, etc. Lower the work function, higher is the reactivity of the material. Hence, it is difficult to use a low work function material such as calcium as cathode which readily oxidizes on exposure to air and moisture. As an alternative, a combination of a very thin layer of lithium fluoride (LiF) and aluminium was selected as cathode for the prototype devices. The thin layer of LiF with aluminium possesses a lower work function of 3.6-3.8 eV [6], when compared to the work function of Al which is 4.2 eV. This combination of LiF/Al leads to an improved charge injection similar to low work function materials. LiF and Al were thermally evaporated on the polymer surfaces using a cluster tool (Doosan DND). The cluster tool consists of a glove box associated with several evaporation chambers. LiF layer of 1.5nm (0.1 Å/second) followed by a layer of aluminium of 200 nm thickness (2Å/second) were thermally evaporated at 2 x 10^{-7} mbar from molybdenum and poly boron nitride boats respectively. The rate of evaporation and hence the thickness of the cathode layers were precisely controlled by a programming console associated with the cluster tool.

6.5.5 Encapsulation of devices

The devices were encapsulated by covering with glass plates, fixed using a UV curable epoxy. The epoxy was inserted around the glass

plates and exposed to a UV source for 5 minutes to achieve good adherence, in order to inhibit the various layers of the device from degradation. The final encapsulated device is shown in figure 6.12.

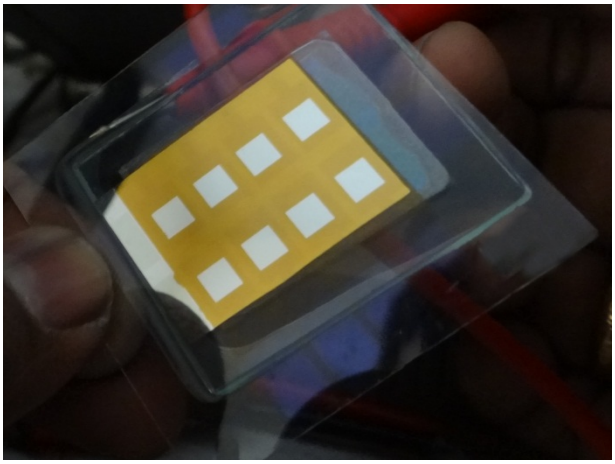

Figure 6.12: Photograph of an encapsulated device with 8 pixels

6.5.6 Energy band diagram of TBPV1 and TBPV2 devices

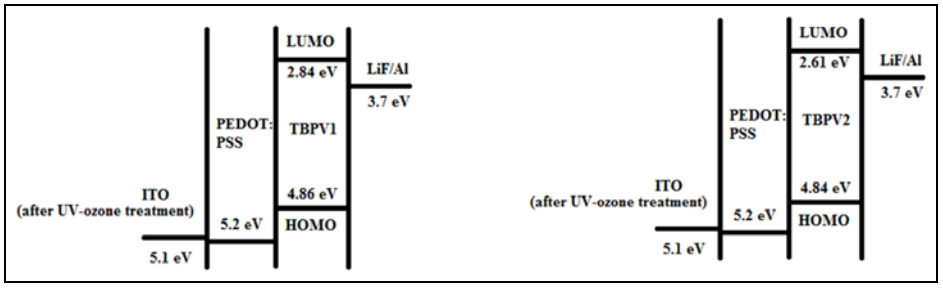

Figure 6.13: Energy band diagrams of ITO/PEDOT:PSS/hybrid-polymer/LiF-Al devices

The energy band diagrams of the fabricated prototypes using TBPV1 and TBPV2 are shown in figure 6.13. The HOMO energy levels of both the emissive polymers have comparable values with that of PEDOT:PSS. LiF-Al layer, when compared to aluminium has a closer work function towards the LUMO energy level of the emissive polymers.

6.6 PLED Characterization

6.6.1 Current-Voltage Characteristics

The current-voltage (I-V) measurements of the prototype devices were carried out using Keithley 2400 source meter interfaced to a computer adopting the standard 2-point probe method. Proper electrical contacts were made from the anode and the cathode of the devices using alligator clips. I-V graphs were plotted using the dedicated program developed in LabVIEW.

I-V graphs of the prototype devices with TBPV1 and TBPV2 as emissive layers are shown in figure 6.14. Both the devices exhibit very good forward diode characteristics which confirm the successful fabrication of the polymer LED with smooth interfaces between the various layers.

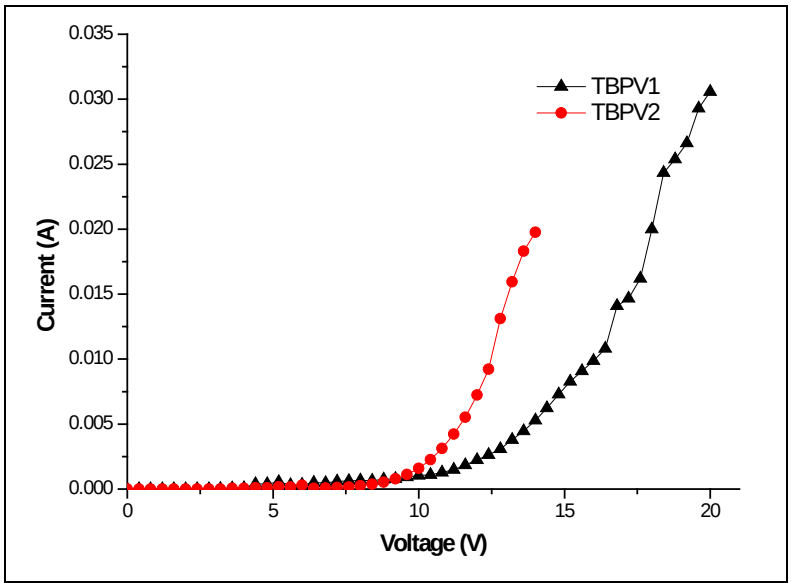

Figure 6.14: I-V plot of prototype devices using TBPV1 and TBPV2

From the figure, the on-set voltages of devices with TBPV1 and TBPV2 as the emissive layers can be identified as 10V and 8V which are slightly high due to the mismatch between the various layers. However, both the devices were found to emit light with moderate intensity in the orange-red region upon the application of the required operating voltage. The operating voltage can be effectively lowered by using suitable electrodes and intermediate, charge transporting layers which facilitate efficient and balanced charge injection.

6.6.2 Spectral distribution and Electroluminescence Studies

The analysis of the spectral distribution and electroluminescence of the devices was performed using Konica Minolta CS1000 spectroradiometer integrated to a computer using a dedicated program. The operating voltages (12 V for TBPV1 device and 11 V for TBPV2 device) as obtained from the I-V graphs were applied to both the devices using Keithley 2400 source meter adopting 2-point probe method. An orange-red emission, at 623 nm for TBPV1 and an orange emission at 601 nm for TBPV2 were observed from the prototype devices. Graphs were plotted with normalised spectral radiance along the y-axis and wavelength along the x-axis and are shown in figures 6.15 (a) and (b) for the devices with TBPV1 and TBPV2 as emissive layers respectively.

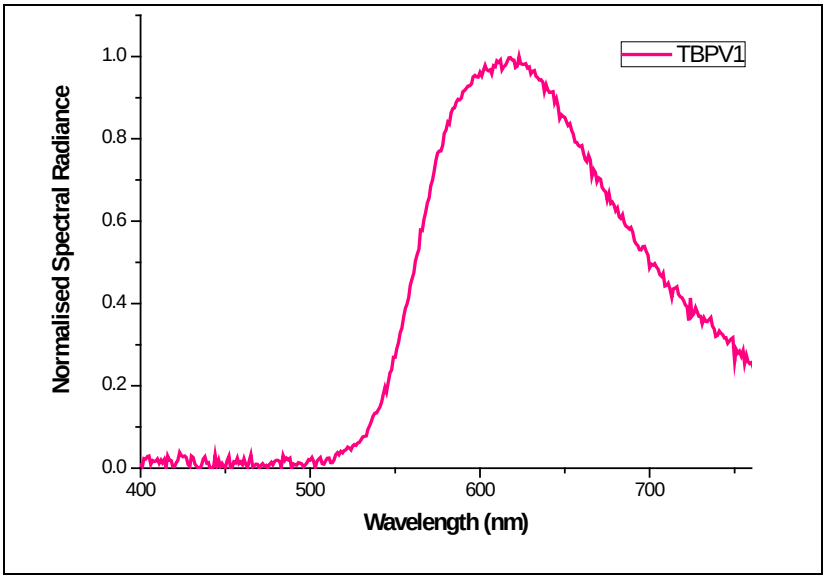

Figure 6.15(a): Normalised spectral radiance against wavelength plot of TBPV1 device

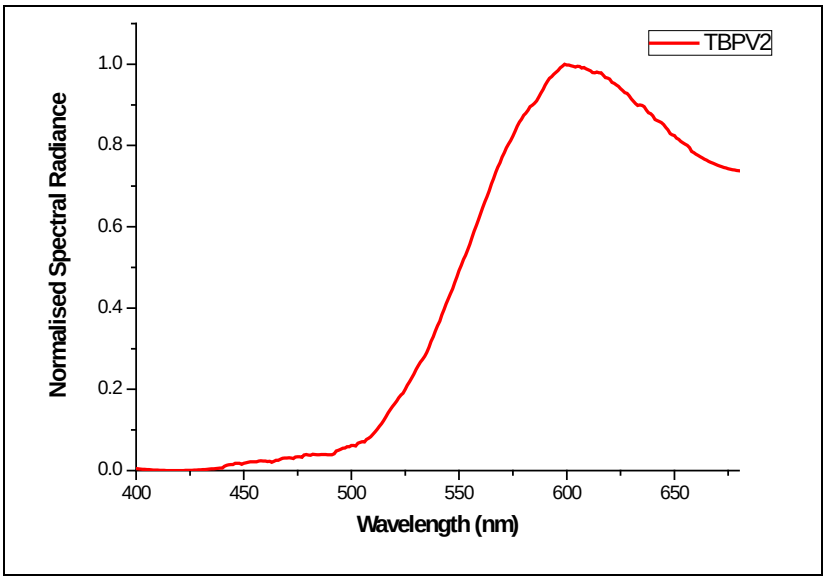

Figure 6.15(b): Normalised spectral radiance against wavelength plot of TBPV2 device

The electroluminescence intensity of the light emitted is not high because of the mismatch between the electrode work functions and the

HOMO-LUMO energy levels of the emissive layers in the devices. The light emission can be fine-tuned for maximum luminescence intensity and life-time by suitably choosing the different layers and optimizing the relevant parameters. The chromaticity coordinates of the emitted light from the prototype devices are shown in table 6.3. The electroluminescence emission from the device using TBPV1 is shown in figure 6.16.

Table 6.3: Chromaticity coordinates of emission from the devices using TBPV1 and TBPV2

Device	x	y	X	Y	Z
TBPV1	0.5727	0.4146	0.6462	0.4678	0.01439
TBPV2	0.5175	0.4342	0.95263	0.79935	0.089023

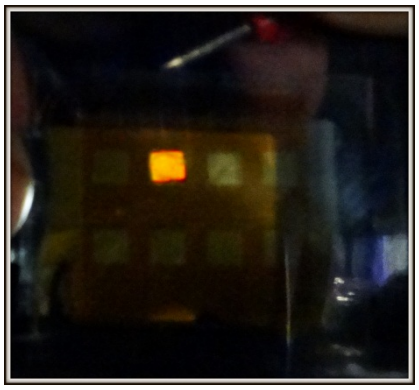

Figure 6.16: Electroluminescence emission from the device with TBPV1 as the emissive layer

6.7 Conclusions

Two novel, thienylene-biphenylenevinylene hybrid polymers (TBPV1 and TBPV2) with excellent PL emission, thermal stability, solubility and semi-crystalline nature have been thoroughly characterized. Current-voltage characteristics of both the polymers with ITO as anode and Al as cathode show well-defined forward and reverse diode

characteristics. The current through the devices with ITO/hybrid polymer/aluminium architecture was found to be very low to light up the device because of the higher barrier height created as a result of mismatch between the various layers. Hence, prototype devices based on these polymers were fabricated with the device architecture ITO/PEDOT:PSS/hybrid polymer/LiF-Al. These devices were found to exhibit excellent forward diode characteristics and electroluminescence emission of moderate intensity in the orange-red region. By suitably choosing the electrode materials and optimizing the relevant parameters of the various layers, the luminescence intensity and life-time of these devices can be considerably enhanced. Highlight of the present work is the identification of two novel hybrid polymers, TBPV1 and TBPV2 as excellent semi-conducting polymers, suitable for realizing efficient polymer light emitting diodes.

References

[1] Mark T.Bernius et al, *Adv. Mater*., 12, 1737-1750 (2000)

[2] David Braun, *Materials Today*, 32-39, June (2002)

[3] Hari Singh Nalwa, *Handbook of Advanced Electronic and Photonic Materials and Devices*, Academic Press, New York (2002), pp 1-102

[4] Miller J.S, *Adv. Mater*., 5, 587-589 (1993)

[5] Miller J.S, *Adv. Mater*., 5, 671-676 (1993)

[6] Zhigang Li and Hong Meng, *Organic Light Emitting Materials and Devices*, Taylor & Francis Group, USA (2007), pp 47-98, 184-213, 303

[7] D. Hohnholz, et al, *Synth. Met.*, 110, 141 (2000)

[8] Y. D. Jin et al, *Synth Met.*, **127**, 155 (2002)

[9] D. Ma, I A Hümmelgen, R. W. C. Li, J Gruber, *J. Phys. D: Appl. Phys*, **33**, 1376 (2000)

[10] Yuning Li et al, *Adv. Mater.*,**18**, 3029–3032 (2006)

[11] Le Huong Nguyen et al, *Sol. Energy Mater. Sol. Cells*, **90**, *2815–2828 (2006)*

[12] Vidya G, *PhD Thesis*, CUSAT, (2012)

[13] T. Yamamoto et al,*Chem. Mater*, **15,**4384 (2003)

[14] R. Resel et al, *Synth. Met.*, **101**, 96 (1999)

…..ஜ۞ஜ…..

Chapter 7

NEW SEGMENTED BLOCK CO-POLYMERS AS EMISSIVE POLYMERS FOR LIGHT EMITTING DIODES

Contents

The possibility of utilizing three novel, segmented block co-polymers based on poly phenylenevinylenes (P1, P2, P3), as emissive layers in polymer light emitting diodes is investigated in detail. This chapter begins with the detailed structural, electrical and optical characterization of these copolymers and evolves into the successful realization of prototype devices with ITO/PEDOT:PSS/SBCs/LiF-Al architecture. These prototype devices are found to exhibit excellent forward diode characteristics and show electroluminescence emission in blue-green/cyan and green regions.

7.1 Introduction

The quest for novel polymers and co-polymers for optoelectronic applications continues, by modelling new architectures, altering the emission characteristics and improving the thermal stability, emission

intensity, and device performance [1]. Blue light emitting polymers have attracted much interest as emissive layers for polymer light emitting diodes (PLED) [2-8] and for the fabrication of blue lasers [9].Tremendous efforts have been put in to improve the stability and performance of the devices based on these polymers. Designing of suitable co-polymers is one of the key solutions for achieving all the necessary characteristics required for the successful realization of optoelectronic devices. Studies related to segmented block co-polymers (SBC) bearing bulky ring substituents are quite scarce and only a very limited number of such co-polymers have been ever synthesized [10, 11, 12]. The SBC's consisting of phenylenevinylene and hexamethylene glycol blocks are novel with their long aliphatic chain and rigid ring substitutions. By combining these groups, the emission can be blue shifted and the solubility can be improved. These polymers consist of conjugated and non-conjugated segments. By suitable substitutions in these SBC's, the emission colour can also be altered to get light emission throughout the whole visible spectrum [13].

In the present study, three, novel, light emitting SBC's have been characterized and the suitability of these polymers as emissive layers in polymer light emitting diodes has been investigated. Detailed investigations on the structural, optical and electrical characteristics of these polymers have been carried out. Prototype devices based on these polymers were fabricated and the current-voltage characteristics were analyzed to assess the suitability of these blue and green light emitting polymers as candidates for emissive layers in PLEDs. The electroluminescence from the prototype devices with ITO/PEDOT:PSS /SBC/LiF-Al architecture

has also been demonstrated. The studies based on these SBC's are quite novel in all respects since there are no previous reports on the synthesis of these polymers and hence on their applicability in PLEDs.

7.2 A short introduction to the new, light-emitting SBCs

Three light-emitting segmented block co-polymers (SBC) based on poly-phenylenevinylene (PPV) were used for the present study. The SBCs were synthesized via Horner-Emmons condensation polymerization* [13]. The abbreviated names of these co-polymers are:

P1 - Poly [1, 6-hexanedioxy-(1, 4 phenylene)-1, 2 ethenylene-(2, 5-dioctyloxy-1, 4 phenylene)-1, 2 ethenylene-(1, 4 phenylene)]

P2 - Poly [1, 6-hexanedioxy-(1, 4 phenylene)-1, 2 ethenylene-(2, 5-dicyclo hexyl methyloxy-1, 4 phenylene)-1, 2 ethenylene – (1, 4 phenylene)]

P3 - Poly [1, 6-hexanedioxy-(2, 6-dimethoxy-1, 4 phenylene)-1, 2 ethenylene-(2, 5-dicyclo hexyl methyloxy-1, 4 phenylene)-1, 2 ethenylene – (3, 5-dimethoxy-1, 4 phenylene)]

The synthesis schemes are shown in figures 7.1(a), (b) and (c).

* *Most part of the synthesis and basic characterizations of these co-polymers were done, in collaboration with The Department of Polymer Science & Rubber Technology and The Department of Applied Chemistry, CUSAT*

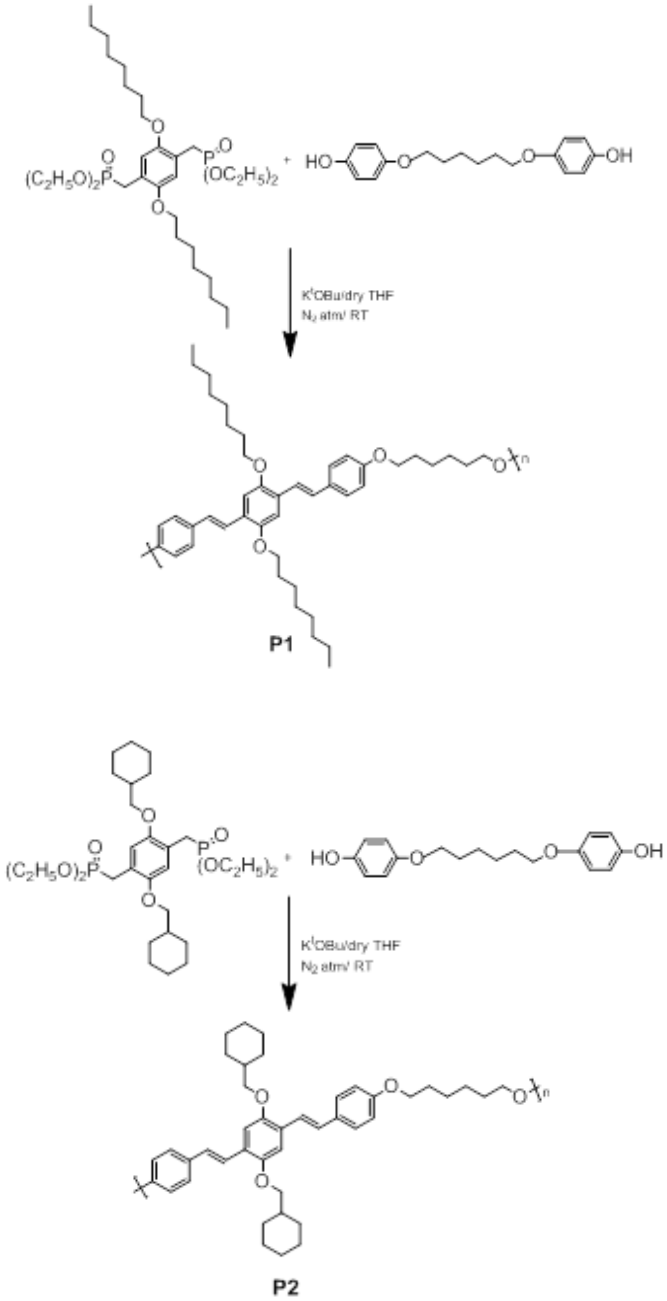

Figure 7.1: Synthesis route of (a) P1 and (b) P2 *via* Horner-Emmons condensation polymerization

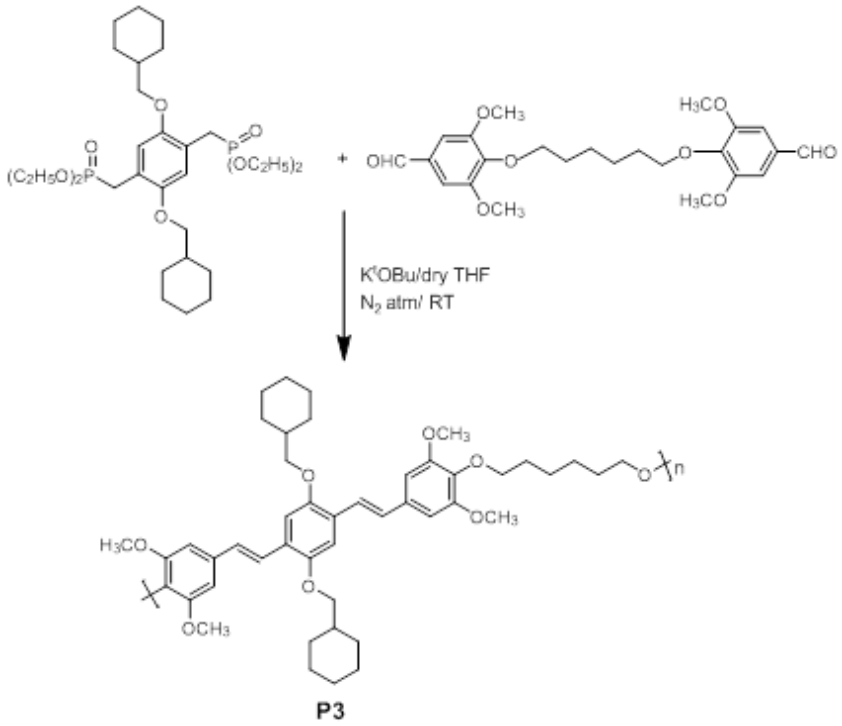

Figure 7.1(c): Synthesis route of P3 *via* Horner-Emmons condensation polymerization

These SBC's combine the qualities of polyphenylenevinylenes and hexamethylene glycol required for the emissive layer in polymer light emitting diode applications. The design and synthesis of monomers, polymers, and the basic characterization of these SBC's are explained in reference 13. These SBCs were found to be highly soluble in dichloromethane (DCM) and quality thin films of these polymers were spin-coated (SPS Spin 150 wafer spinner) on ultrasonically cleaned glass substrates from these solutions.

The important characteristics of P1, P2 and P3 are listed in table 7.1 [13]:

Table 7.1: Physical and thermal properties of P1, P2 and P3

SBCs	P1	P2	P3
Molecular weight (Mw)	14340 $g.mol^{-1}$	12499 $g.mol^{-1}$	12644 $g.mol^{-1}$
Polydispersity Index (PDI)	1.4	1.5	1.6
Degradation temperature (Td)	442^0C	451^0C	422^0C
Glass transition temperature (Tg)	50^0C	82^0C	53^0C

The characteristics listed in table 7.1 indicate that these SBCs are quite pure and their degradation temperatures and glass transition temperatures are high enough for optoelectronic applications.

7.3 Characterization

The optical absorption spectra and photoluminescence spectra of the SBCs in solution and film forms were recorded using Jasco V-500 UV-VIS-NIR spectrophotometer and Fluoromax 3 fluorescence spectrophotometer respectively. The structural characterization of the co-polymers was carried out using Rigaku X-ray diffractometer with Cu-Kα radiation (λ=1.542 Å). The morphological studies of SBCs were carried out using the procedure exactly similar to the one used for the hybrid polymers, explained in chapter 6. As before, the electrical characterization these SBCs was conducted using Keithley 2400 source meter and the electroluminescence studies were carried out using Konica Minolta CS1000 spectroradiometer.

7.3.1 X-ray Diffraction Studies

The X-ray diffraction patterns of P1, P2 and P3 in powder form are shown in figure 7.2 [13].

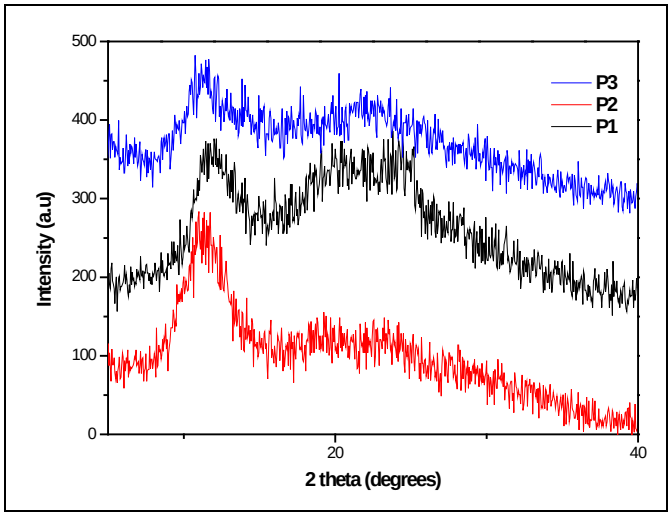

Figure 7.2: XRD patterns of the SBCs

From figure 7.2, it is obvious that all the copolymers are semi-crystalline. The peaks corresponding to d-values 7.44A^0, 7.78A^0 and 7.83A^0 in P1, P2 and P3 respectively, appear as a result of inter-chain scattering of two main chain backbones separated by extended octyloxy side chains. The amorphous diffraction peaks at 24^0 (d = 3.74 A^0), 23^0 (d = 4.27 A^0) and 21.6^0 (d = 4.31 A^0) respectively P1, P2 and P3, originate from the side-to-side distance between loosely packed alkoxy chains [13, 14, 15].

7.3.2 Scanning Electron Microscopy Studies

The FESEM (Hitachi FESEM SU6600) images of P1, P2 and P3 in powder form are shown in figures 7.3(a), (b) and (c). The morphology of P2 and P3 appears to be similar and both P2 and P3 appear to be nano-sized. On the other hand, P1 looks more flake-like and appears to be more crystalline compared to P2 and P3.

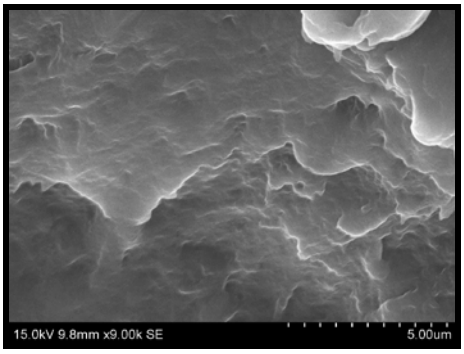

Figure 7.3(a): FESEM of P1 powder

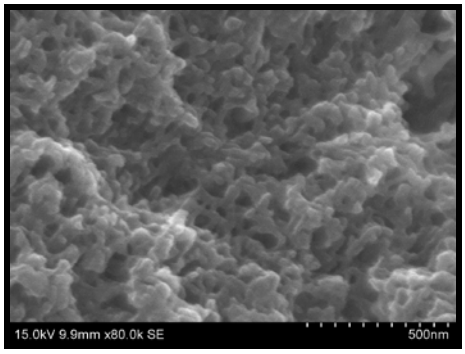

Figure 7.3(b): FESEM of P2 powder

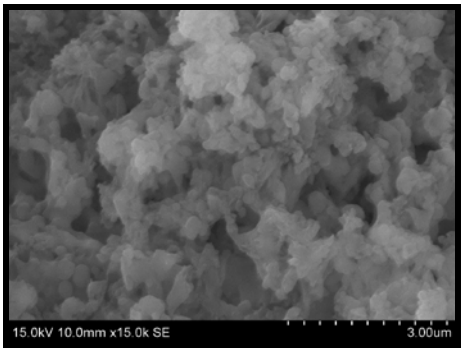

Figure 7.3(c): FESEM of P3 powder

7.3.3 Optical Characterization

The SBCs were dissolved in dichloromethane (5mg in 2 mL DCM) to get homogeneous solutions. Thin films were cast on clean glass slides by spin-coating method. Dilute solutions of these polymers were prepared adopting the same procedure explained in chapter 6. The optical absorption and photoluminescence spectra of the dilute solutions and thin films were recorded as detailed in Chapter 6.The normalised absorption and emission spectra of the dilute solutions and thin films of P1, P2 and P3 are shown in figures 7.4(a), (b) and (c) respectively.

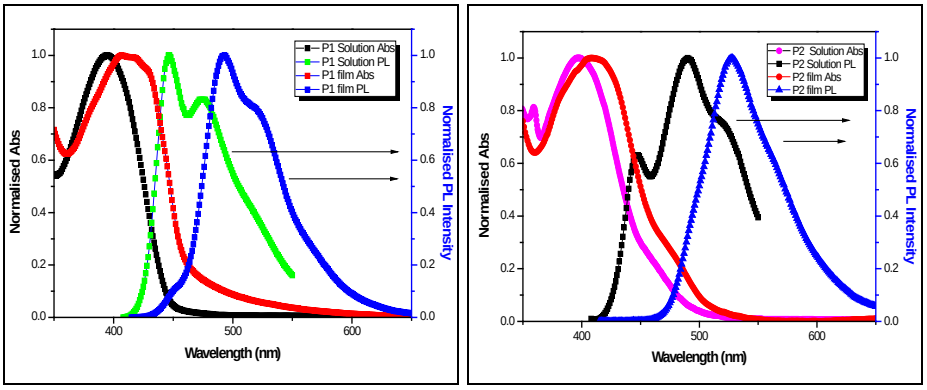

Figure 7.4: UV-Vis absorption and PL spectra of (a) P1and (b) P2

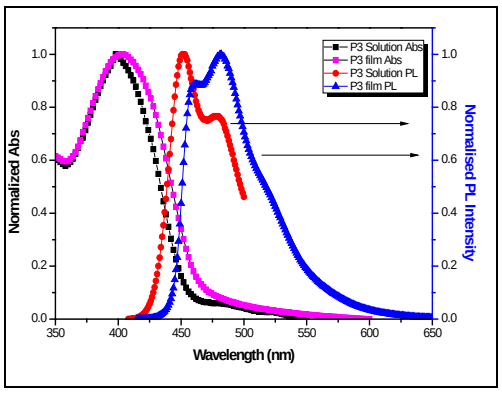

Figure 7.4(c): UV-Vis absorption and PL spectra of P3

The relevant details obtained from the optical absorption and PL spectra of the three SBCs are tabulated in table 7.2.

Table 7.2: Optical absorption and PL emission data of P1, P2 and P3

SBCs	P1		P2		P3	
	solution	film	solution	film	solution	film
Optical absorption peak (nm)	394	410	397	408	399	403
PL peak (nm)	446	492	489	526	451	481

The slight red-shift observed in the optical absorption and PL emission peaks of the thin film samples can be attributed to the

aggregation effects in thin films [16].When the co-polymers were exposed to UV light, the solutions of P1 and P3 show intense blue emission and that of P2 shows intense cyan emission in solution form. The photographs of the polymer solutions and their emissions are shown in figures 7.5(a) and (b) respectively.

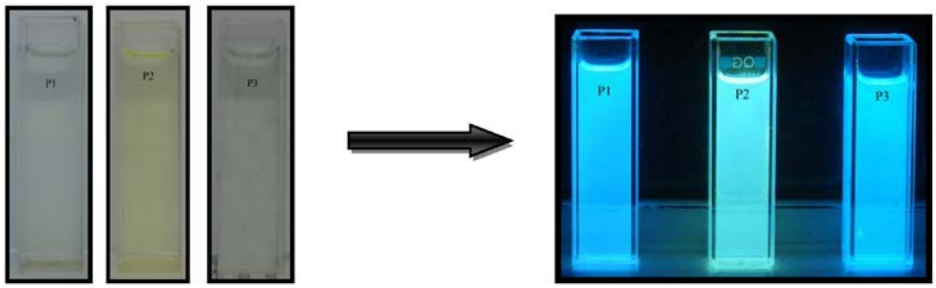

Figure 7.5:(a) Dilute solutions of SBC's in DCM; (b):Emissions from P1, P2 and P3 solutions

7.3.4 HOMO-LUMO energy levels and Band gap

The HOMO-LUMO energy levels and band gap energy estimated from cyclic voltammetry [13] and optical absorption studies are tabulated in table 7.3. The HOMO-LUMO energy levels of emissive polymers determine the nature of the suitable intermediate layers and the electrodes while fabricating the PLED.

Table 7.3: Band-gap and HOMO-LUMO energy values of P1, P2 and P3

SBC's	P1	P2	P3
HOMO (eV)	5.26	5.01	5.23
LUMO (eV)	2.51	2.58	2.529
Band gap (cyclic voltammetry) (eV)	2.747	2.42	2.701
Band gap (UV-Vis absorption) (eV)	2.75	2.46	2.72

7.3.5 Estimation of the CIE coordinates

The CIE coordinates of the light emitted from the solutions and films of the SBCs, P1, P2 and P3 were determined using the program developed in Matlab as described earlier. The screenshots thus obtained for the P1, P2 and P3 solutions and films are shown in figures 7.6(a) to 7.6(f).The screenshots show the PL plots of the SBCs, x, y, tristimulus values (X,Y,Z) and the exact position of the emitted colour in the chromaticity diagram.

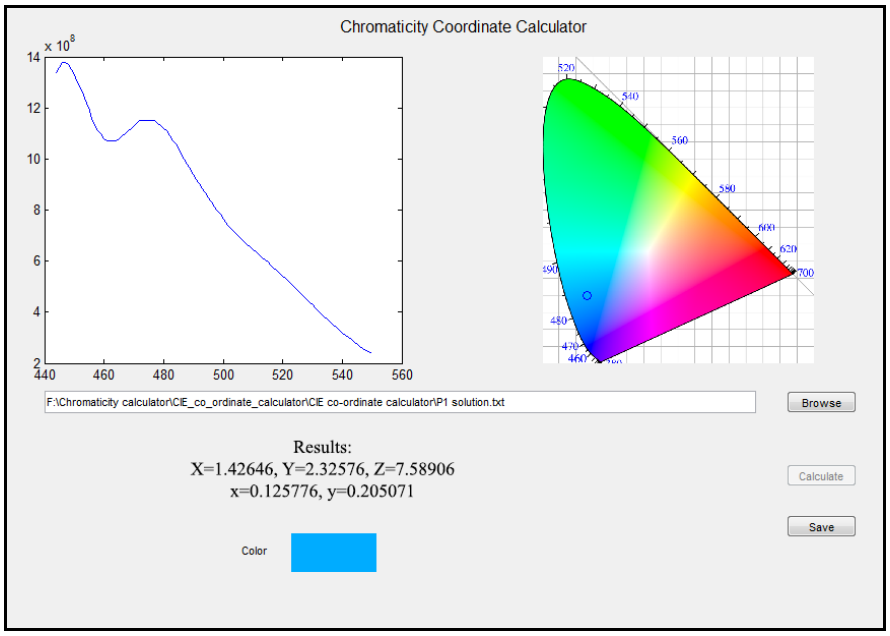

Figure7.6(a): P1 solution

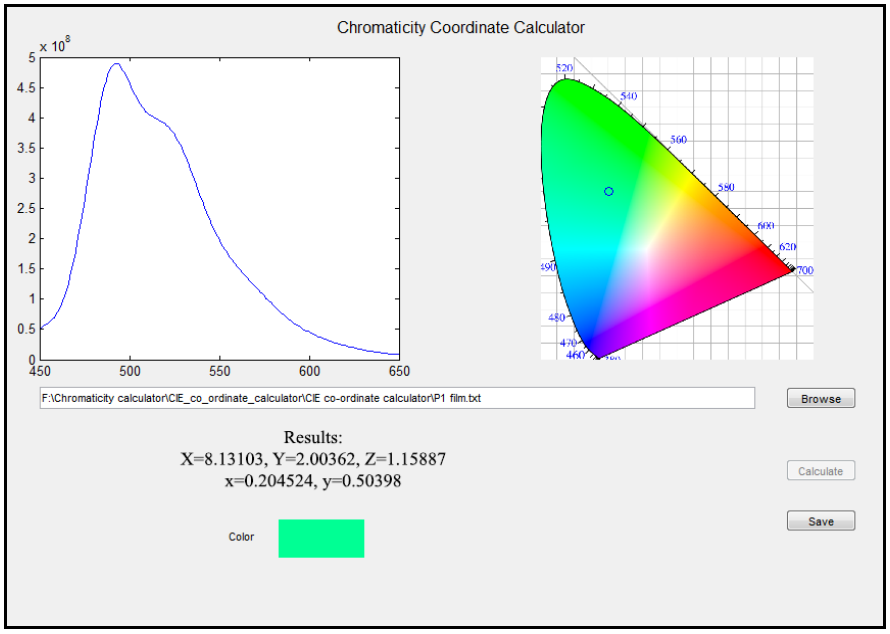

Figure 7.6(b): P1 film

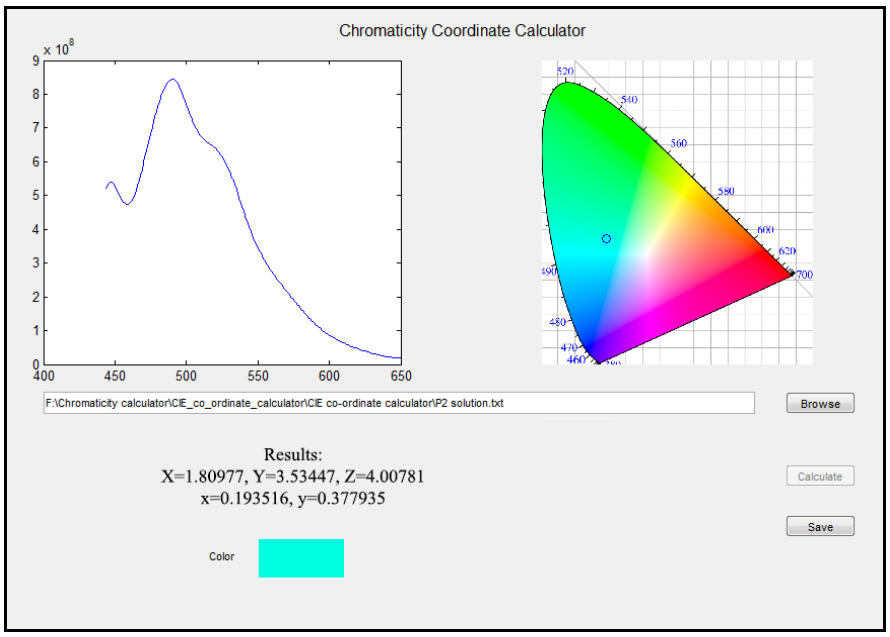

Figure 7.6(c): P2 solution

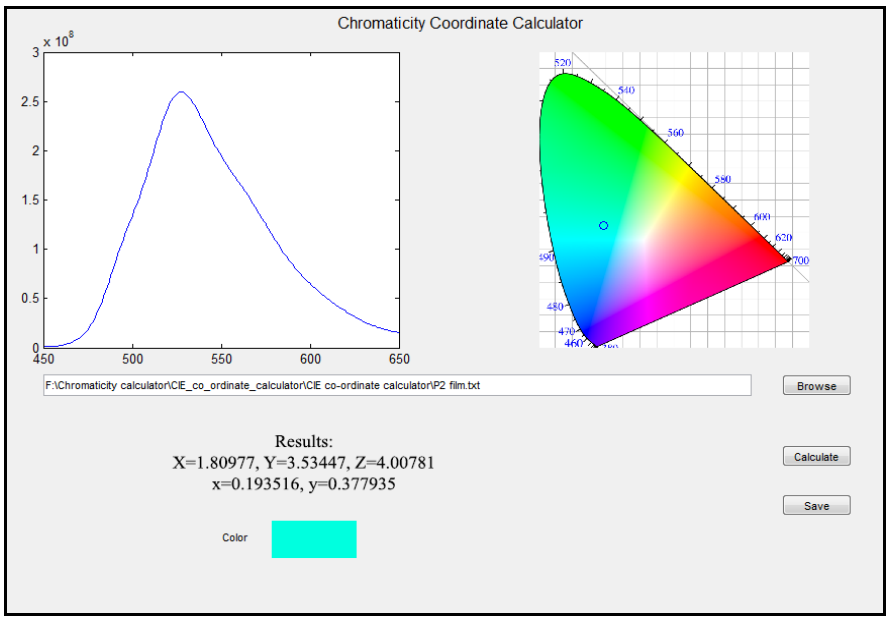

Figure 7.6(d): P2 film

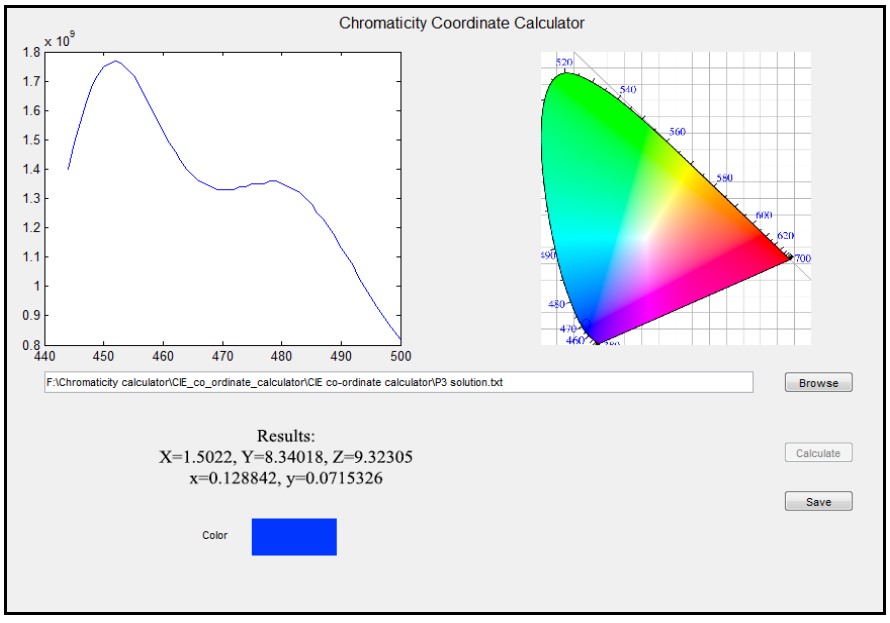

Figure 7.6(e): P3 solution

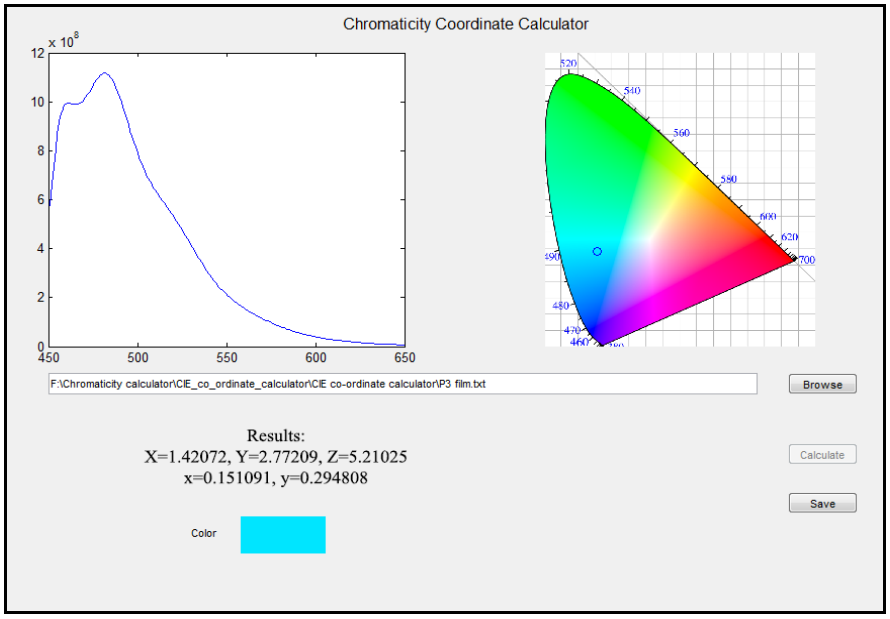

Figure 7.6(f): P3 film

7.3.6 Atomic Force Microscopy Studies

The topographic studies of the thin films of P1, P2 and P3 were conducted using atomic force microscopy technique (Park Systems XC 100) in the non-contact mode. The AFM topography images of P1, P2 and P3 films are shown in figures 7.7(a), (b) and (c). All the three films appear quite smooth with an r.m.s roughness below 5nm.

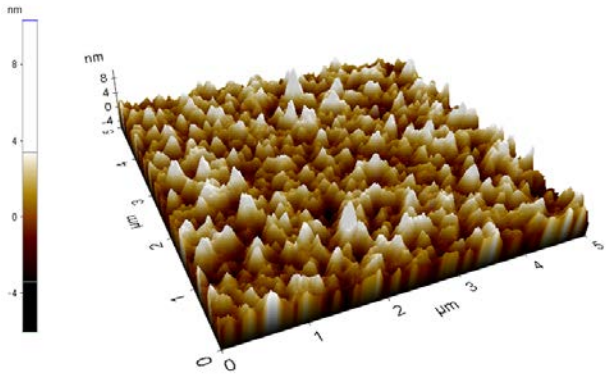

Figure 7.7(a): AFM image of P1 film

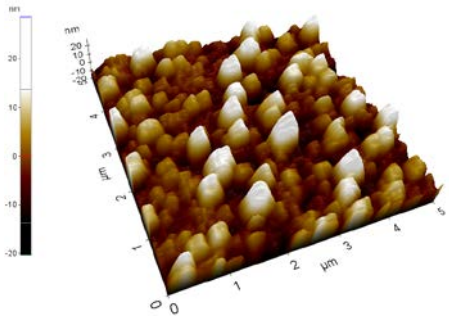

Figure 7.7(b): AFM image of P2 film

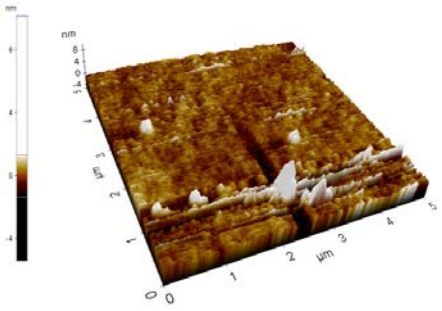

Figure 7.7(c): AFM image of P3 film

7.3.7 Current-Voltage Characteristics of ITO/SBCs/Al structures

The SBC's were spin-coated (2000 rpm, 30 seconds) from solutions in dichloromethane, on ITO coated glass plates. Aluminium contacts of 100 nm thickness were thermally evaporated on top of the co-polymer layers. The current-voltage (I-V) characteristics were recorded using Keithley 2400 source meter adopting the standard 2-point probe method. I-V plots of ITO/SBCs/Al structures in the forward and reverse bias are shown in figures 7.8(a), (b) and (c).

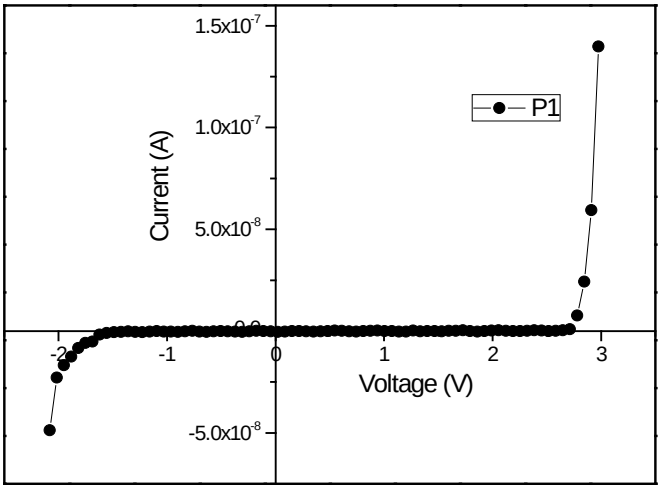

Figure 7.8(a): I-V plot of ITO/P1/Al structure

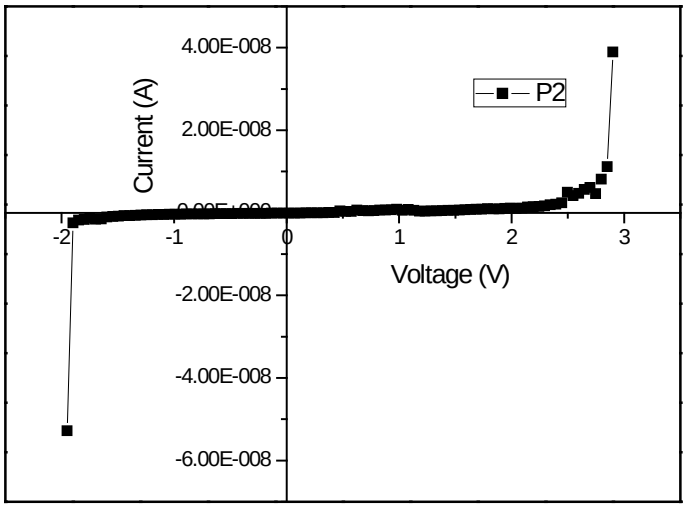

Figure 7.8(b): I-V plot of ITO/P2/Al structure

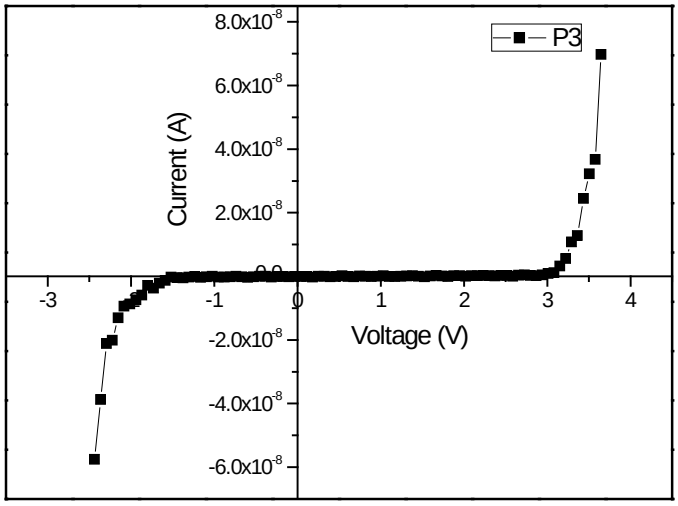

Figure 7.8(c): I-V plot of ITO/P3/Al structure

All the ITO/SBCs/Al structures exhibit well-defined forward and reverse diode characteristics, suitable for polymer light emitting diode applications. It is observed from the I-V plots that the on-set voltages for all the devices are very low. in this architecture. With this architecture, it was not possible to observe electroluminescence as the thickness of the

co-polymer layers was very small. Proper matching of work function of the electrodes with the HOMO-LUMO energy levels of the emissive polymer layer is also mandatory for the occurrence electroluminescence emission.

The band structure of ITO/SBCs/Al or Ca devices is shown in figure 7.9. The work function of ITO is quite close to the HOMO levels of the SBCs and the work function of calcium is close to the LUMO levels of the SBC's. Calcium is the most appropriate cathode material for the devices fabricated with these SBCs. A layer of silver or aluminium has to be evaporated on top of the calcium layer to avoid the oxidation of calcium and associated degradation of the device performance.

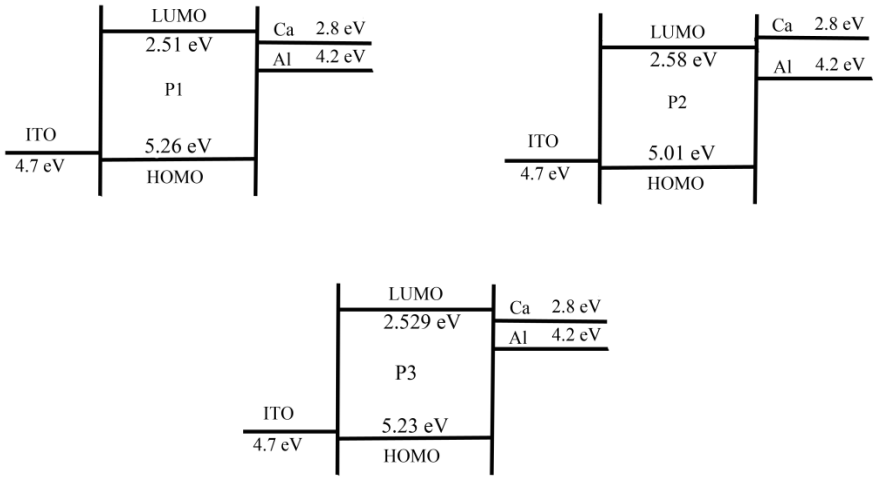

Figure 7.9: The band structure of ITO/SBCs/Al or Ca devices

7.4 Prototype PLED fabrication

As mentioned earlier, the ITO/SBCs/Al devices did not show any electroluminescence emission. Due to technical limitations, it was not possible to use calcium instead of aluminium as the cathode layer.

Hence, the device architecture was modified as ITO/PEDOT:PSS/SBCs/LiF-Al using P1 and P2 as the emissive polymers, following the procedure explained in chapter 6. The devices were encapsulated against degradation inside the glove box associated with the cluster tool (DOOSAN DND, Korea).

The energy band diagram of ITO/PEDOT:PSS/SBCs/LiF-Al devices is shown in figure 7.10.

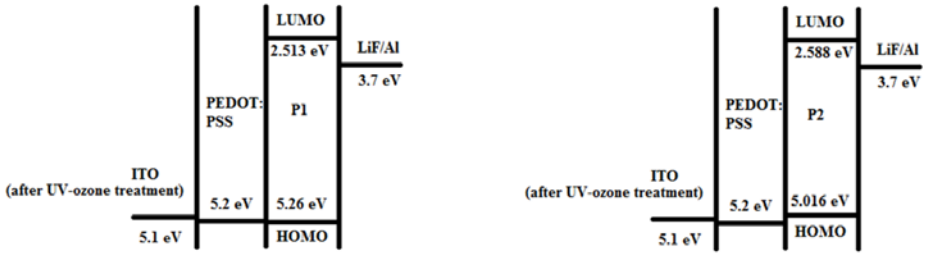

Figure 7.10: Energy band structure of ITO/PEDOT:PSS/SBCs/LiF-Al devices

7.5 Device Characterization

7.5.1 Current-Voltage Measurements

I-V characteristics of the two devices using P1 and P2 as emissive layers were recorded using Keithley 2400 source meter adopting the same procedure detailed in chapter 6. I-V graphs of the devices in the forward bias condition are shown in figures 7.11(a) and 7.11(b). Both the devices show well-defined forward diode characteristics. The observation of the well-defined diode characteristics confirms the successful fabrication of the PLED.

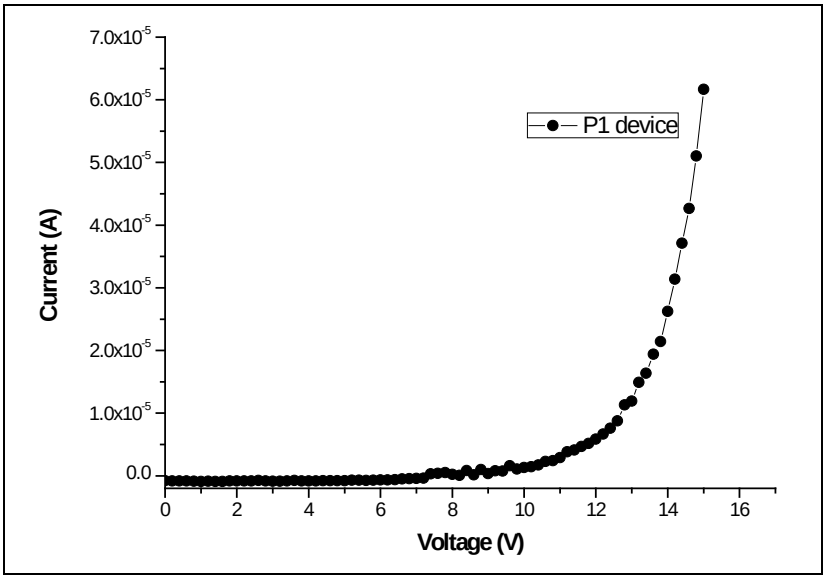

Figure 7.11(a): I-V plot of ITO/PEDOT:PSS/P1/LiF-Al device

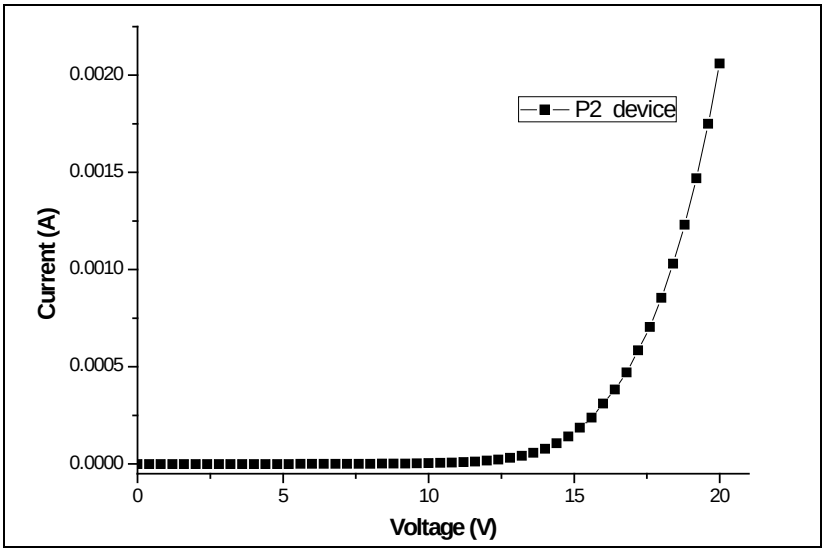

Figure 7.11(b): I-V plot of ITO/PEDOT:PSS/P2/LiF-Al device

7.5.2 Spectral distribution and Electroluminescence Studies

The spectral distribution and electroluminescence (EL) of the two devices were analyzed using the same procedure detailed in chapter 6. The operating voltages of 13 V and 14 V were applied to the devices based on P1 and P2 respectively using Keithley 2400 source meter adopting 2-point probe method. The plots of normalised spectral radiance against wavelength for the devices are shown in figures 7.12(a) and 7.12(b). The device fabricated using P1 was found to show blue-green/cyan, electroluminescence mission at 498nm and the device based on P2 was found to show green emission at 549nm, under forward bias conditions above the respective on-set voltages.

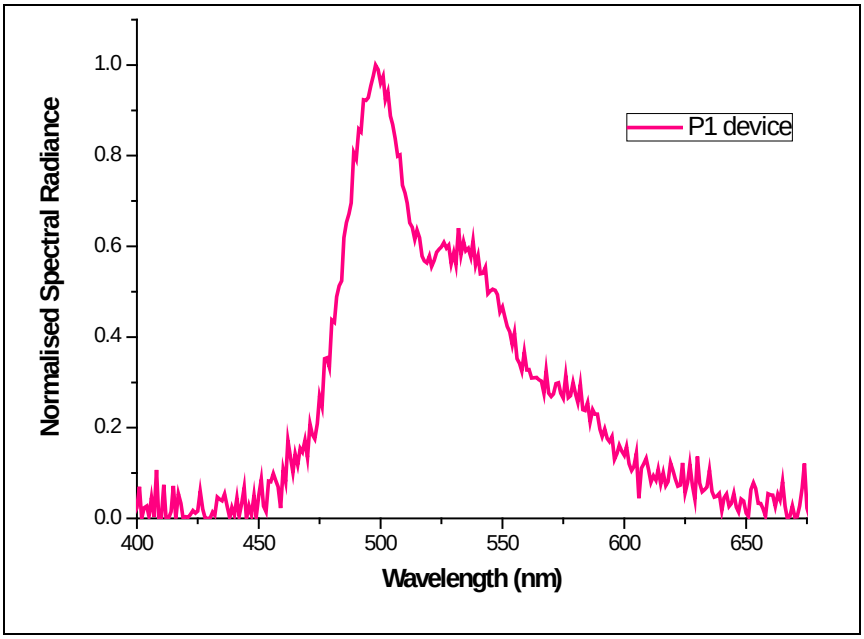

Figure 7.12(a): Normalised spectral radiance against wavelength plot of P1 device

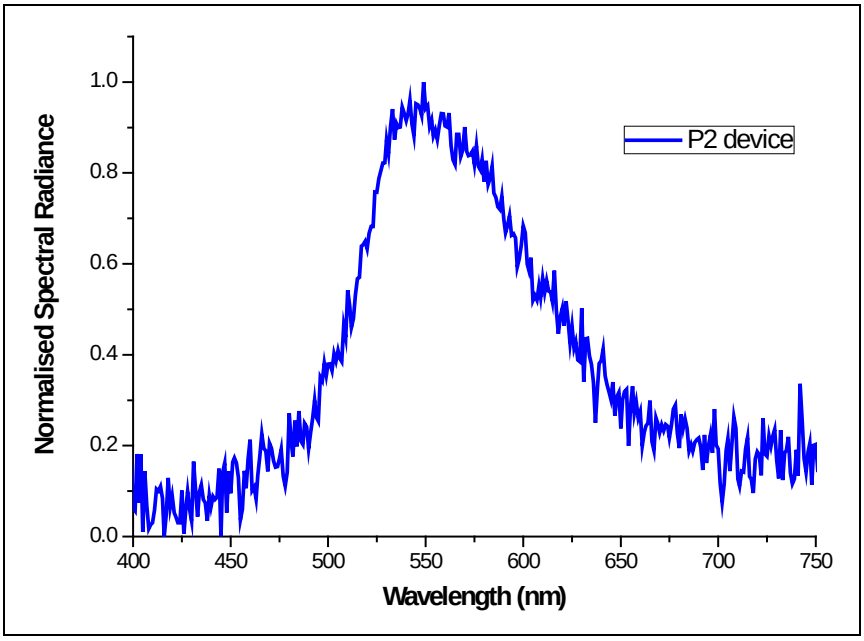

Figure 7.12(b): Normalised spectral radiance against wavelength plot of P2 device

The electroluminescence spectra of the devices appear to be similar in shape to the photoluminescence spectra of P1 and P2 films. This observation indicates that the mechanism of electroluminescence in the devices and that of photoluminescence in P1 and P2 films is similar [17].

The CIE (chromaticity) coordinates of the emitted colours, estimated using the program developed for the CS1000 spectroradiometer are shown in table 7.4.

Table 7.4: CIE coordinates of light emitted from the devices fabricated using P1 and P2

Device	x	y	X	Y	Z
P1	0.2540	0.5249	0.08152	0.1685	0.07095
P2	0.3959	0.5015	0.1059	0.1341	0.02744

The photographs of EL emission from the prototype devices in the forward bias conditions are shown in figures 7.13 (a) and 7.13(b).

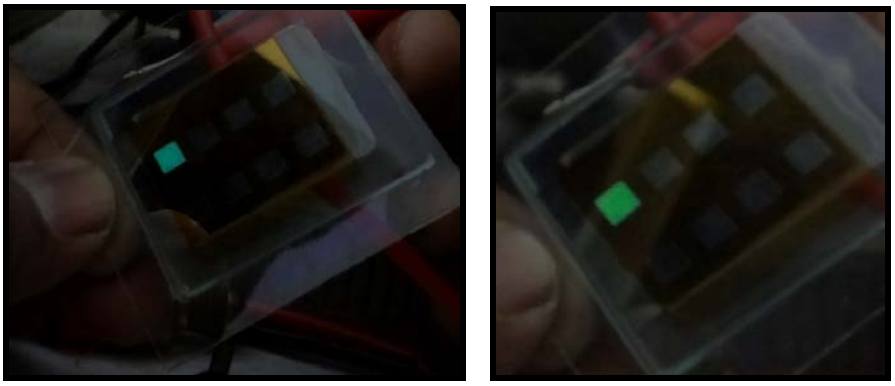

Figure 7.13: Electroluminescence emission from the prototype devices fabricated using (a) P1 (blue-green) and (b) P2 (green) respectively

7.6 Conclusions

A set of novel, segmented block co-polymers (P1, P2, P3) have been extensively characterized optically, structurally and electrically, to assess the suitability of these co-polymers as emissive layers in PLED applications. The devices with ITO/SBCs/Al architecture did not show electroluminescence because of poor carrier injection and interface effects. In order to reduce the mismatch between various layers, and facilitate efficient carrier injection, the device architecture was modified as ITO/PEDOT:PSS/SBCs/LiF-Al, using P1 and P2SBCs as emissive layers. Both the devices are found to exhibit excellent forward diode characteristics and electroluminescence emission in the blue-green (cyan) and green regions. In the light of these observations, the SBCs, especially, P1 and P2, can be identified as excellent candidates for fabricating efficient PLEDs

References

[1] Zhigang Li and Hong Meng, *Organic Light Emitting Materials and Devices*, Taylor & Francis Group, USA (2007), pp 45-294

[2] David Braun, *Materials Today*, 32-39, June (2002)

[3] JH Burroughes et al, Nature, **347,** 539–541, (1990)

[4] M. Schleffer and R. Zimmerman (Editors), *The Physics of Semiconductors*, World Scientific, Singapore, (1996) , pp 35

[5] C Zhang, G Yu, and Y Cao, *U.S. Patent* 5,798,170, (1998)

[6] H Becker et al, *Adv. Mater.*, **12,** 42–48, (2000)

[7] SID 2002 Advance Program. *http://www.sid.org/conf/sid2002/sid2002.html*, (2002)

[8] Samsung SDI, *IMID Exhibition*, Asia Display/IMID'04, Daegu, Korean, August 23–24, (2004)

[9] S.M Sze and Kwok K.Ng, *Physics of Semiconductor Devices*, John Wiley & Sons, New York (1981), pp 3, 124, 602

[10] Igor Sokolik et al, *J. Appl. Phys.***74**, 3584-3586 (1993)

[11] Erica M. Kyllo et al, *Synth. Met.*, **116**, 189-192 (2001)

[12] T.Zyung et al, *Chem. Mater*.**, 7**, 1499-1503, (1995)

[13] Vidya G, *PhD Thesis*, CUSAT, (2012)

[14] Resel et al, *Synth. Met.*, **101**, 96-97 (1999)

[15] Yuning, L. et al, *Adv. Mater*., **18**, 3029–3032 (2006)

[16] Kulkarni AP, Kong X, Jenekhe SA, *J. Phys. Chem. B*, **108,**8689 (2004)

[17] TaehyoungZyung et. al, *Chem. Mater.*,**7**, 1499-1503(1996)

Chapter 8

SUMMARY AND FUTURE PROSPECTS

Contents

8.1 Overview of technologically important conjugated polymers

The interest in intrinsically conducting polymers and conjugated light emitting polymers is growing at a faster pace with the identification of newer application fields and the realization of efficient and stable, polymer based devices. Numerous devices based on these conjugated macromolecules have already been commercialized. Polyaniline is one such polymer that has been commercialized decades ago. Countless research articles based on polyaniline have been published and thousands of patents filed by researchers worldwide.

Polymer light emitting diodes are still intriguing with the possibility of synthesizing a variety of new polymers and co-polymers as emissive layers with excellent thermal stability, solvability and light emission. The search for newer, efficient and stable, conjugated light emitting polymers continues with the vision of overcoming the challenges associated with the device performance and efficiency.

8.2 Missing Links

The enormous number of published articles and patents related to polyaniline and its composites reflect the technological importance of this conducting polymer in various fields of research and industry. In spite of all these, there are many technologically relevant areas in which the potential of polyaniline has not been properly explored. The sensitive dependence of electrical conductivity of polyaniline and its composites, on applied pressure has not been studied in depth, giving emphasis on the structural differences of the polyaniline samples. Quantum confinement effects in inorganic semiconducting nanoparticles and metal nanoparticles have been studied extensively. The quantum confinement effects in conducting polymers, especially polyaniline, have not been addressed in detail. The applications of highly conducting polyaniline have been restricted to those regions where the electrical conductivity that can be achieved through suitable doping has already reached the saturation limits. Further enhancement in conductivity is possible only by improving the order/crystallinity within and among the polymer chains. Not much attention has been given to synthesize polyaniline films with higher extent of crystallinity which in turn can enhance the electrical conductivity and stabilize the overall properties. These areas remain unexplored, and detailed investigations in these directions may unravel newer applications of polyaniline and its composites.

8.3 Motivation for the present studies

Polyaniline is a stable polymer that can be synthesized in bulk quantities using relatively cheaper precursors, employing eco-friendly synthetic routes. Polyaniline and its composites can be effectively used

to develop cost-effective pressure sensors with the prospects of replacing the expensive inorganic pressure sensors. Intrinsically conducting polymers possess the advantageous features of both inorganic materials and polymers. Various inorganic conductors and semiconductors have been effectively replaced by intrinsically conducting polymers in many areas of science and technology. Quantum confinement effects in polyaniline thin films can modify the band gap and hence alter the photoluminescence emission characteristics. Doped polyaniline films with much higher extent of crystallinity can be realized using modified synthetic routes. These highly crystalline polyaniline films are expected to show enhanced electrical conductivity and thermal and environmental stability.

Environmentally and thermally stable, highly soluble and intense light emitting conjugated polymers remain the dream of the scientific community for realizing efficient and stable polymer light emitting diodes. A novel class of hybrid and segmented block copolymers that are capable of delivering stable and efficient light emission has been synthesized. The possibility of electroluminescence emission from devices based on these polymers has not been previously investigated. It is expected that it will be possible to assemble polymer LEDs with these novel polymers as emissive layers with excellent performance characteristics.

8.4 Summary of the work done

Part of the present work involves the studies on the change in electrical conductivity of microstructured and nanostructured polyaniline and its composite samples with applied pressure, synthesized using

chemical oxidative polymerization technique. Appreciable variation in electrical conductivity with applied pressure has been observed in most of the doped PANI samples using HCl, H_3PO_4, CSA and NSA as the acid dopants and the composites of these doped PANI samples with MWNT and PVC. Nanostructured PANI and its composite samples show a superior pressure sensing capability when compared to their microstructured analogues. Nanostructured samples possess a higher saturation limit of above 30MPa for the electrical conductivity change with applied pressure, compared to the micro-structured samples. Based on the percentage variation of electrical conductivity with applied pressure, the maximum sensitivity to applied pressure is observed for the micro-structured PANI-MWNT-PVC composite samples. However, these composite samples cannot be categorized as excellent pressure sensors, due to the inherent hysteresis effect and the lower saturation pressure limit. The nanostructured CSA doped PANI samples are found to exhibit the best pressure sensing characteristics with reproducible results and negligible hysteresis effects. These low-cost, highly sensitive, CSA doped PANI samples can be utilized for realizing foot pressure measurement systems to design footwear to suit the requirements of diabetic patients and sports personnel.

Another phase of the present work involves the search for quantum confinement effects in nanostructured, doped PANI films. The well-known quantum confinement effects in nanostructured inorganic semiconductors have been established in ultra-thin films of CSA doped PANI, using simple spectroscopic methods based on UV-VIS-NIR absorption and photoluminescence studies. In the ultrathin films of

PANI with thickness in the range 50-150 nm, a blue shift of around 100 nm has been observed in the photoluminescence (PL) emission peak compared to that in bulk films (thickness around 4μm). The PL emission in these ultra-thin films occurs in the violet-blue region with much enhanced emission intensity compared to the PL emission in the bulk samples. There is also considerable band gap enlargement of about 0.7 eV for the nanostructured PANI films. These aspects are cited as the evidence for establishing quantum confinement effects in ultra-thin/nanostructured films of CSA doped PANI. The present work highlights the prospects of developing nanostructures such as quantum wells based on these nanometre sized CSA doped PANI films. These ultra-thin PANI films with intense PL emission in the violet-blue region extend ample scope for developing efficient polymer LEDs.

Another gap area which has been investigated in detail in the present work is related to the synthesis of doped polyaniline films with much higher extent of crystallinity. Crystallinity in polymer films, especially in polyaniline films, has not been subjected to detailed analysis. In the present work, the well-known doping-dedoping-redoping process followed by ultrasonication has been adopted as the technique to improve the solubility of doped PANI samples and enhance the crystallinity of PANI films grown by spin coating technique.

Initially, HCl doped PANI powder samples were synthesized using chemical oxidative polymerization technique. These samples were de-doped using ammonia solution and then re-doped with CSA to yield processable and soluble, doped PANI powder. Good quality PANI films

with excellent crystallinity were cast from CSA re-doped PANI powder, dissolved in two different solvents, NMP and m-cresol, under ultrasonication. The PANI films spin-coated from m-cresol solution were found to exhibit very sharp XRD peaks of excellent intensity. Atomic force microscope (AFM) studies of these film samples support the XRD results, showing crystallites of micrometre dimensions. The much higher dc electrical conductivity around 473S/cm and the good thermal stability up to ~250^{0}C exhibited by these PANI films can be attributed to the higher extent of crystallinity and structural order present in these films. The effect of ultrasonication along with the proper combination of primary (HCl) and secondary dopants (CSA, *m*-cresol) can be considered as the prime factors responsible for the enhanced crystallinity and structural order exhibited by the PANI films coated from *m*-cresol solution. The XRD peaks of these PANI films have been indexed to correspond to a simple cubic crystal structure. Polyaniline films co-doped using HCl and DBSA and re-doped using NSA and CSA were also found to exhibit quite high extent of crystallinity when the films were spin coated from solutions in *m*-cresol. The dopants, NSA and CSA were used for re-doping to study the effects of dopants on the crystalline structure, after the formation of the polymer backbone. The resulting polymer film samples were found to have monoclinic and triclinic crystal structures respectively and good thermal stability. The corresponding XRD peaks were successfully indexed and the cell-parameters were evaluated. Crystalline films were also cast from CSA re-doped PANI powder samples synthesized via dispersion polymerization and dissolved in *m*-cresol via ultrasonication. The dispersion polymerized,

CSA re-doped PANI films have been identified as the most conductive films among the set of crystalline PANI film samples investigated.

Single layer polymer LEDs having ITO/emissive polymer/ aluminium architecture were assembled using two novel, highly soluble and thermally stable, light emitting hybrid polymers based on thienylene and biphenylenevinylene, TBPV1 and TBPV2, and three novel, segmented block copolymers (P1, P2 and P3) based on phenylenevinylene and hexamethylene glycol. Even though these devices were found to exhibit well-defined forward and reverse diode characteristics, none of these devices did show any electroluminescence. The mismatch between the different layers of the device structure was identified as the reason for the absence of electroluminescence in these devices. Hence, the device architecture was modified as ITO/PEDOT: PSS/emissive polymer/LiF-Al to overcome this problem, using the hybrid polymers and segmented block copolymers as emissive layers. These modified devices were also found to exhibit well-defined forward diode characteristics. Electroluminescence of moderate intensity, in the orange-red region was observed from the devices based on the hybrid polymers. The devices assembled using the segmented block copolymers P1 and P2 were found to show electroluminescence in the blue-green and green regions respectively.

8.5 Future Prospects

The present investigations extend ample scope for further investigations, suitable modifications and future developments to realize practical devices with characteristics ideal for commercialization, in the following areas.

1) Cost-effective pressure sensors based on nanostructured, doped PANI can be practically realized for foot pressure measurement systems and surveillance applications in both bulk and thin film forms.

2) Attempts can be initiated to fabricate display devices with emission in the blue region using ultra-thin, nanostructured PANI films.

3) Highly crystalline, ordered, highly conducting and transparent PANI films can be realized by modifying the synthesis conditions with the vision of replacing the ITO layer in polymer LEDs.

4) The choice and thickness of the various layers constituting the polymer LEDs, fabricated using the hybrid polymers and segmented block copolymers can be optimized to get higher emission intensity, life-time and efficiency.